The Effect of Lethal Radiation and PDGFBR Signaling on the Contribution of SMC in Atherosclerotic Lesions

Alexandra Annetta Corlis Newman

New York, New York

Bachelor of Science, Biochemistry/Biophysics, Rensselaer Polytechnic Institute, 2010

Master of Science, Biochemistry and Molecular Genetics, University of Virginia, 2015

A Dissertation presented to the Graduate Faculty of the University of Virginia in Candidacy for the Degree of Doctor of Philosophy

Department of Biochemistry and Molecular Genetics

University of Virginia

May 2019

Dr. Gary Owens

Dr. Norbert Leitinger
Dr. Marty Mayo
Dr. Michael McConnell
Dr. David Wotton

Thesis Summary

Thrombosis after rupture or erosion of unstable atherosclerotic lesions is the leading cause of death worldwide. However, despite decades of research, the factors and mechanisms that control lesion stability are poorly understood. Human pathological studies have shown that lesions containing a thin fibrous cap and an abundance of $CD68^+$ relative to $ACTA2^+$ cells are at risk for rupture. CD68 is presumed to be a marker of macrophages (MΦ) and ACTA2 is the most common marker of smooth muscle cells (SMC). However, use of marker proteins alone is insufficient to identify cell lineage and thus, there are major ambiguities as to the origins of these cells as well as the pathways that control their functions within lesions. Herein, we showed that $ACTA2^+$ cells in the fibrous cap derived from SMC seem to be the most effective regulators of lesion stability by three independent methods.

The first method elucidated the effects of radiotherapy on SMC in atherosclerosis. Radiotherapy has well-documented long-term adverse effects on cardiovascular disease (CVD), however, the reasons for this increased risk are not well characterized. Our studies tested whether radiation impairs protective adaptive SMC responses during vascular disease. To do so, SMC-lineage tracing mice were exposed to lethal radiation (1,200 cGy) with bone marrow transplantation (BMT) prior to atherogenesis or vessel injury. In the irradiated animals, there was a complete loss of SMC investment in 100% of carotid artery, aortic arch, and brachiocephalic artery (BCA) lesions, with associated decreases in multiple indices of atherosclerotic lesion stability within the BCA. This was compared to non-irradiated control animals that showed SMC investment in lesions. Importantly, there was no decrease in ACTA2 expression in the cap overall, suggesting after radiation these non-SMC derived $ACTA2^+$ cells are not able to fully maintain lesion stability. Interestingly, we observed anatomic heterogeneity, as SMC accumulated normally into lesions of the aortic root and abdominal aorta. These results revealed an undefined and unintended variable in previous studies using lethal irradiation and may help explain why patients exposed to radiation have increased risk for CVD.

The second method utilized a SMC-specific conditional knockout of the platelet derived growth factor beta receptor (PDGFBR) in $Apoe^{-/-}$ mice that was associated with >94% loss of SMC investment within lesions and the fibrous cap. Unexpectedly, this was not associated with detectable changes in lesion size or indices of plaque stability following 18 weeks of WD feeding. This was due at least in part to compensatory increases in the fraction of $ACTA2^{+}$ fibrous cap cells derived from endothelial cells and MΦ transitioning to a mesenchymal state (EndoMT or MMT). However, this compensation was transient as mice fed WD for 26 weeks showed evidence of plaque instability including reduced collagen content and increased intraplaque hemorrhage, despite persistent increases in EndoMT and MMT. In these studies, we challenged the dogma that $ACTA2^{+}$ cells within the fibrous cap of advanced lesions are nearly if not entirely derived from SMC by showing that up to 40% are derived from other sources.

Finally, we provided evidence based on Imatinib intervention studies and delayed knockout of PDGFBR in SMC that maintenance of a SMC- and ACTA2-rich fibrous cap is dependent on sustained PDGFBR signaling. Using SMC-lineage tracing mice, PDGFBR was knocked out in $Myh11^{+}$ cells between 16-18 weeks of WD. BCA lesions were analyzed eight weeks later and showed significantly reduced $ACTA2^{+}$ SMC and collagen content in the fibrous cap. Global antagonism of PDGFBR in SMC-lineage tracing mice by daily Imatinib administration also resulted in significant loss of total SMC and $ACTA2^{+}$ cells in the fibrous cap and caused morbidity and mortality in 100% of the mice within seven days of injections, compared to 0% in the saline control group. Taken together, these intervention studies demonstrate that sustained PDGFBR signaling is required for maintenance of a protective fibrous cap, and antagonism is associated with deleterious effects on the lesion.

These studies demonstrate that radiation inhibits, and PDGFBR signaling in SMC induces their investment and retention within the fibrous cap, where SMC normally augment lesion stability, but that other cell types also play an underappreciated role in contributing to lesion stability. Furthermore, these studies make a case that fortifying the fibrous cap may be a novel therapeutic target to stabilize existing atherosclerotic lesions.

Dedication

To all those
who have enriched my world
for one second
or for 30 years
thank you

And to you, the reader

Acknowledgements

To my mom, dad, sister, and brother. You have made me everything I am.
You are the driving force of my life. You simultaneously push me forward and give me time to get there on my own. There is nothing I could do and nothing I could be without your support. Mom, you taught me to see the creativity in myself and the world. Dad, you made me curious and then made me find the answers to my own questions. Victoria, you are my singular defender and advocate, my enduring companion. Hunter, you make everything infinitely more fun, I adore the person I have had the privilege of watching grow up. To the rest of my family, we are not quiet, we are not reserved, we do not retreat, we are full of sound and fury, we are full of heart. I can stand up, advocate, and fight for what I think is right and important because of you.

Thank you to my friends from middle and high school, college and grad school, home and away; you bring me so much joy. You are all incredible human beings and wonderfully delightful weirdos. Our friendship is an important and rare thing.

To my lab-mates. You are the reason I joined the Owens lab and the reason I came in every day. To Olga, who convinced me to take on this project and who continually provided support throughout this process. To Delphine, Brittany, and Anh for your invaluable friendship, insight, and guidance; without you, this process would have been much less fun, and much less doable. To Ricky thanks for the badinage and for keeping me on my toes. To Daniel, Gabriel, and Vlad for the conversation and for figures and data. To Rupa, Amber, Coral, Becca, Angie, Missy, and Mary for your support and technical expertise. To Saadhana, my intrepid undergrad. And to the rest, for being incredible coworkers, thank you.

To my teachers, past and present, in any capacity. Especially, to Dr. Gary Owens who has made me a better and more deliberate thinker, doer, and scientist. I owe you a great deal.

Thank you in alphabetical order to my committee members Drs. Norbert Leitinger, Marty Mayo, Michael McConnell, and David Wotton for being an indispensable source of support and encouragement.

To Heller Beethoven Monet

Vonnegut Grateful Dead O'Keefe

Rowling Radiohead Kelly

Remember what the dormouse said

(GS)

Table of Contents

List of Abbreviations

ACTA2 (SMαA) – Smooth muscle alpha actin

Apoe – Apolipoprotein E

BCA – Brachiocephalic artery

BMDC – Bone marrow derived cell

BMT – Bone marrow transplant

CD31 (PECAM-1) – Platelet endothelial cell adhesion molecule

CD45 (PTPRC) – Leucocyte common antigen

CD68 – Macrophage antigen

COL – Collagen type

COX2 – Cyclooxygenase 2

CVD – Cardiovascular disease

EC – Endothelial cell

EMT – Epithelial to mesenchymal transition

EndoMT – Endothelial to mesenchymal transition

FGF – Fibroblast growth factor

(F)ISH – (Fluorescence) in situ hybridization

GWAS – Genome-wide association studies

Hif1α - Hypoxia inducible factor 1 alpha

IKKB - inhibitor of nuclear factor kappa B kinase subunit beta

IL1β – Interleukin 1 beta

IL1R1 – Interleukin 1 receptor 1

ISH-PLA – in situ hybridization-proximity ligation assay

KO – Knockout

LDH – Lactate dehydrogenase

LDLR – Low density lipoprotein receptor

LGALS3 (MAC2) – Galectin 3

LRP – low density lipoprotein related receptor

MΦ – Macrophage

MCP1 (CCL2) – Monocyte chemoattractant protein

MKi67 – Marker of proliferation Ki67

MMP – Matrix metalloprotease

MMT – Macrophage to myofibroblast transition

MRTFB – Myocardin-related transcription factor B

MYH11 – Smooth muscle myosin heavy chain

NSTEMI – Non S-T elevated myocardial infarction

OCT – Optical coherence microscopy

PDGF(BR) – Platelet derived growth factor (beta receptor)

PDH – Pyruvate dehydrogenase

ROS – reactive oxygen species

SCA1 – Stem cell antigen 1

SEM – Standard error of the mean

SM22α (TAGLN) – Smooth muscle protein 22 alpha

SMC – Smooth muscle cell

STEMI – S-T Elevation Myocardial Infarction

TCFA – Thin cap fibroatheroma

TEM – Transmission electron microscopy

TGFβ – Transforming growth factor beta

VCAM1 – Vascular cell adhesion protein 1

WD – Western diet

SMC-lineage tracing: Myh11-CreER^{T2} ROSA26 STOP-floxed eYFP, Apoe$^{-/-}$

EC-lineage tracing: VECadherin-CreER^{T2} ROSA26 STOP-floxed eYFP, Apoe$^{-/-}$

BMDC-lineage tracing: tdTomato^{+} BMT (used less frequently: CD45.1; dsRed)

“Lesion” and “plaque” are used interchangeably

Chapter 1

Introduction

I. The Hitchhiker's Guide to Atherosclerosis

Atherosclerosis, an underlying cause of cardiovascular disease (CVD) burden, is a well-studied but still misunderstood disease. It accounts for one in three deaths worldwide (WHO, 2016). Atherosclerosis is a natural consequence of aging, a chronic inflammatory disease of the vasculature induced by the summed effects of genetic and lifestyle risk factors. It is estimated that lesions begin to form in children by the age of ten (Stary, 1989) and has been seen as early as in utero (Napoli et al., 1997). This disease has plagued humans for millennia, having been unearthed in mummies from places like Ancient Egypt and the Americas, with lifestyles and diets as diverse as those of the Aleutian Unangans to the Ancestral Puebloans (Thompson et al., 2013).

In the modern world, basic research and clinical interventions have yielded great advances in our understanding of atherosclerosis and in reducing CVD incidence. This is due in large part to widespread use of therapies like statins and diet and exercise modifications (Ford and Capewell, 2011; Nissen et al., 2006; Pasterkamp et al., 2017b; Ridker et al., 2008). However, unstable plaque rupture is still largely responsible for ischemic stroke and myocardial infarction (MI) related deaths, and despite decades of research, the factors and mechanisms that regulate stability and pathogenesis of existing lesions remain elusive (Bennett et al., 2016).

Post-mortem histopathology of human autopsy specimens provides compelling evidence that plaque stability and susceptibility to rupture are more highly correlated with cellular composition rather than solely size (Stone et al., 2011; Virmani et al., 2000). Specifically, stable plaques are characterized by a thick extracellular matrix (ECM)-rich protective fibrous cap with a high ratio of $ACTA2^{+}$ cells to $CD68^{+}$ cells, presumed to be smooth muscle cells (SMC) and macrophages (MΦ), respectively (Davies et al., 1993; Libby et al., 2011; Virmani et al., 2000). However, and as outlined later, rigorous lineage tracing studies have proved that these markers are insufficient for identifying the origins or functions of cells within the lesion. In fact, we are only beginning to truly understand the composition, abundance, and function of the many different cells within the lesion.

II. A Brief History of Lesion Development and Classification

What follows is an overview of the events that are thought to underlie atherosclerosis lesion development as they relate to SMC biology.

From Healthy Vessel to Fatty Streak

The vessel wall is a highly specialized conduit that senses and responds to changes in blood pressure and composition. It is made up of three general layers, the endothelium, media, and adventitia. The SMC within the medial layer normally function as the contractile apparatus that constricts and relaxes in rhythm with each heart beat and changes due to cardiac output or blood pressure (Figure 1). High levels of cholesterol and other lipids in the blood, due to factors like an imbalanced diet or genetic mutations, along with turbulent blood flow patterns are sensed in the vessel wall.

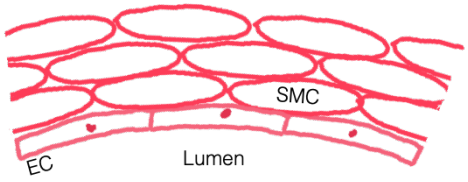

Figure 1

SMC in the healthy vessel are quiescent and reside under the endothelial layer, which lines the lumen.

This causes endothelial cell (EC) activation (expressing VCAM1^{+}) at atheroprone sites along the arteries. In response, circulating white blood cells like leukocytes recognize and accumulate near these activated EC, and thus begins the process of cellular investment into atherosclerosis lesions (Libby et al., 2011). These leukocytes, and particularly monocytes, invest into the sub-endothelial space where they are thought to transition into MΦ (expressing CD68^{+}), and to foam cells, engulfing lipids and debris (called endocytosis). This initial buildup of plaque is called a fatty streak and is represented in histological sections by highly positive staining for lipids and lipid laden foam cells (Figure 2).

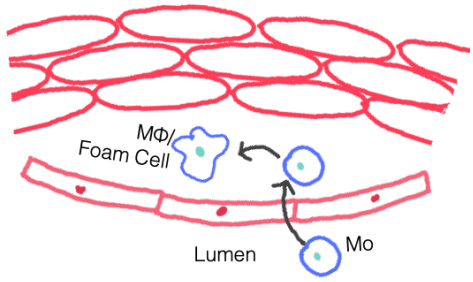

Figure 2

Monocyte accumulation in the sub-endothelial space forms the fatty streak.

Fibroatheroma to Vulnerable Plaque

During this process, the environment changes into a highly inflammatory space, home to multiple cytokines (IL1β, TNF, MCP-1), cholesterol crystals, and apoptotic cells in the necrotic core. This often leads to the formation of a fibroatheroma, characterized by the accumulation of $ACTA2^{+}$ cells, deposition of stiff collagen fibrils and extracellular matrix (ECM), and development of a fibrous cap (Figure 3) that overlies the necrotic core to reduce the risk of rupture (Schwartz et al., 2000; Virmani et al., 2000).

The fibrous cap formation is akin to reinforcing areas of clothing prone to wear and tear like elbow patches on a professor's jacket. Stability is dependent on a higher ratio of beneficial to detrimental cytokines, cells, and ECM. The most vulnerable plaques see a reversal of this ratio, with a larger necrotic core area, increased pathological inflammation, and a thin, ECM-poor fibrous cap (thin cap fibroatheroma, TCFA) (Kolodgie et al., 2001). The fibrous cap of TCFA is subject to high mechanical stress by the blood and is prone to rupture (Ohayon et al., 2008), thus exposing the contents of the lesion to the blood, and leading to formation of a clot at the lesion wound site (Moreno et al., 1996). This clot, when exposed to high blood flow patterns can dislodge, travel downstream to block a smaller artery, and lead to MI or stroke.

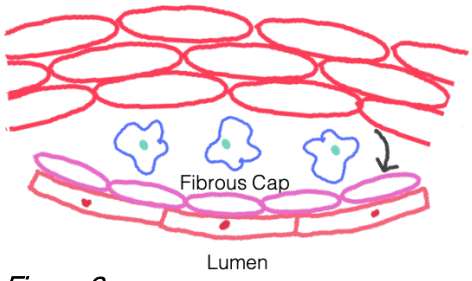

Figure 3

The fibrous cap reinforces the barrier between the lesion contents and blood

Lesion Composition and Atherosclerosis Pathology

For a detailed description of the atherosclerotic plaque classification system, please consult the many published papers on the subject. Below is a summary of a few of the classic criteria that characterize a stable human lesion. Because rupture generally needs to be induced in mouse models of atherosclerosis (Matoba et al., 2013), please note that in mice, we assess the following criteria as "indices of lesion stability".

Classic Criteria of a Stable Lesion, Not Prone to Rupture

1. ACTA2 rich, collagen rich thick (>65μm) fibrous cap
2. Small necrotic core (≤3mm^2)
3. Few CD68$^+$ cells relative to ACTA2$^+$ cells
4. Little calcified nodule presence
5. Little intraplaque hemorrhage

Noticeably absent from the list above is lesion size. In the small-diameter arteries of the heart, this exclusion is primarily due to two factors. The first is that vessels can accommodate the expanding lesion by undergoing positive outward remodeling (Figure 4), in accordance with Glagov's phenomenon. Briefly, the lesion diameter increases in proportion to lesion growth to maintain blood flow (Glagov et al., 1987).

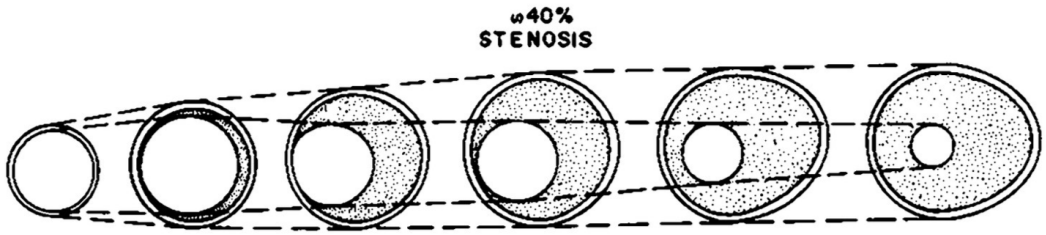

Figure 4

Representation of Glagov remodeling. Lesion develops left to right from a normal artery. Compensatory expansion of the vessel to maintain normal lumen diameter occurs, called positive outward remodeling. Maximum positive remodeling occurs at 40% stenosis, after which, the lumen narrows as lesion expands. Figure from (Glagov et al., 1987).

An occlusive plaque, although sometimes fatal itself, it is easily detectable with proper screening and accordingly can be treated. Small, "clinically silent" lesions therefore arguably pose a bigger threat than large occlusive lesions because they are often not immediately hailed as red flags (Stone et al., 2011). These lesions, often TCFAs, are insidious and rupture, likely due to insufficient amounts of beneficial cellular and extracellular components. However, we have an incomplete understanding of the processes that occur within the environment and mechanisms that maintain lesion stability.

First-line Therapies and Their Relationship to Plaque Stability

Together with lifestyle modifications like cessation of smoking, the advent of anti-hypertensives, anti-thrombotic agents, and lipid lowering drugs have been the best contributors to reduced incidence of vulnerable plaque rupture and subsequent MI or stroke (Endo, 2010; Pasterkamp et al., 2017b). So great was the advent of lipid-lowering drugs that the Nobel prize[1] in Physiology or Medicine was awarded in 1985 "for…discoveries concerning the regulation of cholesterol metabolism". Namely, for the discovery of the LDL receptor, integral for cholesterol re-uptake, the basis of statins. Use of one or more of these therapies has saved countless lives and their effects should not be understated.

However, CVD related events still account for more than 33% of global fatalities and represent a health care cost estimated at about half of one trillion dollars (Khavjou et al., 2016). The reasons for this are varied, notably including that the use of current therapies seems to change the characteristics of plaques that lead to fatalities. This includes the relative rise in non-ST-elevation MI and modest reduction in the percent contribution of plaque rupture to total MI (Pasterkamp et al., 2017b). This is important because statin use is associated with lowered lesion lipids and inflammation and increased collagen content, which are all characteristics I previously described as belonging to a stable plaque. Complications of these lesions seem to arise equally from rupture as from “erosion”, which is thought to be due to sub-endothelial microthrombi and desquamation of the endothelium (Gimbrone Jr and García-Cardeña, 2016; Libby, 2013). Although still unclear, erosion does not seem to destabilize the underlying $ACTA2^{+}$ and ECM-rich layer (Pasterkamp et al., 2017b). Clearly further study is required to identify what constitutes a stable fibroatheroma vs. a statin-modified plaque that can still lead to thrombosis. It is interesting to speculate that the type of ECM or the composition of the cells within the lesion varies substantially between the two (Bentzon and Falk, 2017; Langley et al., 2017). Understanding these mechanisms is vital to protect against MI and stroke.

[1] Thirteen Nobel Prizes have been awarded for research on cholesterol (www.nobelprize.org)

Why Atherosclerosis is Still the Leading Cause of Death Worldwide

1. Despite intervention, risk factors including obesity and Type II Diabetes are increasing worldwide.
2. Despite current therapies, plaque rupture still accounts for the majority of both STEMI and NSTEMI.
3. Current therapies do not specifically focus on stabilizing existing lesions prone to rupture or erosion.

In summary, the findings of histology and imaging studies in human lesions represents the current clinical standard. It is important to reiterate that the bulk of what is known about atherosclerosis plaque rupture as well as the methods for classifying lesions in humans is based on in-vivo imaging techniques (angiography; intravascular ultrasound, IVUS; optical coherence tomography, OCT) (Escaned et al., 1996; Garcia-Garcia et al., 2009; Ivar Seldinger, 2008; Motoyama et al., 2009; Waxman et al., 2009) and histological stains looking at various intra- and extracellular markers that correlate with CVD events (Kolodgie et al., 2004; Virmani et al., 1999; Virmani et al., 2006; Virmani et al., 2000). As will become evident in later sections of this Introduction, these studies provide a solid foundation but an incomplete picture of the origin, function, and complexities of cells within the lesion, including the myriad roles of SMC, our next topic.

III. On the Origin of Smooth Muscle Cells in Atherosclerosis

Historical Identification and (Mis)attribution of ACTA2 to SMC in Atherosclerosis

As briefly stated before, SMC are classically identified within human lesions by expression of ACTA2. This is due in part to the fact that fully differentiated SMC in the vessel media express SMC marker proteins like ACTA2 (and MYH11). However, one of the most important features of SMC biology is that they are not terminally differentiated in the media but exhibit remarkable plasticity in response to disease including atherosclerosis (Alexander and Owens, 2012; Bentzon et al., 2007; Clowes and Schwartz, 1985; Gerthoffer, 2007; Gomez and Owens, 2012). Though multiple mitogens and chemotactic agents have been shown to successfully induce dedifferentiation, proliferation, and/or

migration in culture (Gerthoffer, 2007), neither the mechanisms or cytokines that regulate, nor even the order in which these events occur are clear in the context of atherosclerosis.

Considering the fantastic plastic capabilities of SMC in atherosclerosis (Owens, 1995; Wamhoff et al., 2004), there arises confusion as to how one defines a SMC in the lesion: is it manifestation of functions like collagen synthesis and expression of markers like ACTA2 regardless of origin, or is the label restricted to cells of SMC origin? For ease of the reader, I will differentiate whenever possible between SMC derived cells (that can be either ACTA2^{+} or $^{-}$), non-SMC derived ACTA2^{+} cells, and specifically note when cells are historically identified as “SMC” based on marker protein expression.

Rigorous Lineage Tracing is Essential to Correctly Identify SMC in Mouse Lesions

The presence of SMC-derived cells in the lesion was able to be confirmed only with the advent of rigorous SMC-lineage tracing models in mice and humans when just prior to the start of my PhD candidacy, our lab developed the most rigorous SMC-lineage tracing mouse model. This is predicated on the fact that mature SMC in healthy animals are the only known cells that express MYH11 (Madsen et al., 1997; Miano et al., 1994; Nagai et al., 1988; Rovner et al., 1986). Thus, MYH11-driven conditional CreER^{T2} (Myh11-CreER^{T2} ROSA26 STOP-floxed eYFP) allows for specific and faithful labeling of mature SMC after tamoxifen if administered in healthy animals (Gomez et al., 2013). The complex genetics of the mouse coupled with the timing of tamoxifen injections prior to atherogenesis means that any eYFP^{+} lineage tagged cell in the lesion must have originated from a previously tagged eYFP^{+} cell.

This SMC-lineage tracing mouse is the gold standard for SMC biology. By using this SMC-lineage tracing model, our lab and subsequently others showed that about 30-70% of total lesion cells are derived from a pre-existing mature SMC (Chappell et al., 2016; Shankman et al., 2015). We also showed that about 80% of eYFP^{+} SMC downregulate marker protein expression within the brachiocephalic artery (BCA) lesions of the mouse (Shankman et al., 2015), thereby reinforcing the notion that it is nearly impossible to identify SMC in lesions solely by staining for MYH11 or ACTA2.

Identifying SMC in Human Lesions

We are also able to confirm the presence of phenotypically modulated (e.g. ACTA2^{-} MYH11^{-}) SMC in human lesions, albeit not quantitatively, using a novel method developed in our lab combining in situ hybridization with proximity ligation assay (ISH-PLA). This technique is predicated on the fact that SMC but not non-SMC can express and retain certain epigenetic markers including H3K4me2 on the MYH11 promoter even after dedifferentiation (McDonald et al., 2006). ISH-PLA labels SMC with about 70% efficiency in atherosclerosis, and we have provided evidence of PLA^{+} detection in SMC that have downregulated their characteristic marker proteins in both human and mouse lesions (Gomez et al., 2013).

SMC Populate the Lesion in by Clonal Expansion

SMC in the media are derived from multiple progenitor sources that form a mosaic of differentiated cells that become contractile vascular SMC (Benditt and Benditt, 1973; Chung et al., 1998; Misra et al., 2018; Schwartz and Murry, 1998). From this mosaic, it has been established that medial SMC give rise to the lesion SMC. Although decades prior to rigorous lineage tracing models, evidence of possible SMC clonality was observed in human lesions through detection of X-linked inactivation of the glucose-6-phosphate dehydrogenase enzyme presence in micro-dissected lesion samples. Briefly, autopsy sections of female patients showed that there was a higher percentage of cells in the fibrous cap with a single enzyme isotype than in the underlying media, which nearly always contained an equal mixture of both isotypes (Benditt and Benditt, 1973). Since the lesion contains multiple other cell types like MΦ or EC, it is not possible to be certain the source of sampled cells. Recent use of multi-color SMC-lineage tracing in mice additionally showed that lesion SMC were derived from clonal expansion of a small number of medial SMC. Importantly, any particular SMC clone was able to contribute to both the lesion cap and core and to give rise to many different SMC-derived phenotypes including SM-derived MΦ or ACTA2^{+} cells (Chappell et al., 2016; Feil et al., 2014; Jacobsen et al., 2017; Misra et al., 2018). Yet, how SMC clonal expansion is regulated in atherosclerosis is still a question (Gomez and Owens, 2016). Studies have started to elucidate these

regulatory mechanisms, including evidence that BM-derived integrin b3 is required for clonality (Misra et al., 2018).

Non-SMC Derived ACTA2^{+} Fibrous Cap Cells: A Rose by Any Other Name?

The ACTA2^{+} cells in the lesion are generally thought to be nearly entirely derived from SMC. However, it is also postulated that they come from multiple sources like cells in the adventitia (Hu et al., 2004; Kramann et al., 2016; Sartore et al., 2001), circulating BM cells (Sata et al., 2002), or EC (Beranek and Cavarocchi, 1990; DeRuiter et al., 1997).

It has been shown that non-SMC including MΦ and EC within lesions can express SM markers like ACTA2 or SM22a in mice and humans (Gomez and Owens, 2012; Sata et al., 2002). Using Y-chromosome FISH, lesions from human patients who received cross gender bone marrow transplant demonstrated that ~10% of the BMDCs that accumulate within coronary lesions co-express ACTA2 and CD68 (Caplice et al., 2003), which suggests they have undergone MΦ to mesenchymal transition (MMT). Further, approximately 50% of foam cells within human lesions have been shown to co-stain with ACTA2 (Allahverdian et al., 2012), although it is unclear if this is evidence of MMT or phenotypic switching of another cell type. These mesenchymal transitions may be mediated by TGFβ signaling, which has been shown to induce ACTA2 expression in SMC, MΦ, and EC (Hautmann et al., 1999; Medici et al., 2011; Ninomiya et al., 2006; Stewart et al., 2009).

Additionally, various EC-lineage tracing studies in mice show that approximately 10% of EC undergo endothelial to mesenchymal transition (EndoMT) in a TGFβ and bFGF dependent manner (Chen et al., 2012), where they express both EC-markers like CD31 and SM-markers. Keeping the caveat about marker protein identification of phenotypically modulated cells in mind, in human lesions, cells that co-stain with EC and SMC markers are considered to have undergone EndoMT (Chen et al., 2015; Evrard et al., 2016). As these studies represent discrete points in time, it is unknown what proportion of the ACTA2^{+} cells are derived from such mesenchymal transitions and if they are beneficial or detrimental to human lesion stability.

At this point, I would like to reiterate that use of classic marker protein staining (ACTA2 and CD68) to determine cell identity within lesions formed the basis of

classification of cells and our understanding of human lesion development. However, and this is an important qualification, cell-specific lineage tracing experiments have recently shown that these markers alone are unreliable for identifying the origins and abundance of cells within lesions. Understanding a cell's function and its contribution to pathology is of utmost importance when considering the well-being and continued survival of patients, and may illuminate some limitations of current therapies. With this consideration, I will focus the next sections on elucidating the role of cells of SM-origin within the lesion, including how they might differ from non-SMC derived ACTA2$^+$ cells.

IV. War and Peace: How Smooth Muscle Cell Fate Regulates Stability

As the lesion develops, mature SMC from the media accumulate in the lesion core and fibrous cap. Within the lesion, we have determined that almost half of SMC express markers of other cell types including: myofibroblast (MF) cells (12%, ACTA2, PDGFBR), stem cells (7%, SCA1), or MΦ (30%, LGALS3, F4/80, CD11b) (Chappell et al., 2016; Feil et al., 2014; Gomez et al., 2013; Shankman et al., 2015). Although the prevailing dogma is that the principal role of SMC in atherosclerosis is protective, maintaining the fibrous cap and preventing rupture (Libby et al., 2011), certain SMC transitions have been associated with detrimental effects on the lesion.

Evidence that SMC Phenotype Affects Function and Lesion Stability

The good

A general consensus between various SMC-specific gene KO studies in SMC is that more ACTA2$^+$ SMC in the lesion is generally associated with increased collagen and decreased inflammation. One example demonstrates that OCT4 plays a protective role in SMC, directing them to populate the lesion (Cherepanova et al., 2016). Genetic KO of OCT4 in SMC-lineage tracing mice fed WD for 18 weeks showed that OCT4 plays a role in SMC investment into the fibrous cap and ACTA2 expression. In conjunction, ex vivo explants and in vitro migration assays showed a marked inhibition of SMC migration in OCT4 KO compared to OCT4 WT SMC. It is important to note that this KO study represents the net effect of loss of a single gene specifically in SMC during atherogenesis and

secondary changes, rather than direct effects of SMC alone. However, this data supports the classic idea of a stable plaque: abundant ACTA2^{+} SMC in a thick fibrous cap.

The Bad

Based on studies of SMC-KLF4 KO, we suggest that KLF4 expression in SMC contributes to the detrimental SMC phenotypes in the lesion. Additionally, KLF4 was recently identified as a human risk factor locus by GWAS, leading to increased CAD incidence (van der Harst and Verweij, 2018). Interestingly, KLF4 seems to be rate-limiting for the SMC transition to a MΦ marker^{+} foam cell state, as indicated by presence of lipid vacuoles in vivo. SMC-KLF4 KO likewise resulted in reduced bead uptake in cultured SMC, a surrogate for phagocytosis. Phagocytosis by SMC in a MΦ-like state was demonstrated in vivo by engulfment morphology by TEM (Shankman et al., 2015). The notion that SMC-derived MΦ are not capable of fully recapitulating proper debris clearing functions is supported by additional studies that may in part explain the detrimental pathology observed (Vengrenyuk et al., 2015). This is corroborated in human lesions showing SMC-derived MΦ (defined as CD45^{-} ACTA2^{+} CD68^{+}) do not effectively export cholesterol through ABCA1-dependent mechanisms (Allahverdian et al., 2014).

And the Ugly

In lesions that lack SMC there are associated detrimental effects overall on stability. In SMC-OCT4 KO mice there are fewer ACTA2^{+} fibrous cap cells, increased lipids, and increased intraplaque hemorrhage (Cherepanova et al., 2016). Additional studies looking at SMC KO of either IL1R1 (Gomez et al., 2018) or COL15A1 (Durgin et al., 2017) resulted in small lesions devoid of collagen and a fibrous cap after 18 weeks of WD. These lesions are correspondingly abundant in MΦ, which taken together is indicative of a vulnerable plaque phenotype. This suggests these factors play a critical role in seeding and formation of a SMC- and ECM-rich lesion.

To elucidate the effect of loss of SMC in advanced lesions, studies specifically ablated SM22a^{+} cells[2] via diphtheria toxin administration (SM22a-hDTR). These lesions exhibited multiple indices of plaque destabilization including reduced collagen, a thin fibrous cap, and increased cellular debris (Clarke et al., 2006). Together, these studies show that SMC indeed play a functional role in regulating lesion stability because selective loss of SMC themselves, or SMC-specific loss of the genes described above, results in detrimental alterations of multiple lesion parameters.

The preceding results provide incontrovertible evidence that SMC play a critical direct functional role in regulating lesion pathology and increasing beneficial SMC populations represents a viable heretofore untapped therapeutic target. The fact that SMC can not only play a beneficial role in lesion pathology per long-standing dogma, but can also play a detrimental role depending on the nature of their phenotypic transitions, further confounds our understanding of the factors that contribute to lesion stability. However, there are a number of remaining questions including what the factors and mechanisms are that stabilize the lesion, and specifically, the SMC to MF transitions thought to strengthen the fibrous cap.

Modulating SMC Phenotype by Targeting Inflammation

Considering the general chronic inflammatory nature of atherosclerosis despite statin treatment and lifestyle interventions, a focus has been on globally suppressing inflammation to reduce the incidence of atherosclerosis. Studies using genetic KO of IKKB in an SM22a-Cre; LDLR$^{-/-}$ mouse model showed that IKKB in SMC (as compared to Cre-less, IKKB$^{F/F}$, LDLR$^{-/-}$ controls) increases pathological inflammation. This study showed loss of IKKB reduced inflammatory cytokines (MCP-1, IL1β, COX2, VCAM1) in the vascular wall and reduced lesion area (Sui et al., 2014). Further, KO of IKKB was associated with resistance to diet induced obesity and metabolic disorders. This suggests that SMC in an inflammatory state (characterized as secreting multiple pro-atherogenic cytokines)

---

[2] SM22a is a commonly used but less rigorous method of targeting SMC lineage as it also is expressed in fibroblasts and cardiac cells

may have detrimental effects on the lesion itself, and on the systemic factors that lead to atherosclerosis. Recall also that SMC-IL1R1 KO resulted in lesions resembling a vulnerable plaque (Gomez et al., 2018)

Our lab further assessed the role of IL1 signaling by testing if global suppression of inflammation by antibody antagonism of IL1β in mice with established atherosclerotic lesions resulted in beneficial changes in the lesion. Surprisingly, anti-IL1β treatment reduced multiple indices of stability including collagen deposition and fibrous cap thickness, and showed a decrease in SMC but an increase in MΦ proliferation (Gomez et al., 2018). That is the opposite of the desired effect of a treatment, namely, of increased proliferation and/or recruitment of SMC from the media, and maintenance of a fibrous cap with abundant ACTA2^{+} cells and ECM deposition. These studies, along with results of the CANTOS clinical trial (Ridker et al., 2017a), suggest that global suppression of IL1β in the context of persistent hyperlipidemia induces a false sense of inflammation resolution with associated lesion destabilization. Thus, a critical need remains for additional therapies and strategies to reduce adverse outcomes of atherosclerosis plaque rupture.

Embryonic Origin Affects SMC Function

There are at least eight distinct embryonic origins of SMC within the vasculature (Figure 5, selected vessels), which seems to result in differential susceptibility to disease and response to stimuli (Madura et al., 1996; Majesky, 2007; Topouzis and Majesky, 1996). For example, initial derivation of SMC from the neural crest (NC) but not from the mesoderm seems to require TGFβ and MRTFB dependent differentiation (Li et al., 2005), and mature SMC from the NC but not the mesoderm increase DNA synthesis in vitro in response to TGFβ stimulation (Gadson Jr et al., 1997; Jaffe et al., 2012; Topouzis and Majesky, 1996).

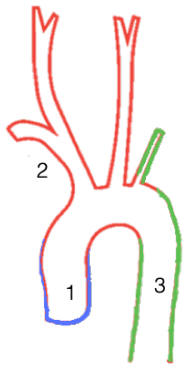

Figure 5

SMC in vessels of the aortic outflow tract are derived from three (of eight currently known) distinct origins: the (1) secondary heart field, (2) neural crest and (3) mesoderm.

In disease, these intrinsic differences in SMC origin manifest as a susceptibility of certain vascular beds to develop calcification (Leroux-Berger et al., 2011) or aneurysm (Jaussaud et al., 2013), the latter of which often occurs at the boundary between two

distinct origins. Evidence SMC origin plays a role in atherosclerosis lesion development is given using homograft transplants of atheroprone (abdominal aorta) and atheroresistant (thoracic aorta) arteries. The transplanted atheroresistant artery into the prone area did not develop atherosclerosis, and vice versa (Haimovici and Maier, 1964). In human lesions, distinctive lesion development and presentation patterns were observed corresponding to vascular bed assessed (DeBakey and Glaeser, 2000). Together, these studies show that SMC from different origins exhibit distinct atherosclerosis responses, independent of hemodynamics and systemic risk factors.

To summarize, SMC can play a beneficial or detrimental role in lesion pathology, which may inform future therapies. However, defining the direct functional roles of SMC and non-SMC on lesion pathology remains a challenge. Outlined below are a number of unresolved questions that remain.

Critical Unresolved Questions that Remain:

1. What are the origins of the ACTA2^{+} fibrous cap cells and does this impact their functional properties and in particular, ECM production and the overall stability of the lesion?
2. What are the mechanisms and factors that promote formation and maintenance of a protective fibrous cap?
3. How can we develop novel therapies to stabilize the lesion and prevent rupture in humans?

V. The Importance of PDGFBR in Atherosclerosis

PDGF and its cognate receptor tyrosine kinase (PDGFRs) were discovered and isolated from platelets in the 1970s-1980s with the idea that in vascular disease, SMC respond to the growth promoting factors released from platelets that have adhered to regions of endothelial damage (Bowen-Pope and Raines, 2011; Ross, 1986). Platelets are not the only source of PDGF however, with it being synthesized by EC and MΦ, and PDGF receptors being expressed on stromal cells like SMC and fibroblasts. There are four isoforms of PDGF (A-D) that bind and activate the receptors (α and β),[3] with distinct

[3] The beta form of the receptor is written from here on out in my preferred way: PDGFBR

but overlapping effects in SMC. For the purposes of this thesis, we are going to focus on PDGFBB, the most studied ligand of PDGFBR. Although PDGFDD plays a very similar role to PDGFBB (Thomas et al., 2009) and is specific to PDGFBR (Bergsten et al., 2001), it is not nearly as well characterized.

PDGFBR Regulates Vascular Development and Repair

PDGFBR signaling is highly evolutionarily conserved, especially its role in cardiovascular development and directed migration of mesenchymal cells like SMC and pericytes (Hoch and Soriano, 2003). Pericytes are specialized SMC within the basement membrane of EC in capillaries (Rouget, 1874). During development, PDGBB is secreted by EC and acts in a paracrine manner to recruit SMC or pericytes to the site of blood vessel development (Hellstrom et al., 1999; Lindblom et al., 2003). Global conventional PDGFBB or PDGFBR KO is embryonic lethal due to multiple defects in the development of the cardiovascular system, which are likely secondary to SMC hypoplasia (Andrae et al., 2008; Hellstrom et al., 2001; Leveen et al., 1994; Lindahl et al., 1997; Soriano, 1994).

There is a well-documented role of PDGF activation of PDGFBR in disease, including being necessary for SMC expansion to distal arteries in pulmonary hypertension (Sheikh et al., 2015), to induce SMC-mediated neointima formation after vascular injury (Clowes et al., 1983; Jawien et al., 1992), and in wound healing where PDGFBB exerts pleotropic effects during all stages and on multiple cell types involved in the process (Pierce et al., 1991).

Evidence Supports PDGFBR as a Target for SMC Function in Atherosclerosis

Decades of culture studies testing the action of PDGFBB on SMC show it is a potent mitogen and chemotactic agent, mediating SMC growth and migration as well as inducing matrix synthesis (Amento et al., 1991; Blank and Owens, 1990; Grotendorst et al., 1982). Importantly, these are all capabilities one would want to augment in order to maintain a SMC-rich fibrous cap within lesions. Based on localization and electron microscopy studies, it was presumed that SMC that accumulate within the lesion were responsible for the matrix deposition within atherosclerotic lesions (Ross, 1971; Ross and Klebanoff, 1971). Additionally, studies by our lab have shown that reducing SMC matrix

production capabilities (IL1β/Col15a1) and/or migratory or modulatory state (KLF4/OCT4) can influence lesion development and stability metrics (Cherepanova et al., 2016; Durgin et al., 2017; Gomez et al., 2018; Shankman et al., 2015). However, no one has tested if PDGFBR signaling is necessary to form and maintain an ACTA2^{+} SMC- and ECM-rich fibrous cap.

Why Have Previous Studies Not Already Looked at Directly Augmenting SMC in Advanced Atherosclerosis?

In spite of highly compelling human histological data correlating lesions containing a thick ACTA2^{+} fibrous cap to stability, there is a misguided pervasive dogma in the field that inhibiting SMC migration and proliferation would somehow induce beneficial changes in lesion pathogenesis. This rationale is likely inappropriately extrapolated from studies of restenosis after vascular injury where SMC accumulation in the neointima is maladaptive (Ferns et al., 1991; Jawien et al., 1992). Previous studies have largely focused on antagonizing PDGFBR in order to reduce SMC proliferation and thus atherosclerosis burden, however, we postulate that this strategy would have detrimental effects on the lesion as a whole.

Notably, one study had attempted to augment PDGFBR in an atherosclerotic setting. Researchers artificially overexpressed a constitutively active mutant PDGFBR in SM22a^{+} cells throughout embryonic and adult development, which was associated with multiple vascular abnormalities and exacerbation of atherosclerosis (He et al., 2015).[4] This study indicates that lifelong uncontrolled PDGFBR activation results in multiple vascular defects, but does not tell us its normal role in atherosclerosis and fails to test if augmenting PDGFBR signaling in advanced lesions would result in beneficial effects.

Antagonism of PDGFBR Signaling in Atherosclerosis

Multiple previous studies tested the effects of loss of PDGFBR signaling on atherosclerotic lesions. Global chemical antagonism of PDGFBR or hematopoietic loss of the

---

[4] Interestingly, these studies demonstrate a model of coronary vessel atherosclerosis, an effect not often seen in mice

PDGFBB ligand ($PDGFBB^{-/-}$ chimeras) during lesion development generally resulted in reduced ECM in $Apoe^{-/-}$ mice, greater numbers of $LGALS3^{+}$ MΦ in the lesion, and led to delayed development of a thick fibrous cap (Kozaki et al., 2002). The $PDGFBB^{-/-}$ chimeras did not show a difference in fibrous cap thickness or in ECM accumulation when the study was extended by 10 weeks, which could be due to delayed SMC responses, or to other cell types secreting ECM and contributing to the fibrous cap in the absence of a SMC response.

Similarly, PDGFBR specific antibody treatment in animals during the second half of lesion development resulted in the reduction of $ACTA2^{+}$ cells by 80% and lesion area by 67% in the aortic root (Sano et al., 2001). These animals were treated between 12-18 weeks of WD, which roughly corresponds to the time that advanced lesions begin to form in mice. This suggests that PDGFBR blockade affects the development of ACTA2-rich lesions, consistent with fibroatheroma. However, none of these previous studies have specifically tested if PDGFBR signaling in SMC is required for their investment into the fibrous cap, or whether global inhibition of PDGFBR signaling in mice with established advanced atherosclerosis is associated with detrimental or beneficial changes in lesion cellular composition or indices of plaque stability.

Remaining Questions:

1. What is the effect of PDGFBR signaling on SMC vs. non-SMC in lesion development and pathology?
2. Does global antagonism of PDGFBR in developed lesions result in a less stable fibrous cap and lesion that is prone to rupture?
3. How can this information be used to develop better therapies to stabilize atherosclerotic lesions?

VI. The Strange Case of Cancer and CVD

Genetic and environmental drivers of cancer and CVD are increasingly recognized as being linked, as are anti-cancer therapies and development of CVD. Clinically, it is well-documented that anti-cancer therapies often contribute to atherosclerosis

development or pathology. Receptor tyrosine kinase inhibitors including those that target PDGFBR like Imatinib (Gleevec® Novartis) are often associated with developing occlusive artery disease (Giles et al., 2013; Kim et al., 2013). Additionally, multiple reports and clinical observations show that patients who receive radiotherapy for cancer have a dose-dependent increase in developing CVD or experiencing MI (Darby et al., 2003; Mertens et al., 2008; Weintraub et al., 2010). Furthermore, in mouse models of atherosclerosis, radiation resulted in acceleration of lesion development and exacerbation of existing lesions, multiple decreased indices of lesion stability including reduced collagen content, increased MΦ staining, and increased intraplaque hemorrhage (Gabriels et al., 2014; Schiller et al., 2001; Stewart et al., 2006).

This suggests that there is some overlap between the molecular pathways that govern both diseases and highlights the need to evaluate CVD risk in patients receiving treatment for cancer. To this end, studies in this thesis evaluated the effect of radiation and the anti-PDGFBR antagonist Imatinib in murine atherosclerosis. Both of these treatments were associated with surprising changes in lesion content and/or pathology.

VII. Précis

Through SMC-specific KO of PDGFBR or lethal irradiation in long term WD fed SMC-lineage tracing Apoe$^{-/-}$ mice, we observe the following surprising and novel results.

First, PDGFBR signaling in SMC is required for investment into lesions in that SMC were almost completely absent within advanced atherosclerotic BCA lesions after SMC-PDGFBR KO. Loss of SMC was similarly observed in lesions of lethally irradiated mice.

Second, studies show that SMC normally make up about 60-70% of the ACTA2^{+} fibrous cap cells in advanced BCA lesions, and EndoMT and MMT marker^{+} cells make up the bulk of the remaining cells.

Third, after 18 weeks of WD, there were observed reductions in indices of stability in lethally irradiated mice, but not in SMC PDGFBR KO mice, where it seems EndoMT and MMT can contribute to stability.

Fourth, ACTA2^{+} fibrous cap cells derived from EndoMT and MMT can only transiently compensate for loss of SMC in SMC-PDGFBR KO mice as we observed reduced indices of plaque stability following longer term WD despite sustained ACTA2 expression.

Fifth, we show that global inhibition of PDGFBR signaling in Apoe$^{-/-}$ mice with advanced lesions was associated with significantly decreased SMC and ACTA2^{+} cells overall. Further, Imatinib treatment was associated with 100% mortality. These results provide novel evidence that SMC are normally the major and most effective, but not the only, cell type responsible for formation of the protective ACTA2 rich fibrous cap, and that this process is dependent on PDGFBR signaling.

Sixth, transcriptional profiling of lesion cells and energetic assessments of SMC are beginning to uncover the functionality of SMC within the lesion, and of the lesion as a whole.

Chapter 2

Irradiation Abolishes Smooth Muscle Investment into Vascular Lesions in Specific Vascular Beds

Alexandra A.C. Newman,* Richard A. Baylis,* Daniel L. Hess, Steven D. Griffith, Laura S. Shankman, Olga A. Cherepanova, and Gary K. Owens

*equal contribution

Published: JCI Insight August 9, 2018 (Cover article)

I. Abstract

The long-term adverse effects of radiotherapy on cardiovascular disease are well documented. However, the underlying mechanisms responsible for this increased risk are poorly understood. Previous studies using rigorous smooth muscle cell (SMC) lineage tracing have shown abundant SMC investment into atherosclerotic lesions, where SMCs contribute to the formation of a protective fibrous cap. Studies herein tested whether radiation impairs protective adaptive SMC responses during vascular disease. To do this, we exposed SMC lineage tracing (Myh11-ERT2Cre YFP^{+}) mice to lethal radiation (1,200 cGy) followed by bone marrow transplantation prior to atherosclerosis development or vessel injury. Surprisingly, following irradiation, we observed a complete loss of SMC investment in 100% of brachiocephalic artery (BCA), carotid artery, and aortic arch lesions. Importantly, this was associated with a decrease in multiple indices of atherosclerotic lesion stability within the BCA. Interestingly, we observed anatomic heterogeneity, as SMCs accumulated normally into lesions of the aortic root and abdominal aorta, suggesting that SMC sensitivity to lethal irradiation occurs in blood vessels of neural crest origin. Taken together, these results reveal an undefined and unintended variable in previous studies using lethal irradiation and may help explain why patients exposed to radiation have increased risk for cardiovascular disease.

II. Introduction

Since its introduction in 1951, radiation exposure followed by bone marrow transplantation (BMT) has become a key technique for both medical practice and biomedical research (Lorenz et al., 1952). Indeed, this procedure has been used in over 100,000 basic science papers and stem cell transplantation has been used to treat over a million patients (Gratwohl et al., 2015). Although it has greatly improved the survival rates for multiple malignancies, exposure to levels of radiation necessary to deplete the bone marrow have long-term side effects including a profound increase in cardiovascular disease (CVD). Indeed, pediatric cancer patients, who are often treated with radiotherapy or BMT, are seven times more likely to die from a cardiovascular complication, making CVD the leading cause of non-malignant death in these patients (Mertens et al., 2008). Further, women treated with radiotherapy for breast cancer have a dose-dependent increase in CVD risk, which was shown to be independent of traditional risk factors (Darby et al., 2003). This has motivated extensive research on the cardiovascular effects of radiation in mouse models of atherosclerosis. Consistent with the clinical data, multiple studies have shown that lethal irradiation results in decreased indices of atherosclerotic lesion stability including reduced collagen content, increased macrophage marker staining, and increased intraplaque hemorrhage (Gabriels et al., 2014; Schiller et al., 2001; Stewart et al., 2006). However, there is a high level of unexplained variability in the literature as to the effect of radiation exposure on different vascular beds. For example, lesion size has been shown to increase in the aortic sinus yet decrease in the aortic arch (Schiller et al., 2001). Although there are many possible causes for this heterogeneity, we hypothesize that it is due in part to differences in the sensitivity of SMC to radiation in different vascular beds.

A critical role for SMC in atherosclerosis has become increasingly clear due in large part to the development of rigorous SMC lineage tracing and simultaneous conditional gene knockout studies in long term Western diet (WD) fed $Apoe^{-/-}$ mice (Cherepanova et al., 2016; Gomez et al., 2013; Shankman et al., 2015). Briefly, studies have shown that lesion SMC are derived from a subset of mature $Myh11^{+}$ medial SMC

that clonally expand to populate the lesion (Chappell et al., 2016; Jacobsen et al., 2017; Murry et al., 1997). Further, >80% of the SMC within atherosclerotic lesions lack expression of characteristic SMC markers, and of these, nearly 50% have activated markers of macrophages (MΦ), mesenchymal stem cells, or myofibroblasts, and thus would have been missed or misidentified in previous studies (Shankman et al., 2015). Moreover, SMC-specific knockout studies have shown that SMC can have key beneficial or detrimental effects on lesion pathogenesis depending on the nature of their phenotypic transitions (Cherepanova et al., 2016; Durgin et al., 2017; Gomez et al., 2013; Shankman et al., 2015). For example, Klf4-dependent transitions, including formation of SMC-derived MΦ-marker+ foam cells exacerbated lesion pathogenesis while Oct4-dependent transitions (Cherepanova et al., 2016) were protective, including being critical for investment of SMC into the fibrous cap. The studies herein examine the effects of lethal irradiation to the contribution of SMC to atherosclerosis lesion pathology and surgically induced neointima formation.

III. Results

To determine the effect of lethal gamma radiation on SMC during atherosclerosis, we injected SMC lineage tracing Myh11-ERT2Cre ROSA-STOP-eYFP Apoe$^{-/-}$ (SMC-YFP, Apoe$^{-/-}$) mice with tamoxifen from 6-8 weeks of age (Figure 1A). Mice were then exposed to whole body lethal radiation (1200cGy) using a Cesium-137 irradiator with subsequent BMT at 9 weeks of age, followed by 6 weeks of rest to allow for bone marrow engraftment. Non-irradiated non-BMT littermates were used as controls. We placed mice on Western diet (WD) for 18 weeks to induce atherogenesis (Figure 1B). Flow cytometric analyses of blood at the time of harvest showed >95% bone marrow engraftment (S. Figure 1). Vessels were harvested and analyzed for indices of lesion stability and cellular composition. Of major significance, we found that SMC failed to accumulate in any of the brachiocephalic artery (BCA) lesions from lethally irradiated mice, as assessed by YFP staining at multiple locations along the length of the BCA (Figure 2 B,C). In contrast, in the control mice, >85% of the BCA lesions had YFP^{+} SMC accumulation, consistent with the hundreds of SMC-YFP, Apoe$^{-/-}$ mice previously analyzed in our lab and others (Figure 2 A,C) (Chappell et al., 2016; Cherepanova et al., 2016; Durgin et al., 2017; Gomez et al., 2013; Shankman et al., 2015). Furthermore, to assess the functional consequences of SMC loss in the BCA, we found that BCA lesions from irradiated mice exhibited decreases in multiple induces of lesion stability including: significant increases in both intraplaque hemorrhage and necrotic core area, and a significant reduction in collagen content (Figure 2 D,E,F). However, despite reductions in multiple indices of lesion stability, we found that vessel morphology including EEL and lesion area was not significantly changed (Figure 2 G,H). Importantly, these observations were consistent despite using multiple bone marrow donor lines including from CD45.1, tdTomato, or dsRed mice (see methods, Figure 1 B). Taken together, radiation induces loss of SMC accumulation and results in detrimental effects on multiple indices of lesion stability within BCA lesions, highlighting an unexpected and highly significant side effect of lethal irradiation.

To determine if other vascular beds exhibited a similar loss of SMC accumulation, we examined multiple vascular locations, including the aortic arch, aortic root, and abdominal, renal, and iliac arteries. Similar to our observations in the BCA, lesions in the aortic arch of all irradiated animals lacked SMC accumulation (Figure 3 A,B,G). However, all other vascular beds showed similar SMC accumulation in both the irradiated and control mice including in the aortic root (Figure 3 C,D,H) and the abdominal aorta (Figure 2E,F,I), renal and iliac arteries, suggesting that the SMC of aortic arch and BCA are uniquely sensitive to radiation. Of interest, SMC from these two sites, unlike any of the other vascular sites tested, are derived from the neural crest (Majesky, 2007).

To determine if ionizing radiation has a direct effect on the vascular SMC that could explain their absence in BCA lesions, we harvested vessels from mice at 1, 4, and 7 days post irradiation and BMT, and from age-matched non-irradiated controls (Figure 1C). Of major interest, lethal irradiation resulted in significantly increased YFP^+ $TUNEL^+$ cells in the BCA vessel media at 1 and 4 days post irradiation, which decreased to the level of the control by 7 days (Figure 4 A,B). Surprisingly, increased YFP^+ $TUNEL^+$ staining was not observed in the aortic root, coronary or pulmonary vessels (Figure 4 C,D,E), suggesting that the medial $Myh11^+$ SMC from various vascular beds have different susceptibilities to radiation-induced DNA double strand breaks. In the BCA media, the increased YFP^+ $TUNEL^+$ staining was not associated with a decrease in the number of YFP^+ cells (Figure 4 F). To determine if the double strand DNA breaks were associated with increased SMC apoptosis, we assessed the percentage of YFP^+ cleaved $Caspase3^+$ cells in the BCA and found >1% apoptotic SMC at day 1 and 4 (Figure 4 G), suggesting that the vast majority of $TUNEL^+$ SMC did not undergo subsequent apoptosis. At the time of radiation exposure, we injected mice with a single pulse of BrdU to assess SMC proliferation directly after radiation. Consistent with the literature, we found that very few medial SMC proliferate in the absence of vascular injury, and even after irradiation, the maximum percent of proliferating YFP^+ cells was <2% (Figure 4 H), which was confirmed by Ki67 staining. Thus, SMC within the BCA appear to be uniquely susceptible to gamma radiation demonstrated by increased TUNEL staining, which suggests that part of the effect

of lethal irradiation-induced loss of SMC accumulation in lesions is intrinsic to SMC in this vascular bed.

To determine if the loss of YFP^+ SMC accumulation was unique to atherosclerosis, we performed two models of surgically-induced vascular injury, carotid ligation and femoral injury, on Myh11-ERT2Cre, ROSA26 STOP-flox $eYFP^{+/+}$ with and without Apoe knockout (SMC-YFP) following irradiation and BMT. Consistent with results in the BCA and aortic arch, we observed a profound reduction in SMC investment into neointimal lesions resulting from carotid ligation (Figure 1 D, Figure 5). Indeed, none of the irradiated mice demonstrated SMC investment into the neointima (Figure 5 B,C), whereas 90% of the control mice had significant YFP^+ SMC investment (Figure 5 A,C). However, SMC accumulation in the neointima induced by femoral injury showed SMC accumulation regardless of radiation exposure. These data are consistent with our results in atherosclerosis, indicating that radiation has different effects on SMC accumulation in different vascular beds. Moreover, these additional models indicate that the observed results were not a function of the mouse age, diet, type of vascular insult, BMT donor, or hyperlipidemia.

IV. Discussion

Taken together, the present study reveals that an unintended and highly unexpected consequence of lethal irradiation is a profound impairment of SMC accumulation in vascular lesions that form in the BCA, aortic arch, and carotid artery. It is interesting to speculate based on the vascular patterning of these effects that they are due to differences in the embryologic origin of the SMC. Indeed, fate mapping studies have revealed that SMC develop from at least eight unique embryologic origins, which appears to impact the behavior of the mature SMC (Majesky, 2007). For example, TGFβ stimulation of neural crest (NC)-derived cultured SMC results in increased DNA synthesis while mesoderm-derived SMC show the opposite response (Gadson Jr et al., 1997; Jaffe et al., 2012; Lee et al., 2012; Topouzis and Majesky, 1996). Loss of SMC accumulation in vascular lesions is highly consistent with vessels where SMC are derived from the NC. This is perhaps best illustrated by the profound effect of whole body gamma radiation in the aortic arch but no effect in the adjacent aortic root.

Although studies provide compelling evidence that investment of NC-derived SMC within lesions is lost following lethal irradiation, results do not distinguish if this is driven by direct intrinsic effects of radiation on SMC themselves or through secondary effects on other cell types, tissues, or the lesion microenvironment. The fact that we only observed this phenotype in NC-derived vascular beds despite using whole body radiation, suggests that the local environment plays a critical role. However, the underlying mechanisms are likely to be highly complex. For example, radiation-induced damage to local endothelial cells could inhibit the expression of factors required to stimulate SMC investment or induce secretion of factors that inhibit investment into lesions (Lee et al., 2012). It is also possible that functional changes in the engrafted hematopoietic stem cells that seed the BM niche following BMT selectively impact SMC, or that radiation may impact one or more of the other NC-derived cell populations shown to play a critical role in the remodeling of the branchial arch vessels during vascular development (Kirby and Waldo, 1995).

Our observations of increased YFP^{+} TUNEL^{+} cells selectively in the BCA suggest that radiation is directly and/or selectively impacting the Myh11^{+} medial SMC population and preventing them from accumulating within lesions. However further study is required to determine if there are other contributing factors from circulating cells or the local environment. If radiation was directly targeting the NC-derived SMC, this would appear to be inconsistent with the widely-accepted dogma that radiation primarily impacts highly proliferative and poorly differentiated cells (Bergonie and Tribondeau, 1959). Indeed, SMC are known to have a very low proliferation rate within mature blood vessels (~0.1%) (Olson et al., 1992; Reidy, 1990) and are therefore considered one of the most radioresistant cell types. However, several recent studies (Chappell et al., 2016; Jacobsen et al., 2017) using multicolor SMC clonal analysis, have shown that SMC in BCA and carotid lesions are derived from oligoclonal expansion of a small number of medial SMC. Thus, it is possible that a subpopulation of medial Myh11^{+} SMC in NC-derived vascular beds are poised to undergo clonal expansion, and perhaps these cells are susceptible to radiotherapy. Interestingly, SMC located at the tip of muscularized pulmonary arterioles, which are also NC-derived (Jiang et al., 2000), have been shown to be primed to clonally expand following hypoxia-induced pulmonary hypertension (Sheikh et al., 2015). Perhaps there is a similar subpopulation among the aortic SMC. Consistent with this idea, a recent study (Majesky et al., 2017) has shown that a subset of differentiated SMC (using Myh11-ER^{T2}Cre) express the mouse stem cell marker, SCA1. It is interesting to speculate that the subpopulation of primed Myh11-derived SMC may be uniquely sensitive to radiation due to their increased plasticity, which would presumably be associated with a more open chromatin state that may increase their susceptibility to radiation-induced DNA damage independent of proliferation status. However, it will be extremely difficult to directly test this possibility given that SCA1 is expressed by many cell types other than SMC. As such, studies would require development of a sequential dual recombinase lineage tracing mouse that allows selective lineage tracing of the subset of Myh11 expressing SMC that subsequently activate SCA1.

An alternative possibility is that radiation may induce terminal differentiation of a proliferation competent subset of medial SMC exclusively in NC-derived vascular beds. This idea is supported by a previous study showing that radiation-induced coat greying, which is normally maintained by a NC-derived melanocyte stem cell population, was due to radiation-induced terminal differentiation of the stem cell population (Inomata et al., 2009). To extrapolate from these studies, perhaps the SMC population primed to oligoclonally expand is terminally differentiated following radiation, impairing their ability to populate BCA, carotid, and aortic arch lesions. However, the appropriate dual lineage tracing mouse model systems required to test this hypothesis are also not currently available.

We believe that the results of these studies are of great interest to multiple fields of basic and clinical biology. However, the preceding points make it clear that many intrinsic and extrinsic mechanisms may be responsible for radiation selectively abrogating the ability of SMC in the BCA, carotid artery, and aortic arch from investing into lesions. Thus, extensive further studies will be necessary to elucidate the underlying mechanisms for these effects, understand the possible implications of our results for clinical medicine, and interpret the findings of the more than 100,000 previous publications that have employed BMT as a primary experimental approach.

V. Acknowledgements

The authors thank D Gomez and BG Durgin for their input, and acknowledge A Saenz and CM Kasden for aid in tissue harvest, A Washington for assistance with histology, TCS Keller IV for assistance with data collection, A Young for performing surgeries, and the UVA CCM for use of equipment and support.

AACN and RAB performed the bulk of the experiments, data collection, and analysis, and wrote the manuscript. DLH performed surgeries and contributed editorially to the manuscript. SDG performed surgeries and contributed to data collection. LSS initiated BMT studies. OAC performed surgeries and provided guidance throughout the project. All authors conceived of and intellectually contributed to the experimental design. GKO supervised the entire project and had a major role in experimental design, data interpretation, and writing the manuscript.

VI: Figures

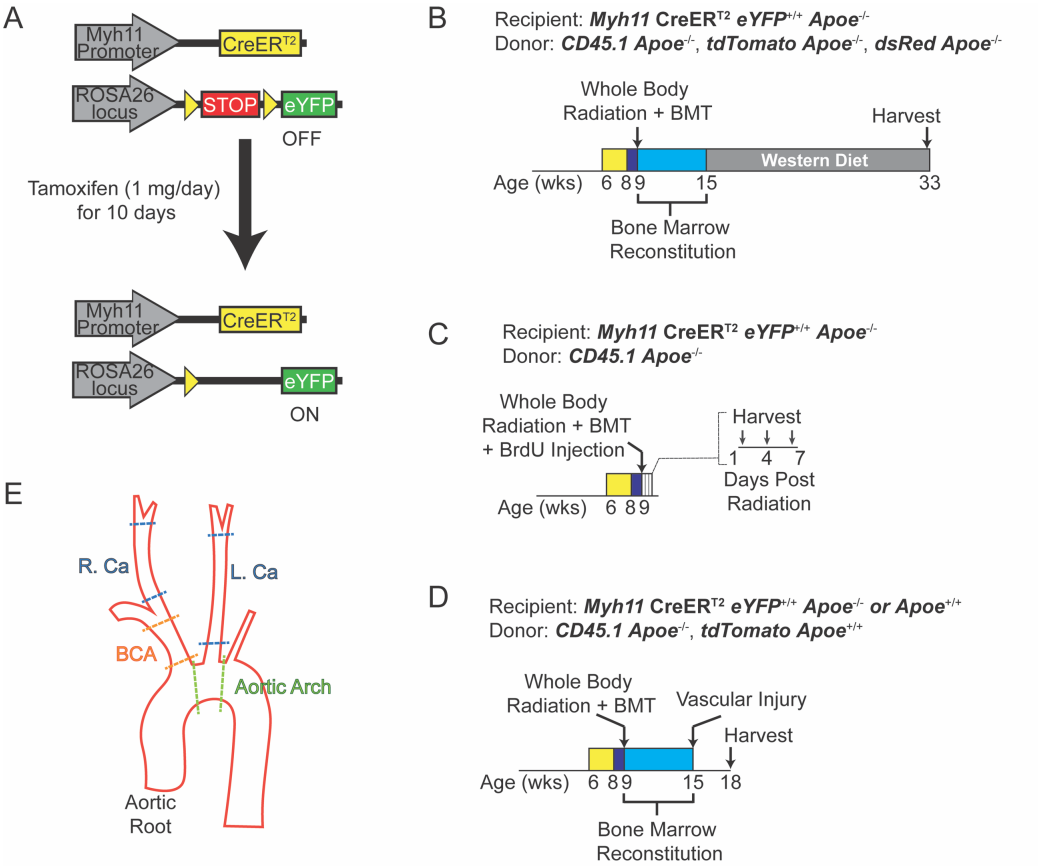

Figure 1

Experimental design. (**A**) Schematic of *Myh11*-CreER^{T2}, ROSA*26* STOP-flox eYFP$^{+/+}$ (SMC-YFP) mice. Upon tamoxifen injection, any cell transcribing MYH11 underwent excision of a floxed STOP codon in front of an eYFP transgene driven by the ROSA26 locus, allowing for permanent eYFP labeling of SMCs and their progeny. (**B**–**D**) SMC-YFP, Apoe$^{-/-}$ littermates at 9 weeks of age were subjected to 0 (nonirradiated, non-BMT controls) or 1,200 cGy of ionizing radiation and then administered >1 × 10^6 bone marrow cells (BMT). (**B**) Following 6 weeks of recovery to allow bone marrow engraftment, the mice were placed on a Western diet for 18 weeks to induce atherosclerosis formation. (**C**) Directly after radiation, mice were given a single BrdU pulse (10 mg/ml) and harvested at 1, 4, or 7 days after irradiation or 5 days after BrdU pulse for nonirradiated, non-BMT controls. (**D**) Following 6 weeks of recovery to allow bone marrow engraftment, mice underwent carotid ligation or femoral wire injury for 21 days. Bone marrow donor lines are indicated for each experiment. (**E**) Delineation of cut sites for vessels excised from the aortic outflow tract.

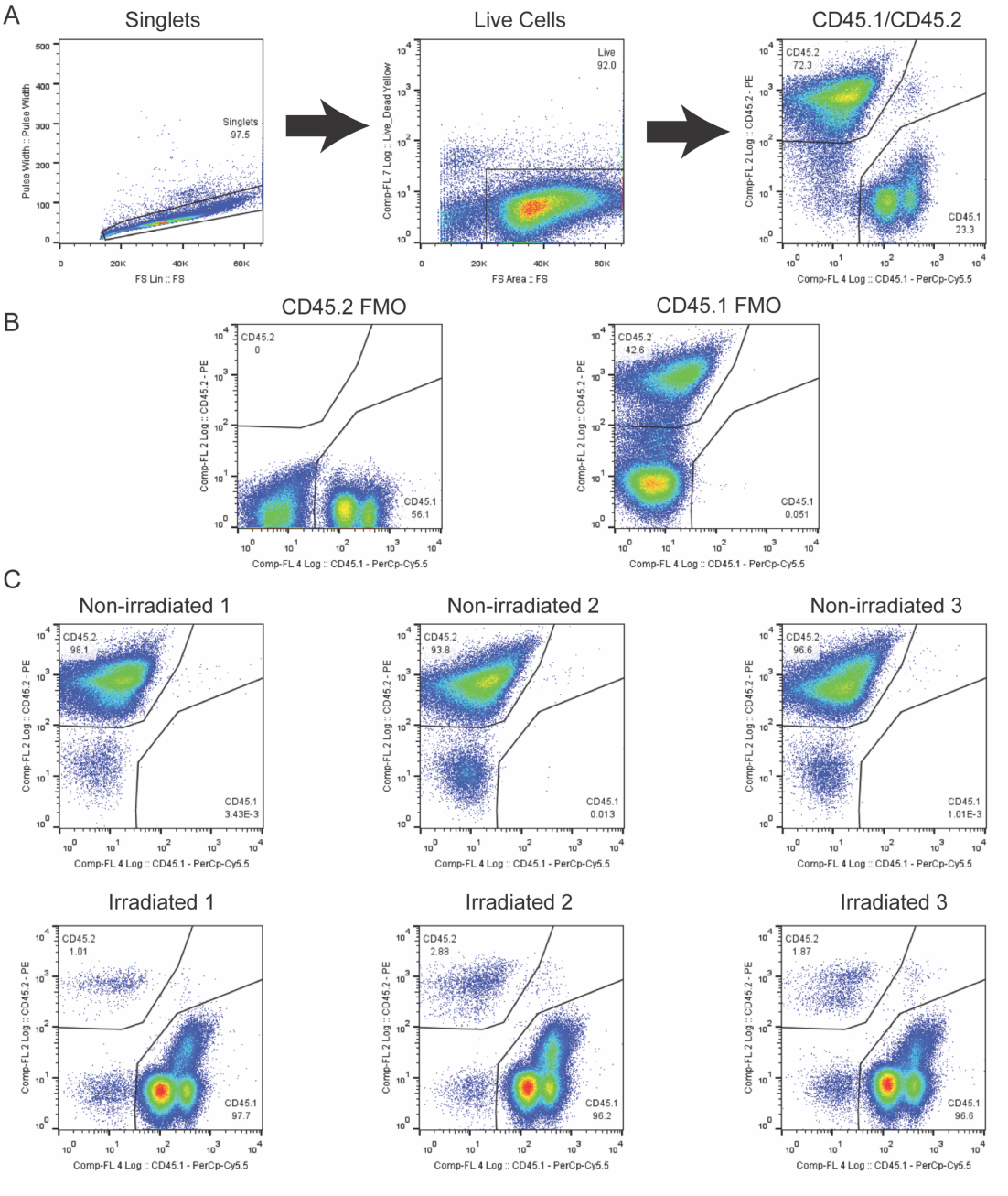

Supplemental Figure 1

Effective bone marrow reconstitution following lethal irradiation. (**A**) Gating strategy for determining bone marrow engraftment efficiency. Cell aggregates and dead cells were removed in (left) and (middle). Donor and recipient cells were identified in this example using CD45.1 and CD45.2 specific antibodies (right). (**B**) Fluorescent minus one (FMO) controls for CD45.1 and CD45.2. (**C**) Percentage of CD45.1 and CD45.2 cells in three representative control and irradiated animals based on FMO.

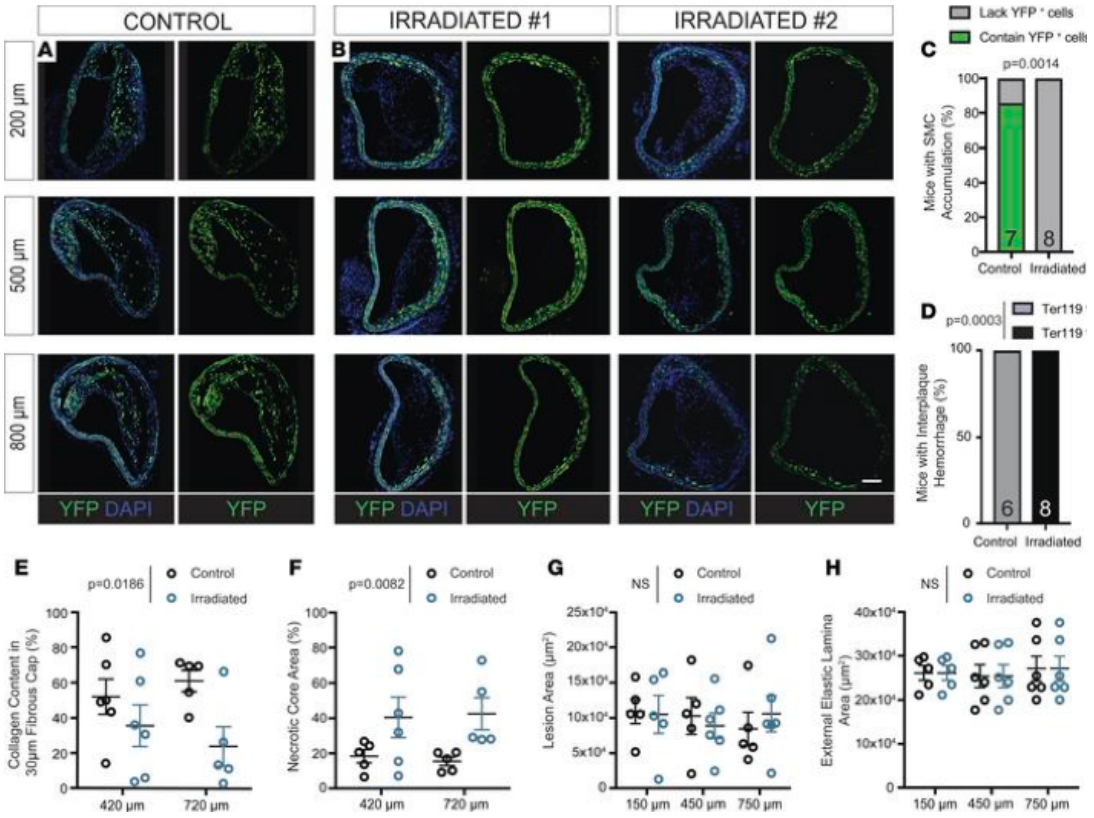

Figure 2

SMCs fail to invest within brachiocephalic atherosclerotic lesions following lethal irradiation and BMT; these changes are associated with decreased indices of lesion stability. SMC-YFP, Apoe$^{-/-}$ mice received 1,200-cGy whole-body radiation and BMT followed by 18 weeks of WD to induce atherosclerosis lesion development. (**A**) High-resolution confocal imaging shows consistent YFP^{+} cell accumulation in brachiocephalic (BCA) lesions of control mice. (**B**) Lethally irradiated animals show loss of YFP^{+} cell accumulation in BCA lesions at 3 locations past the aortic arch. (**C**) Fisher's exact test quantifying the percentage of control and irradiated animals that demonstrate YFP^{+} cell accumulation in BCA lesions. (**D**) Fisher's exact test quantifying the percentage of animals with intraplaque hemorrhage in at least 1 of 3 locations along the BCA. (**E**) The percentage of collagen pixels in the 30-µm lesion cap area was significantly decreased after lethal irradiation. (**F**) The necrotic core area was significantly increased in BCA lesions after lethal irradiation. (**G** and **H**) Lesion area (**G**) and external elastic lamina area (**H**) were not changed between control and radiated animals **E**–**H**. Data were assessed by 2-way ANOVA. Data represent mean ± SEM. Sample number is indicated in the graph. Scale bar: 100µm.

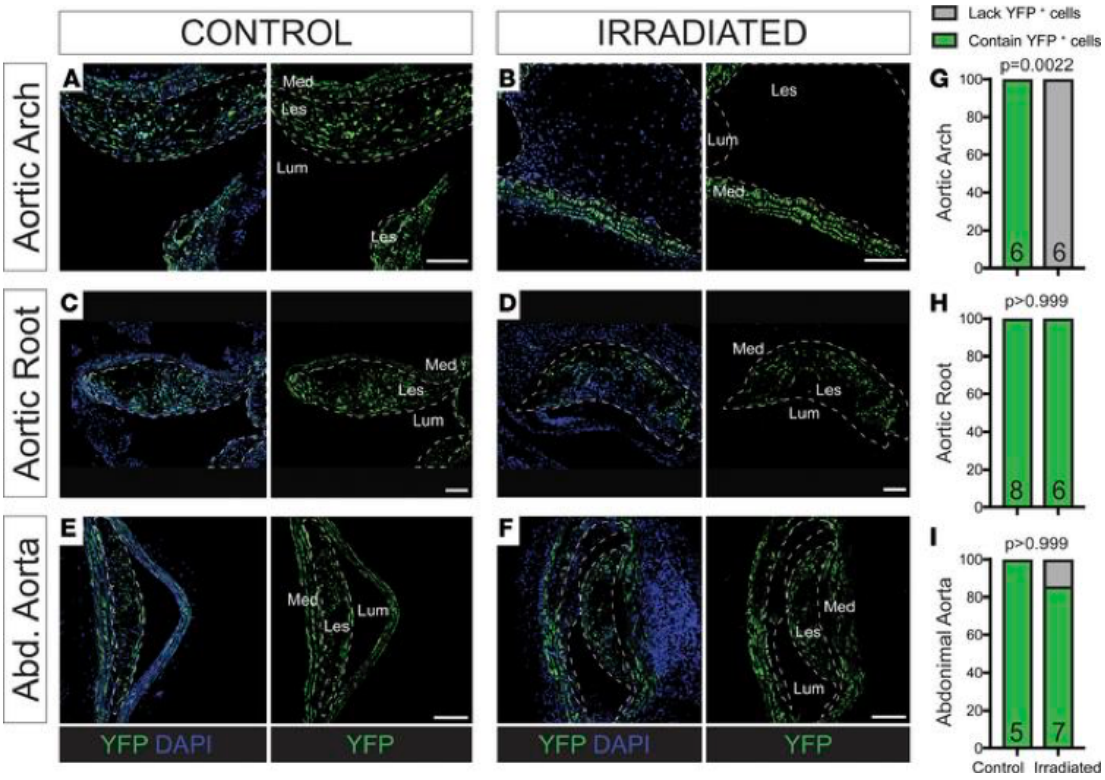

Figure 3

Vascular SMCs show heterogeneous investment in atherosclerotic lesions depending on vascular bed. (A and B) YFP+ cell accumulation was not observed in irradiated lesions but was observed in controls within the aortic arch. (C and D) Lesions within the aortic root and (E and F) abdominal aorta consistently had YFP+ cell accumulation in both control and irradiated mice. (G–I) Fisher's exact test quantifying the percentage of control and irradiated animals with lesions that demonstrate YFP+ cell accumulation at each location. Sample number is indicated in the graph. Scale bar: 100μm.

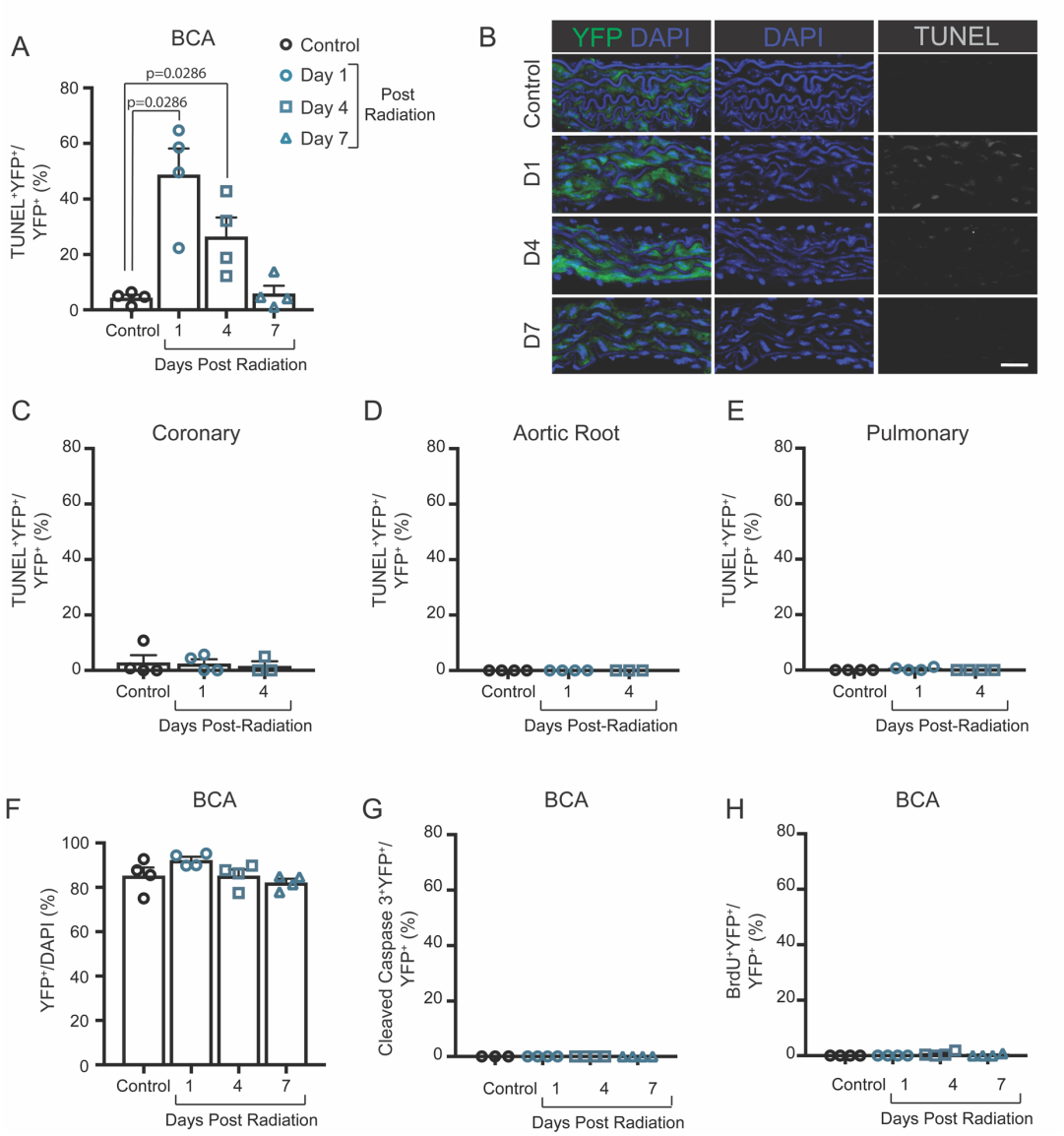

Figure 4

Radiation induces DNA damage only in BCA SMCs but does not result in increased apoptosis or proliferation. (A and B) Lethal radiation exposure results in significantly more TUNEL$^+$ YFP$^+$ cells within the brachiocephalic artery (BCA) at day 1 and 4 after radiation. (C–E) SMCs do not show increased TUNEL$^+$ cells in the media of the coronary (C), aortic root (D), or pulmonary vessels (E). (F) There was no difference in the number of YFP$^+$ cells in the media of the BCA. (G) There was no difference in the number of cleaved caspase-3$^+$ YFP$^+$ cells in the media of the BCA. (H) Nor was there any change in the number of cells incorporating BrdU following lethal radiation exposure. Data were assessed by Mann Whitney U test. Data represent mean ± SEM. Sample number is indicated in the graph. Scale bar: 25μm.

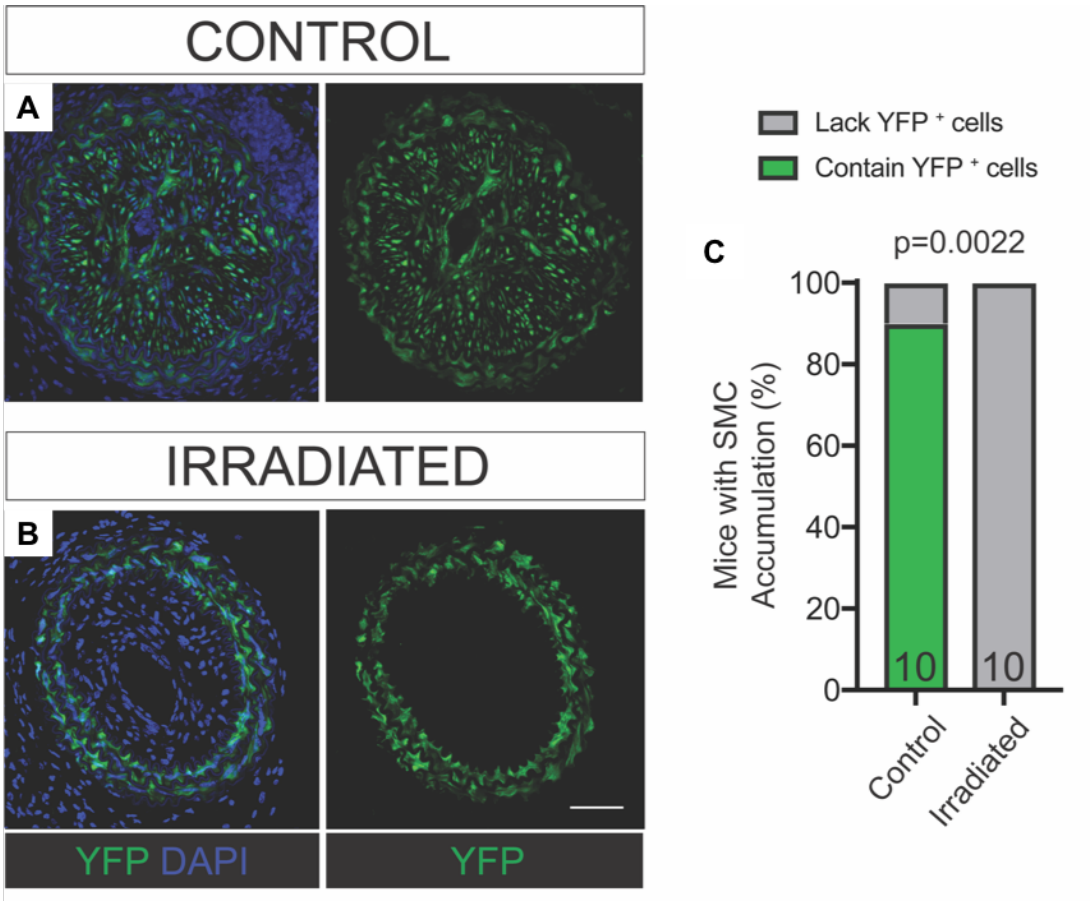

Figure 5

The carotid artery neointima lacks YFP+ SMC investment following lethal irradiation and BMT. (A) YFP+ SMC accumulate in the neointima that form after carotid ligation surgery. (B) Lethal irradiation ablated YFP+ cell accumulation in the carotid artery neointima. (C) Fisher's exact test quantifying the percentage of animals that demonstrate YFP+ cell accumulation in neointima with and without radiation. Sample number is indicated in the graph. Scale bar: 50μm.

Chapter 3

Platelet Derived Growth Factor Receptor Beta Signaling is Required for Maintenance of a Protective Atherosclerotic Fibrous Cap

Alexandra A.C. Newman, Olga A. Cherepanova, and Gary K. Owens

Adapted to become a manuscript submitted to Nature

I. Abstract

Thromboembolic events secondary to rupture or erosion of atherosclerotic lesions are the leading worldwide cause of death. Although human pathological studies show lesions with a high ratio of CD68 to ACTA2 cells are at risk for rupture, there are major ambiguities regarding the origins of these cells and pathways that control their functions within lesions. Platelet derived growth factor receptor beta receptor (PDGFBR) is shown to play a critical role in smooth muscle cells (SMC) but its impact on lesion pathogenesis is poorly understood. SMC-specific PDGFBR KO with simultaneous lineage tracing in atherosclerotic mice resulted in nearly complete failure of SMC to invest within lesions, with associated increases in mesenchymal transitions of endothelial cells and macrophages (EndoMT/MMT). Unexpectedly, these non-SMC derived cells could temporarily contribute to lesion stability. We additionally provided evidence based on late-stage intervention studies with Imatinib that maintenance of an ACTA2 and collagen rich fibrous cap was dependent on sustained PDGFBR signaling. Remarkably, mice with advanced atherosclerosis treated with Imatinib exhibited marked increases in morbidity and mortality of 100% of mice within seven days of onset of treatment. These studies demonstrate that PDGFBR signaling is required for plaque stabilizing SMC investment and retention within the fibrous cap, but that other cell types also play an underappreciated role in contributing to lesion stability.

II. Introduction

Despite widespread use of statins, anti-hypertension drugs, and lifestyle modifications, rupture or erosion of atherosclerotic plaques resulting in myocardial infarction or stroke are the leading worldwide causes of death (WHO, 2016). Indeed, despite decades of research, the mechanisms that regulate stability of late stage lesions are poorly understood (Bennett et al., 2016). Post-mortem human pathology studies provide compelling evidence that the composition of the lesion, rather than size, best correlates with stability. Specifically, stable plaques are characterized by a thick extracellular matrix (ECM)-rich protective fibrous cap with a high ratio of ACTA2$^+$ cells to CD68$^+$ cells, presumed to be smooth muscle cells (SMC) and macrophages (MΦ), respectively (Davies et al., 1993; Libby et al., 2011; Virmani et al., 2000).

However, recent studies using lineage tracing techniques in mouse and human lesions have challenged this dogma by showing that these markers alone are unreliable for identifying the origins and abundance of lesion cells (Cherepanova et al., 2016; Feil et al., 2014; Shankman et al., 2015). In fact, our previous studies have shown that >80% of the SMC within atherosclerotic lesions lack ACTA2, and almost half of these SMC exhibit markers and/or functions characteristic of MΦ, mesenchymal stem cells, or myofibroblast (MF) cells (Shankman et al., 2015). Moreover, many non-SMC within lesions have been shown to express SM markers like ACTA2, including MΦ (Albarran-Juarez et al., 2016; Allahverdian et al., 2012; Caplice et al., 2003) and endothelial cells (EC) (Gomez and Owens, 2012). For example, humans who underwent cross gender bone marrow transplantation demonstrated that ~10% of the ACTA2$^+$ cells in coronary lesions are of myeloid origin (Caplice et al., 2003), which suggests they have undergone MΦ to mesenchymal transition (MMT). Additionally, 50% of foam cells based on Oil Red O co-stained with ACTA2 in human lesions, (Allahverdian et al., 2014). Further, EC lineage tracing studies have shown that approximately 10% of EC undergo endothelial to mesenchymal transition (EndoMT), where they express both EC and SMC-markers (Chen et al., 2015; Evrard et al., 2016). However, it is unknown what proportion of the ACTA2$^+$ cells are derived from such mesenchymal transitions and if they are beneficial or detrimental

to lesion stability. In addition, although there is evidence showing that artificial enhancement of EndoMT through genetic approaches exacerbates lesion pathogenesis (Chen et al., 2012), and a number of human studies have suggested that EndoMT contributes to plaque erosion (Chen et al., 2015; Evrard et al., 2016; Pasterkamp et al., 2017a), there is no direct evidence that this is the case. In fact, we postulate that these mesenchymal states can be beneficial depending on the specific nature of their phenotypic transitions and the lesion environment. Indeed, recent studies by our lab involving simultaneous SMC lineage tracing and SMC-specific knockout (KO) of the stem cell pluripotency genes Oct4 or Klf4 have provided compelling evidence that SMC transitions can have either beneficial or detrimental effects on indices of lesion stability. For example, Oct4-dependent changes appeared to be required for SMC migration into lesions and formation of a protective fibrous cap (Cherepanova et al., 2016). In contrast, Klf4-dependent changes were detrimental including being required for transition of SMC to a macrophage-like state (Shankman et al., 2015).

There are a number of critical unresolved questions including: 1) What proportion of ACTA2^{+} fibrous cap cells are derived from SMC, EC, MΦ, or other sources? 2) Does the origin of ACTA2^{+} fibrous cap cells impact their function and in particular ECM production and overall plaque stability? 3) What are the mechanisms and factors that promote formation and maintenance of a protective fibrous cap?

Platelet derived growth factor beta receptor (PDGFBR) activation is a potent mitogen and chemotactic factor for cultured SMC (Blank and Owens, 1990; Heuchel et al., 1999; Holycross et al., 1992; Myllarniemi et al., 1997), and is critical for recruiting SMC to nascent vessels during angiogenesis (Hellstrom et al., 2001; Hellstrom et al., 1999). PDGFBR is upregulated in human lesions (Raines, 2004; Shankman et al., 2015) and interestingly, nearly all previous studies in atherosclerosis have attempted to antagonize PDGFBR to inhibit SMC migration and proliferation and presumably reduce lesion burden (Boucher et al., 2003; Kozaki et al., 2002; Sano et al., 2001). However, we believe this notion is not only mistaken but potentially deleterious to lesion stability. Instead, we hypothesize that augmenting PDGFBR signaling and SMC investment would induce

beneficial changes to lesion composition (Bennett et al., 2016). Indeed, this is supported by studies that show hematopoietic loss of PDGFBB or chemical antagonism of PDGFBR during atherogenesis delayed fibrous cap formation (Kozaki et al., 2002), and anti-PDGFBR antibody treatment starting at 12 weeks of WD resulted in 80% fewer ACTA2^{+} cells in the lesion (Sano et al., 2001). Taken together, these results suggest that PDGFBR signaling plays a critical role in regulating fibrous cap development. However, these previous studies involved global inhibition of PDGFBR, and failed to provide direct insight as to the mechanisms for the observed effects, including determining the role of PDGFBR signaling in SMC in lesion stability and pathogenesis.

Herein, we show that SMC-specific KO of PDGFBR in long term Western diet (WD) fed SMC-lineage tracing Apoe$^{-/-}$ mice results in several surprising findings. First, studies show that SMC normally make up about 60-70% of the ACTA2^{+} cap cells in advanced brachiocephalic artery (BCA) lesions, and cells expressing EndoMT and MMT markers make up the bulk of the remaining ACTA2^{+} cap cells. Second, PDGFBR signaling in SMC is required for their investment into lesions in that SMC were almost entirely absent within advanced atherosclerotic BCA lesions after PDGFBR KO. Third, despite the complete absence of SMC within these lesions, there was no change in multiple indices of plaque stability following 18 weeks of WD feeding likely due in part to a compensatory increase in ACTA2^{+} fibrous cap cells derived from EndoMT and MMT. However, it seems that increased EndoMT and MMT can only transiently compensate for loss of SMC in lesions as we observed reduced indices of plaque stability following longer term WD feeding despite sustained ACTA2 expression. Fourth, we show that global inhibition of PDGFBR signaling in Apoe$^{-/-}$ mice with advanced lesions was associated with significantly decreased SMC and ACTA2^{+} cells overall and premature death in atherosclerotic mice. Taken together, these results provide novel evidence that SMC are normally the major and most effective, but not the only, cell type responsible for formation of the protective ACTA2 and ECM rich protective fibrous cap, and that this process is dependent on PDGFBR signaling.

III. Results

PDGFBR Signaling in SMC is Required for Their Investment within the BCA Lesion and Fibrous Cap

Whereas there is clear evidence that lesions containing a thick fibrous cap enriched in ACTA2^{+} cells are more stable, the mechanisms that regulate this process are poorly defined. To test the hypothesis that PDGFBR signaling in SMC is critical for formation and/or maintenance of a stable fibrous cap, we generated tamoxifen inducible SMC-PDGFBR KO mice with SMC lineage tracing (eYFP^{+}) on an Apoe$^{-/-}$ background (PDGFBR-Flox or -WT Myh11-CreER^{T2}/Rosa Flox-Stop/eYFP; Apoe$^{-/-}$, henceforth PDGFBR$^{SMC\Delta/\Delta}$ or $^{WT/WT}$, S. Figure 1A).[5] Littermate controls were injected with tamoxifen between 6-8 weeks of age, before being placed on Western diet (WD) to induce atherosclerosis development (S. Figure 1 B). BCA lesions were assessed at proximal, middle, and distal locations past the aortic arch (S. Figure 1 C). Tamoxifen injected mice show >99% activation of eYFP lineage tracing within medial SMC within the aorta. Excision of PDGFBR was confirmed by PCR with excision primers, and PDGFBR immunofluorescence staining (S. Figure 1 D, E) analyses showed effective knockout of the PDGFBR in >96% of SMC. PDGFBR$^{SMC\Delta/\Delta}$ was not associated with significant changes in body weight, cholesterol, or triglyceride levels after WD.

Results of high-resolution z-stack confocal microscopy analyses (Figure 1) showed a >90% reduction in investment of eYFP^{+} SMC within the brachiocephalic artery (BCA) lesions (eYFP^{+}/DAPI, Figure 1 A,C,E) and >94% reduction in eYFP^{+} SMC within the fibrous cap after 18 weeks of WD (measured as the 30μm sub-luminal space, Figure 1 B,D,F) after PDGFBR KO (Figure 1 C,D) as compared to WT animals (Figure 1 A,B). The reduction in SMC investment was not associated with reduced cell density between PDGFBR$^{SMCWT/WT}$ and PDGFBR$^{SMC\Delta/\Delta}$ animals (based on DAPI^{+}/area). These data show that

[5] Author's note: this alternate format for genotype is analogous to SMC-PDGFBR WT and KO, which is used elsewhere

PDGFBR signaling is required for SMC to populate BCA lesions and the fibrous cap, where they are thought to contribute to plaque stability.

To determine the mechanism responsible for the virtual absence of lesion SMC in PDGFBR$^{SMC\Delta/\Delta}$ mice, we analyzed SMC accumulation after 10 weeks of WD as well as the effects of SMC-PDGFBR KO on SMC proliferation and phenotypic modulation in the media following 18 weeks of WD (S. Figure 2), as these processes are thought to underlie the SMC response to atherosclerosis. After 10 weeks of WD feeding, most of the PDGFBR$^{SMCWT/WT}$ animals have lesions with eYFP^{+} SMC investment, whereas only one in seven PDGFBR$^{SMC\Delta/\Delta}$ animals had any eYFP^{+} SMC investment (data not included). This demonstrates that SMC accumulation in lesions after SMC-PDGFBR KO is impaired throughout atherosclerosis development, rather than SMC loss resulting from initial SMC investment in lesions and then subsequent apoptosis. Further support for this comes from data showing no discernable differences in the total number of apoptotic cells, or in the fraction of SMC undergoing apoptosis between PDGFBR$^{SMCWT/WT}$ and PDGFBR$^{SMC\Delta/\Delta}$ animals (data not included).

PDGFBR activation induces dedifferentiation of cultured SMC, which is characterized by the downregulation of SMC markers including ACTA2 (Blank and Owens, 1990; Holycross et al., 1992). As such, we expected that loss of PDGFBR signaling in SMC would be associated with impaired dedifferentiation and reduced numbers of eYFP^{+} ACTA2^{-} SMC in the media. However, surprisingly, we observed no change in the frequency of these cells within the media of PDGFBR$^{SMC\Delta/\Delta}$ mice as compared to littermate controls (eYFP^{+} ACTA2^{-} /DAPI, S. Figure 2 A,B). To determine if SMC can transition to other phenotypes after SMC-PDGFBR KO, we assessed SMC specific expression of a marker of phagocytic MΦ, LGALS3, which our lab has previously shown to be expressed in eYFP^{+} SMC in the media (Cherepanova et al., 2016). We found that there was a significant 65% increase in the SMC that express LGALS3 within the media of PDGFBR$^{SMC\Delta/\Delta}$ BCAs (eYFP^{+} LGALS3^{+} /DAPI, S. Figure 2 C,D), indicating that SMC-PDGFBR KO does not impair their capacity to dedifferentiate and phenotypically modulate. SMC-PDGFBR

KO also resulted in a surprising 3-fold increase in proliferation of SMC in the media ($eYFP^+$ $Ki67^+$/DAPI and $Ki67^+$/DAPI, S. Figure 2 C,E). Taken together, these results indicate that the profound reductions in SMC within lesions of $PDGFBR^{SMC\Delta/\Delta}$ mice was due to impaired migration of SMC rather than reduced phenotypic modulation, proliferation, or increased apoptosis.

Loss of $eYFP^+$ SMC Does Not Result in Fewer $ACTA2^+$ Cells in the Fibrous Cap or Reduced Indices of Stability after 18 Weeks of WD

Given the well-established dogma that lesions with a thicker fibrous cap enriched in $ACTA2^+$ SMC and ECM are more stable, we anticipated that loss of SMC would result in a profound decrease in indices of lesion stability. However, completely unexpectedly, we found no significant changes in any of the multiple indices of plaque stability examined including collagen content as determined by PicroSirius Red staining (Figure 2 A) in the lesion (Figure 2 B) or fibrous cap (Figure 2 C). There was also no change in intraplaque hemorrhage based on RBC marker TER119 (Figure 2 B,E), or necrotic core area (Figure 2 F). Also, $PDGFBR^{SMC\Delta/\Delta}$ mice showed no differences in lesion area (S. Figure 3 A,B), or remodeling indices (EEL area, S. Figure 3 A,C) and lumen area (S. Figure 3 A,D), as compared to littermate control $PDGFBR^{WT/WT}$ mice.

Due to the profound decrease in SMC investment in lesions, we expected to see reduced numbers of $ACTA2^+$ cells within lesions after SMC-PDGFBR KO. However, we were again surprised to find no changes in the ratio of MΦ- to SM-marker$^+$ cells in the cap ($LGALS3^+$:$ACTA2^+$, Figure 2 G) nor in the percentage of total $ACTA2^+$ cells in the lesion or fibrous cap at three locations in the BCA in $PDGFBR^{SMC\Delta/\Delta}$ animals after 18 weeks of WD ($ACTA2^+$/DAPI, Figure 2 H) as compared to WT controls. Taken together results suggest that in the absence of SMC investment into lesions, non-SMC are able to fully compensate not only in terms of maintenance of an $ACTA2^+$ fibrous cap, but also for the indices of plaque stability evaluated. These observations were totally unexpected and seem to be contrary to long established dogma in the field that SMC are the primary cell type responsible for the formation of the protective $ACTA2^+$ fibrous cap.

A Substantial Portion of ACTA2^{+} Fibrous Cap Cells are Derived from EndoMT and MMT Rather than from Pre-existing SMC

To further characterize the source of ACTA2^{+} fibrous cap cells, we completed more rigorous high-resolution z-stack confocal analyses of advanced BCA lesions in our SMC lineage tracing Apoe$^{-/-}$ mice after 18 weeks of WD. Of major interest, we found that SMC only make up approximately 60% of the ACTA2^{+} cells in the fibrous cap in PDGFBR$^{SMCWT/WT}$ mice, and are decreased to <1% in PDGFBR$^{SMC\Delta/\Delta}$ mice (eYFP^{+} ACTA2^{+} /ACTA2, Green, Figure 3 C). To demonstrate that not all ACTA2^{+} cells are derived from SMC in human lesions, we performed ISH-PLA on human coronary sections. With the caveat that ISH-PLA is not quantitative and has a relatively high false negative rate (Gomez et al., 2013), we determined that similar to what we see in mice, 50-60% of the ACTA2^{+} cells are also PLA^{+} after correction (Figure 3 F; see methods).

To identify the potential origins of these non-SMC derived ACTA2^{+} cells, we performed immunofluorescence staining for eYFP along with putative markers of EC (CD31) and MΦ (LGALS3) to assess the potential contributions of EndoMT (Figure 3 A) and MMT (Figure 3 B) respectively, to the fibrous cap with and without KO of PDGFBR in SMC. Co-localization of ACTA2 with CD31 was chosen based on previous studies in atherosclerosis indicating that CD31 persists for some period following EndoMT (Chen et al., 2015; Chen et al., 2012; Evrard et al., 2016). LGALS3 was chosen as a marker based on previous studies showing increased expression of the protein by pro-fibrotic M2 cells (Vernon et al., 2010). Notably, it is not possible to employ independent Cre recombinase EC and Mo/MΦ lineage tracing models to rigorously address this question, since our biological effect is dependent on Myh11-CreER^{T2}-KO of PDGFBR.

Of major interest, results of our analyses suggest that 32% of the ACTA2^{+} cell population in the cap of PDGFBR$^{SMCWT/WT}$ mouse BCA lesions expresses markers consistent with them having been derived by MMT (eYFP^{-} LGALS3^{+} ACTA2^{+}, Lilac) or EndoMT (eYFP^{-} CD31^{+} ACTA2^{+}, Violet). In PDGFBR$^{SMC\Delta/\Delta}$ lesions, 76% of the ACTA2^{+} cells in the cap appear to be derived by MMT or EndoMT (Figure 3 E, Lilac and Violet together). An additional 24% of eYFP^{-} fibrous cap ACTA2^{+} cells are of undetermined origin, although

we cannot rule out that some or all of these may have resulted from EndoMT and/or MMT but with cells having lost their residual EC or macrophage lineage protein markers. Importantly, these results reveal that there is a basal level of EndoMT and MMT marker^{+} cells that normally contribute to the ACTA2^{+} fibrous cap cells in WT lesions, but also that in response to PDGFBR-dependent loss of SMC-derived ACTA2^{+} cells, EndoMT and MMT increase and appear to effectively maintain plaque stability at least after 18 weeks of WD feeding.

Non-SMC Can Only Transiently Compensate for PDGFBR-dependent Loss of SMC Investment into Lesions

Considering the chronic nature of atherosclerosis, we next tested if non-SMC were capable of compensating for loss of lesion SMC for longer periods of WD feeding by performing vessel and lesion composition analyses on PDGFBR$^{SMCWT/WT}$ and PDGFBR$^{SMC\Delta/\Delta}$ mice after 26 weeks of WD (S. Figure 4 A). Similar to at 18 weeks of WD, we observed a >90% reduction in eYFP^{+} cells in the lesion (S. Figure 4 B) and cap (S. Figure 4 C). However, at this very late timepoint, BCA lesions of PDGFBR$^{SMC\Delta/\Delta}$ mice showed multiple reductions in indices of plaque stability including reduced collagen deposition within the lesion (Figure 4 A,C) and cap (Figure 4 A,D) and significantly increased intraplaque hemorrhage (Figure 4 B,E) compared to littermate PDGFBR$^{SMCWT/WT}$ control mice. There remained no differences in necrotic core area (Figure 4 F), LGALS3:ACTA2 ratio (Figure 4 G), nor in most vessel parameters (S. Figure 4 D) including lesion (S. Figure 4 E) or lumen (S. Figure 4 F) areas, although EEL area was increased (S. Figure 4 G).

Similar to data at 18 weeks of WD, there was no decrease in the percentage of ACTA2^{+} cells in the fibrous cap (Figure 4 H) although there was a similar significant decrease in the SMC-derived ACTA2^{+} cells of about 90% between PDGFBR$^{SMCWT/WT}$ and PDGFBR$^{SMC\Delta/\Delta}$ mice (S. Figure 5, Green). Maintenance of the ACTA2^{+} cap was again due to compensatory increases in non-SMC eYFP^{-} cells (eYFP^{-} ACTA2^{+} /ACTA2 S. Figure 5, Grey). However, the contribution of presumptive EndoMT (five-fold increase, p=0.0006; S. Figure 5, Lilac) was significantly increased relative to MMT (two-fold increase

p=0.0753; S. Figure 5, Violet) at this later time point. Taken together, the preceding data show that while lesion stability can be maintained by non-SMC after PDGFBR-dependent loss of SMC investment into BCA lesions, this compensation is not sustained over long term atherosclerosis development. In addition, these data indicate that EndoMT and MMT can be beneficial processes at least in the context of our model system.

Sustained PDGFBR Signaling in SMC is Required for Maintenance of ACTA2^{+} SMC within the Fibrous Cap

Thus far, we have presented data showing that PDGFBR signaling is required for SMC investment within the BCA lesion and fibrous cap. We next wanted to test if persistent PDGFBR signaling is required for SMC retention within the fibrous cap and if its loss would reduce the population of ACTA2^{+} SMC in the fibrous cap and adversely affect lesion stability. PDGFBR-Flox or -WT Myh11-CreER^{T2}/Rosa Flox-Stop/eYFP; Apoe$^{-/-}$ littermate mice were treated with tamoxifen between 16 and 18 weeks of WD (Figure 5 A) after advanced lesion formation, to induce eYFP^{+} lineage tracing of Myh11^{+} cells, with and without PDGFBR KO (PDGFBR$^{Myh11Cre\Delta/\Delta}$ and PDGFBR$^{Myh11Cre\ WT/WT}$, Figure 5 B,C). At 18 weeks of WD, 80% of ACTA2^{+} SMC express Myh11 (eYFP^{+}ACTA2^{+}Myh11^{+}/eYFP^{+} ACTA2^{+}) by high resolution confocal microscopy. Thus, after delayed tamoxifen injections, any cell labeled with eYFP had been expressing multiple SMC marker proteins. This represents >60% of the SMC in the fibrous cap (Figure 3 E) and approximately 20% of total lesion SMC (Shankman et al., 2015).

Eight weeks of WD post tamoxifen showed significant reductions in the percentage of eYFP^{+} cells (eYFP^{+} /DAPI) (Figure 5 D) and in the eYFP^{+} ACTA2^{+} cells in the cap (eYFP^{+}ACTA2^{+} /ACTA2, Figure 5 F). This was also associated with a significant decrease in the collagen content within the cap (Figure 5 G), despite no changes in total ACTA2^{+} cells (ACTA2^{+} /DAPI, Figure 5 E). These results indicate that persistent PDGFBR signaling is required to maintain the ACTA2^{+} SMC population within the fibrous cap, and that collagen deposition is likely reliant on the sustained presence of ACTA2^{+} SMC.

Imatinib Treatment Potently Reduced SMC and ACTA2$^+$ Cells in the Fibrous Cap

Previous studies using chemical or antibody antagonism of PDGFBR signaling resulted in reduced ACTA2$^+$ staining in atherosclerotic lesions (Kozaki et al., 2002; Sano et al., 2001) but did not examine multiple indices of plaque stability or unambiguously identify the key cell types that comprise the fibrous cap. To test if therapeutic antagonism of PDGFBR would adversely affect lesion stability, we administered 100mg/kg/day of Imatinib Mesylate (STI571, Gleevec) to mice via i.p. injection to SMC-lineage tracing mice with advanced lesion development (Figure 6 A). Western diet fed littermate controls were injected with saline. Imatinib Mesylate is a commonly used anti-cancer agent that targets PDGFR, c-Kit, and BCR-ABL, which is well-tolerated in humans at up to 800mg/day (Novartis, 2018). The dose of 100mg/kg/day in mice is well within range of the human dose and was chosen based on previous literature (see methods for detailed description).

BCA lesions were analyzed and showed a striking decrease in total SMC and total ACTA2$^+$ cells and the percentage of ACTA2$^+$ SMC in the fibrous cap (eYFP$^+$, ACTA2$^+$, eYFP$^+$ ACTA2$^+$/DAPI, Figure 6). These results were noteworthy because Imatinib injection also resulted in early terminal end points (significant weight loss, sudden death, lower limb paralysis) in 100% (5/5) of Imatinib treated mice within 7 injections versus 0% (0/5) in saline treated control mice. Results indicate that even a surprisingly short period of Imatinib treatment resulted in marked reductions in indices of plaque stability and increased mortality. Whereas the exact cause of death in Imatinib treated mice is unknown, the appearance of mice exhibiting deficits in motor control are consistent with possible stroke.

IV. Discussion

For decades it was widely accepted that SMC dedifferentiate, accumulate within atherosclerotic lesions, contribute to fibrous cap development, and promote lesion stability (Libby et al., 2011; Virmani et al., 2000). Only recently has high-fidelity lineage tracing and single cell epigenetic marker analyses directly confirmed SMC investment in mice and humans (Albarran-Juarez et al., 2016; Feil et al., 2014; Gomez et al., 2013; Shankman et al., 2015). However, the mechanisms of how this occurs and the precise functions of SMC once they are in the lesion are still not well defined. Herein we present compelling evidence that PDGFBR signaling in SMC regulates beneficial plaque stabilizing events within advanced atherosclerotic lesions, including being required for SMC investment in and maintenance of the fibrous cap. This should perhaps not be surprising given that PDGFBR signaling induces SMC to invest in vessels during angiogenesis (Andrae et al., 2008). However, with multiple factors such as IL1β, bFGF, and TGFβ that are shown to promote SMC migration based on studies in culture (Gerthoffer, 2007), the environmental milieu within lesions is far different. Our findings indicate that PDGFBR signaling in SMC is indispensable, at least in atherosclerosis, and may regulate events that make SMC permissive to respond to these other factors.

Results herein suggest that in atherosclerosis, the major role for PDGFBR is in SMC migration rather than proliferation, which agrees with studies of arterial injury in chimeric animals with PDGFBR-expressing (WT) and PDGFBR-deficient (null) cells that found more null cells in the media than the neointima (i.e. no migration), and an increased percentage of WT cells in the neointima compared to null (i.e. migration) (Buetow et al., 2003). Furthermore, because our model lacks the PDGFBR protein itself only in SMC, it seems that SMC migration is due to cell autonomous, not secondary effects of the PDGF-PDGFBR axis, including permissive ECM rearrangement or release of other chemotactic cytokines.

It has yet to be elucidated why other migratory agents cannot induce migration of SMC lacking PDGFBR. PDGFBR may be a marker of the expansion competent mature medial SMC that oligoclonally populate the atherosclerotic lesion (Chappell et al., 2016;

Jacobsen et al., 2017; Sheikh et al., 2015). Indeed, there is a subset of primed SMC marked by PDGFBR expression that oligoclonally expand to muscularize distal pulmonary arteries shown in a mouse model of pulmonary hypertension (PAH) (Sheikh et al., 2015). In this case, EC and MΦ-derived PDGFBB acting through PDGFBR regulates distal migration. We suggest that similar to PAH, the expansion-competent cells in the BCA media must activate PDGFBR, but the question then becomes, why, if nearly all the medial SMC express PDGFBR (S. Figure 1 D), does only one (or a very few) give rise to the SMC in the lesion?

There seem to be two possibilities, the first being that most or all PDGFBR$^+$ medial SMC are capable of expansion, possibly cycling between competence and incompetence. The second is that there are rare PDGFBR$^+$ SMC uniquely equipped to give rise to the lesion SMC. The first scenario would indicate that many, if not all medial PDGFBR$^+$ SMC have the ability to expand into the lesion and random chance allows for oligoclonal expansion. For example, cycling of certain genes may allow for stochastic expression of a protein or set of proteins required for the initial clonal events, and subsequent active negative regulation prevents competition by other SMC. In light of our data, the yet unknown secondary signals may be downstream of PDGFBR activation. The latter would require the expansion-competent medial SMC to be rare enough in the vessel wall so that plaques are comprised of just one SMC clone that proliferates until it meets another SMC clone. These boundaries may be pre-determined by a competing clone releasing negative regulatory signals. Overall, it is clear that further study is needed to fully elucidate the mechanisms of SMC migration and expansion into the lesion. Our studies show, though, that persistence of a protective ACTA2- and collagen-rich fibrous cap requires PDGFBR-mediated SMC accumulation in the lesion.

SMC are generally thought to mostly, if not entirely, derive the plaque stabilizing, ECM producing, protective cells in the cap based on ACTA2 staining (Libby et al., 2011; Pasterkamp et al., 2017a). In these studies, we show that while the majority of the ACTA2$^+$ cells are indeed of a SMC origin in mice and humans, over 30% are of alternate cell origins, including from EndoMT or MMT. The abundance of these transitions is higher

than we expected, higher than previously appreciated in the field, and raises questions as to the function of the mesenchymal transitioned non-SMC. Although not equal to SMC in maintaining stability over the very long term, our longitudinal studies show that these ACTA2^{+} cells seem to temporarily maintain a collagen rich cap. The fact that the presence of SMC in the fibrous cap keeps EndoMT and MMT at a relatively low level suggests that SMC actively inhibit these transitions, which may be an effort to preserve the normal functions of EC and MΦ including maintaining proper barrier function and phagocytic clearance of lipids and cell debris. It is possible that EndoMT and MMT are only ever meant to be temporary stewards of stability, subbing in for SMC until they can sufficiently proliferate within the growing lesion.

It is also possible that similar to previous observations of SMC phenotype, EndoMT and MMT can have the same duality of beneficial and detrimental effects depending on the lesion environment. Deliberate temporary mesenchymal transitions of EC occur during development or injury, where EC provide initial stromal investment in nascent vessels (Red-Horse et al., 2010; Welch-Reardon et al., 2015). Additionally, MMT has been shown to produce and organize collagens and other ECM (Wang et al., 2016b) in wound healing (beneficial) and various fibrotic diseases (detrimental) (Braga et al., 2015; Iwata et al., 2013). The question to be addressed is, if co-opting these events in atherosclerosis ameliorates or exacerbates human lesion pathology.

The field generally concludes that in lesions EndoMT and MMT are detrimental, with MMT contributing to inflammation and instability through increased MMP production, and because co-incident EndoMT staining correlates with worsening AHA lesion classification (Chen et al., 2015; Evrard et al., 2016; Iwata et al., 2010; Metharom et al., 2008; Sata et al., 2002; Yu et al., 2011). However, EndoMT also correlates with increased collagen type I content (Chen et al., 2015; Evrard et al., 2016). Clearly, it is important to determine the context in which these mesenchymal transitions may ameliorate or exacerbate pathology in part to better classify stable lesions, and in part because augmenting ACTA2^{+} cells globally could represent a novel therapeutic target.

Still, the majority of studies in atherosclerosis focus on inhibiting SMC proliferation and accumulation within lesions, the presumed source of ACTA2^{+} cells, in order to reduce overall lesion burden. If this is done to prevent lesion development, with therapy starting at a young age, then inhibiting SMC accumulation, similar to cases of restenosis after angioplasty (Ferns et al., 1991), may reduce lesion size. However, considering the timeline of purported therapeutic intervention, i.e. after SMC have already accumulated within an established lesion, increasing ACTA2 and beneficial SMC phenotypes is paramount for plaque stability. In fact, studies that result in reduced SMC in lesions generally demonstrate a thinner, collagen and ACTA2^{+} poor fibrous cap and overall decreased indices of lesion stability (Cherepanova et al., 2016; Durgin et al., 2017; Gomez et al., 2018; Newman et al., 2018; Shankman et al., 2015). For example, anti-IL1β antibody administration to Apoe$^{-/-}$ mice with developed atherosclerosis showed surprising marked reductions in SMC and ACTA2 cells and collagen in the fibrous cap, as well as inhibition of beneficial outward remodeling. (Gomez et al., 2018) Moreover, it hints that a possible therapeutic would involve the synergistic interaction of PDGF and IL1β to maintain beneficial SMC phenotypes within the fibrous cap (Chen et al., 2006).

Previous studies of murine atherosclerosis that have antagonized PDGFBR signaling to inhibit SMC accumulation and thus lesion burden, resulted in multiple characteristics of an unstable plaque. This includes delayed fibrous cap development and fewer ACTA2^{+} cells overall and demonstrate a key protective role of PDGFBR in development of a thick, ACTA2^{+} rich fibrous cap (Kozaki et al., 2002; Sano et al., 2001).

Fibrous cap formation is reminiscent of mechanisms that regulate vascular repair following injury including requiring PDGF-mediated recruitment of SMC to the endothelium. Thus, PDGFBR agonism may represent a novel therapeutic target. This would require development of a novel small molecule PDGFBR agonist or a non-redundant downstream mediator (Yang et al., 2014a), which may be feasible based on screening studies that identify discrete downstream events of differential phosphorylation outcomes, including activating specific inositol phosphate second messengers (Williams, 1989). To test this would require interventional studies similar to those outlined in Figure 6 A to assess

agonism on the atherosclerotic lesion. It would also be necessary to test off target effects of PDGFBR agonism by looking at disease or repair mechanisms like angiogenesis or tumor growth.

Finally, results of our Imatinib intervention studies may have important implications for understanding the link between cancer treatment and incidence of cardiovascular disease (CVD) (Aprile et al., 2013; Bloom et al., 2016; Chai-Adisaksopha et al., 2015; Clarke et al., 2005; Darby et al., 2003; Giles et al., 2011; McGale et al., 2011). Targeting PDGFBR chemically is a potent anti-cancer therapy for leukemias like CML and ALL, and sarcomas like GIST (Druker, 2002). Treatment with Imatinib, although generally well-tolerated, has been associated with peripheral artery occlusive disease, ischemic heart disease, and ischemic cerebrovascular disease (Giles et al., 2013; Hochhaus et al., 2016; Kalmanti et al., 2015; Kim et al., 2013; Larson et al., 2014), although there is no recommendation to exclude its use as a first-line treatment (Steegmann et al., 2016). One can speculate that the increased risk of cancer survivors for CVD is due in part to MI or stroke resulting from destabilization of the $ACTA2^{+}$ and SMC-rich fibrous cap, which we show requires sustained PDGFBR signaling. Particularly concerning is that treatment of our advanced atherosclerotic mice with Imatinib resulted in markedly premature death in spite of the dosage being within the level shown to be well-tolerated not only in humans but also non-atherosclerotic mice (Pouwer et al., 2018; Reber et al., 2017; Rossi et al., 2010). In fact, high doses of Imatinib in mice may represent a novel mechanism of murine plaque rupture and stroke.

Taken together, our data suggest that it is worth at least reexamining the criteria that determines which patients receive Imatinib and other RTK inhibitors, and possibly, any anti-cancer treatment. It also shows for the first time in vivo that PDGFBR signaling is an indispensable cog in the protective machinery that typifies a stable atherosclerotic lesion. We hope that data herein urges the field to reevaluate the idea that therapies should be almost exclusively aimed at preventing progression of lesions, and shift to attempting to stabilize lesions that have already formed and are most likely to rupture.

V. Acknowledgements

Authors want to thank DG and BGD for being a sounding board for experiments and ideas. AW and MB for their support in histology. AHS and RAD for their help with mouse work. RAB for editing assistance. SK for data collection and analysis.

AACN conducted all experiments and was primary writer of the manuscript. OAC provided guidance throughout the project and helped with analysis and editing of the manuscript. GKO supervised the entire project and had a major role in experimental design, data interpretation, and writing of the manuscript.

VI. Figures

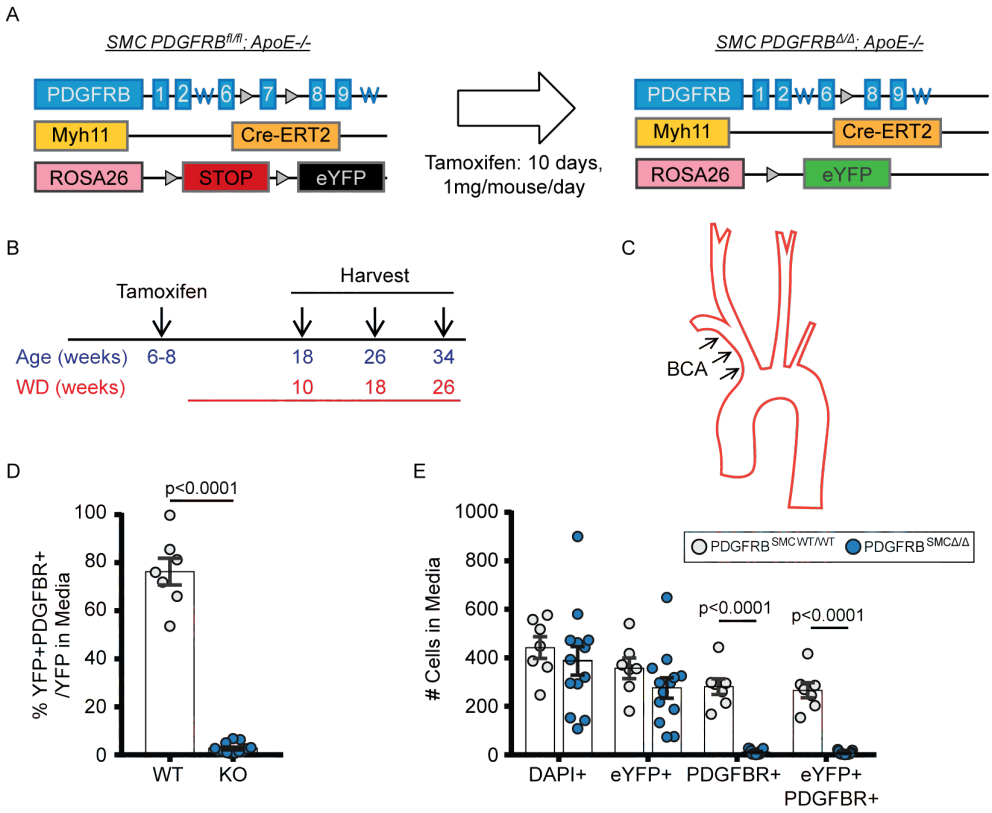

Supplemental Figure 1

Generation and validation of SMC-specific conditional PDGFBR KO SMC lineage tracing mice. (**A**) Myh11-CreER^{T2}/Rosa Flox-Stop/eYFP; Apoe$^{-/-}$ mice were crossed with a PDGFRB-Flox mouse to generate PDGFRB Fl/Fl and WT/WT animals. Heterozygote animals were bred as follows: PDGFRB Fl/WT; Myh11-CreER^{T2}/Rosa Flox-Stop/eYFP; Apoe$^{-/-}$. Littermate WT controls were used in all experiments. (**B**) Mice were injected with tamoxifen at 6-8 weeks of age and prior to the onset of Western diet feeding. Mice were harvested 10, 18, and 26 weeks later to assess different stages of lesion development. (**C**) Analyses were conducted on the brachiocephalic artery (BCA), at multiple locations past the aortic arch in order to assess patterns across the entire region. (**D**) Quantification of IF staining at 18 weeks of WD in the media of BCA lesions showed efficient KO of PDGFBR in >94% of SMC. (**E**) PDGFBR KO in SMC is not associated with decreases in the total number of DAPI^{+} or eYFP^{+} cells (SMC) in the media, but there was a significant reduction in the total number of PDGFBR^{+} cells and eYFP^{+} PDGFBR^{+} cells. Graphs were analyzed using Mann-Whitney U test, error bars represent mean ± SEM.

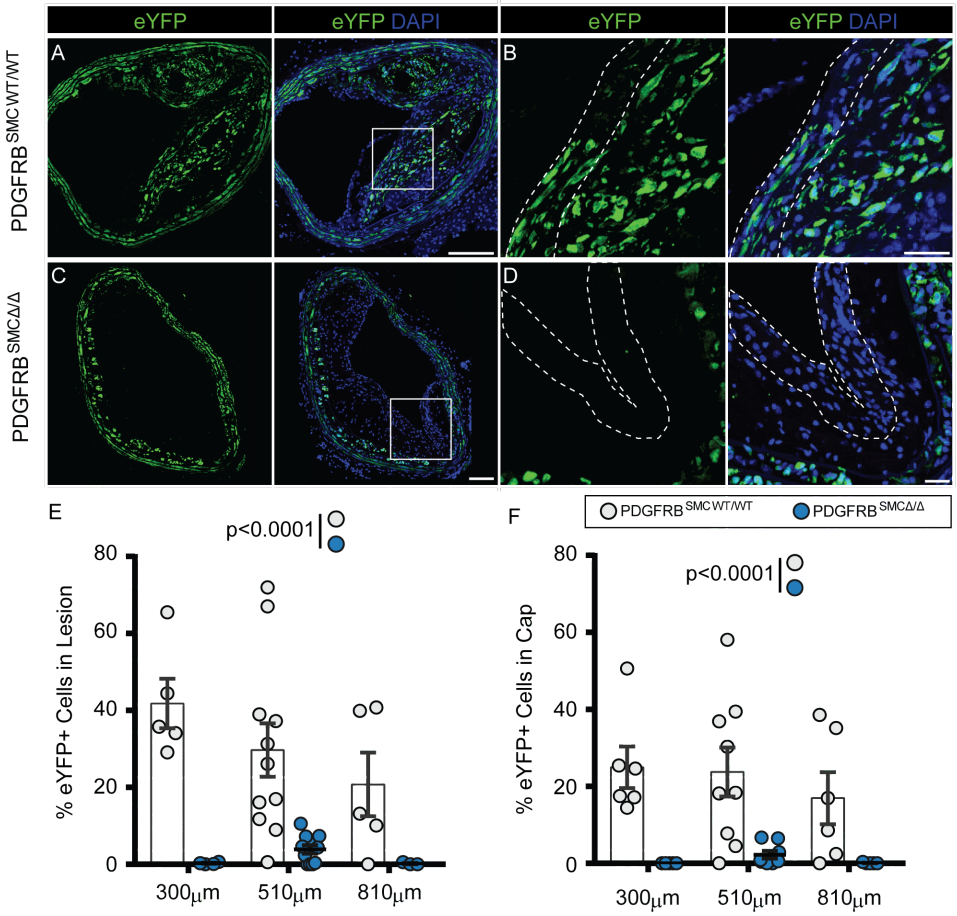

Figure 1

SMC-PDGFBR KO resulted in marked impairment of SMC investment into BCA lesions and the fibrous cap following 18 weeks of WD feeding. BCA lesions of PDGFBR WT and KO litter-mate mice fed WD for 18 weeks were harvested and analyzed for SMC content. (**A**) PDGFBR WT mice exhibited robust SMC accumulation within the lesion and (**B**) fibrous cap, outlined by dashed lines. (**C**) PDGFBR KO mice showed greatly reduced numbers of SMC within the lesion and (**D**) fibrous cap. Quantification of single cells counting of eYFP/DAPI within the lesion (**E**) and fibrous cap (**F**) at three locations. Scale bar: 100μm (**A,C**) or 20μm (**B,D**). X-axis values represent distance past the aortic arch. Graphs were analyzed using two-way ANOVA, error bars represent mean ± SEM.

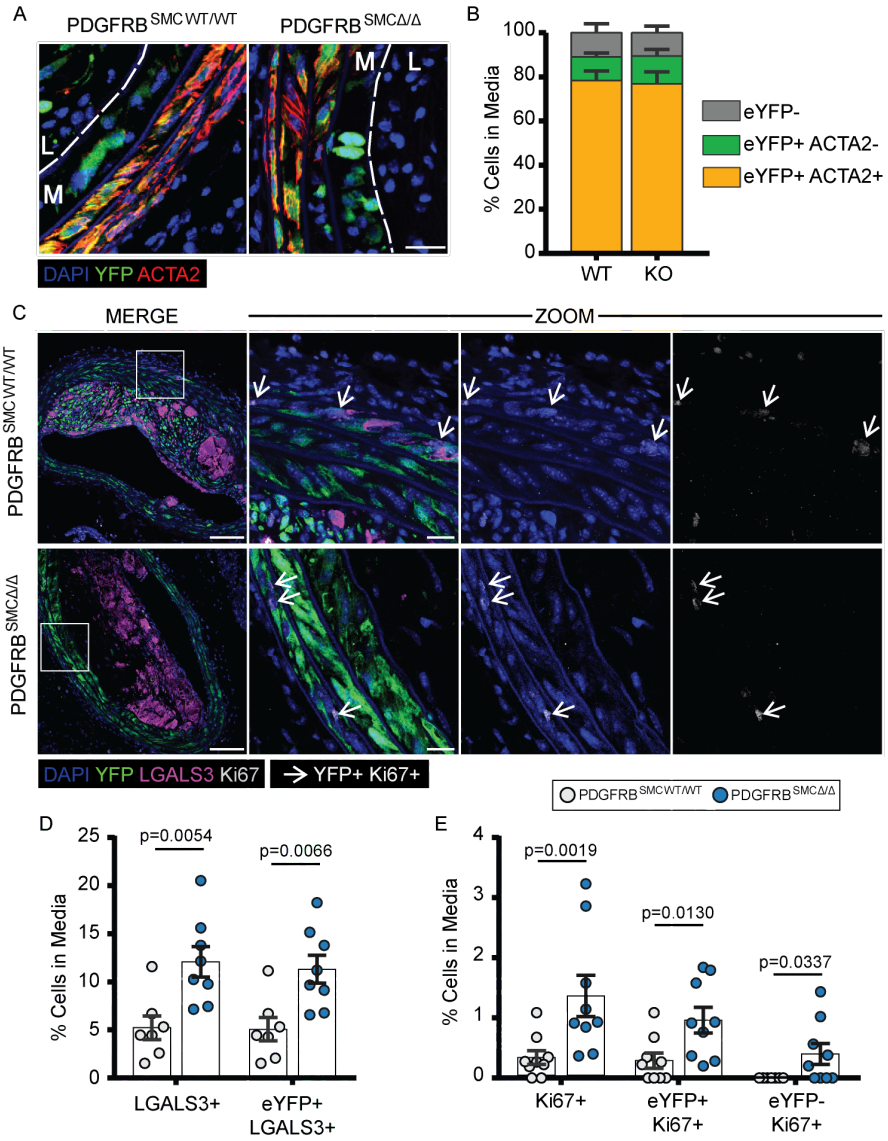

Supplemental Figure 2

SMC-PDGFBR KO did not reduce dedifferentiation, phenotypic modulation or proliferation of medial SMC following 18 weeks of WD. (**A**) Representative image of media of the BCA of PDGFBR$^{SMCWT/WT}$ and PDGFBR$^{SMCΔ/Δ}$ mice show ACTA2 downregulation in the innermost layer of the media. (**B**) Quantification of (**A**). (**C**) Representative image of Ki67 and LGALS3 staining in eYFP^{+} SMC in the media. (**D**) Quantification of SMC phenotypic modulation to an LGLAS3^{+} state. (**E**) Quantification of Ki67 expression in the media, representing proliferation. Scale bar: 100μm (whole lesion) or 20μm (zoom). Graphs were analyzed using Mann-Whitney U test, error bars represent mean ± SEM.

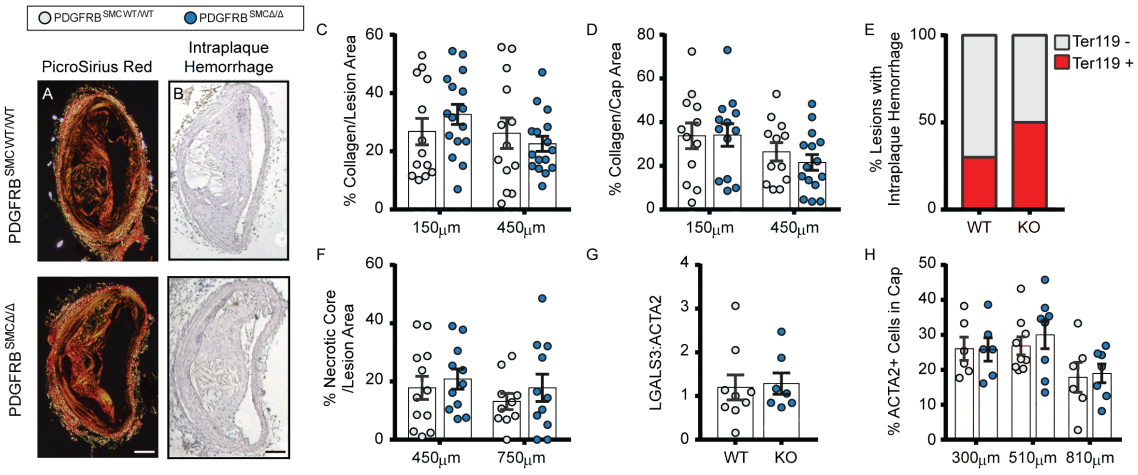

Figure 2

SMC PDGFBR KO did not alter multiple indices of plaque stability following 18 weeks of WD feeding. Representative images of (**A**) PicroSirius Red staining representing collagen deposition and (**B**) Ter119 staining for Intraplaque hemorrhage within PDGFBR$^{SMCWT/WT}$ and PDGFBR$^{SMCΔ/Δ}$ mice after 18 weeks of WD. No significant changes were observed for collagen deposition within the lesion (**C**) and fibrous cap (**D**), percent of lesions with intraplaque hemorrhage (**E**) nor necrotic core area (**F**). The ratio of LGALS3:ACTA2 cells was unchanged within the fibrous cap (**G**), as was the total percentage of ACTA2^{+} cells (**H**). Scale bar: 100μm. X-axis values represent distance past the aortic arch. Graphs were analyzed using two-way ANOVA, except in G, which was analyzed by Mann-Whitney U test. Error bars represent mean ± SEM.

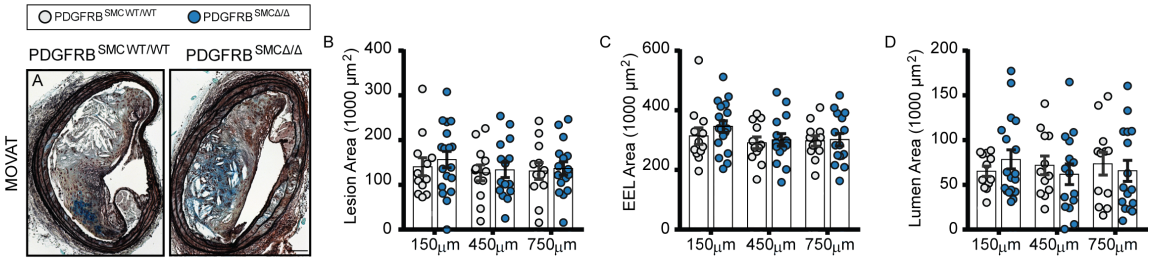

Supplemental Figure 3

SMC-PDGFBR KO did not result in differences in BCA lesion size or remodeling indices after 18 weeks of WD. (**A**) MOVAT representation of PDGFBR$^{SMCWT/WT}$ and PDGFBR$^{SMCΔ/Δ}$ mice after 18 weeks of WD. (**B**) Lesion, (**C**) external elastic lamina (EEL), (**D**) or lumen area were not significantly changed at three locations. Scale bar: 100μm. X-axis values represent distance past the aortic arch. Graphs were analyzed using two-way ANOVA, error bars represent mean ± SEM.

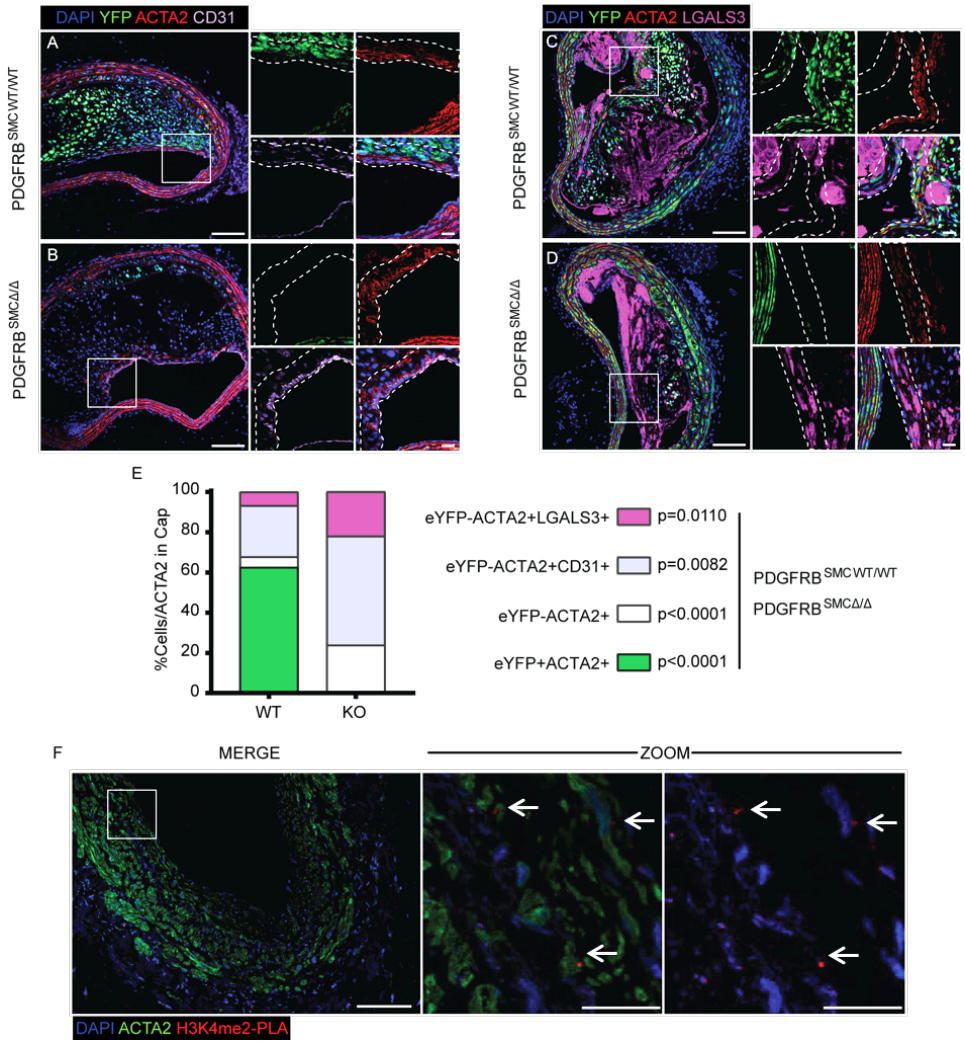

Figure 3

SMC-PDGFBR KO resulted in marked increases in the fraction of ACTA2^{+} fibrous cap cells derived from EndoMT and MMT rather than from pre-existing SMC following 18 weeks of WD feeding. Representative images of advanced BCA lesions from PDGFBR$^{SMCWT/WT}$ and PDGFBR$^{SMCΔ/Δ}$ mice following 18 weeks of WD feeding. Results show that whereas the majority of ACTA2^{+} fibrous cap cells are eYFP^{+}, up to 40% are derived from EndoMT (**A**) or MMT (**C**), with these contributions increasing dramatically following SMC-PDGFBR KO (**B,D**). (**F**) Representative human lesion showing ACTA2 are PLA^{+} (white arrows) and PLA^{-} (PLA = H3K4me2 on the Myh11 promoter), i.e. a portion are not derived from SMC. Data were obtained by rigorous single-cell counting for co-localization of DAPI, eYFP, ACTA2, and CD31 (Lilac) or LGALS3 (Violet) or PLA. Scale bar: 100μm (**A,C,F** merge) or 20μm (**B,D,F** zoom). Graphs were analyzed using Mann-Whitney U test.

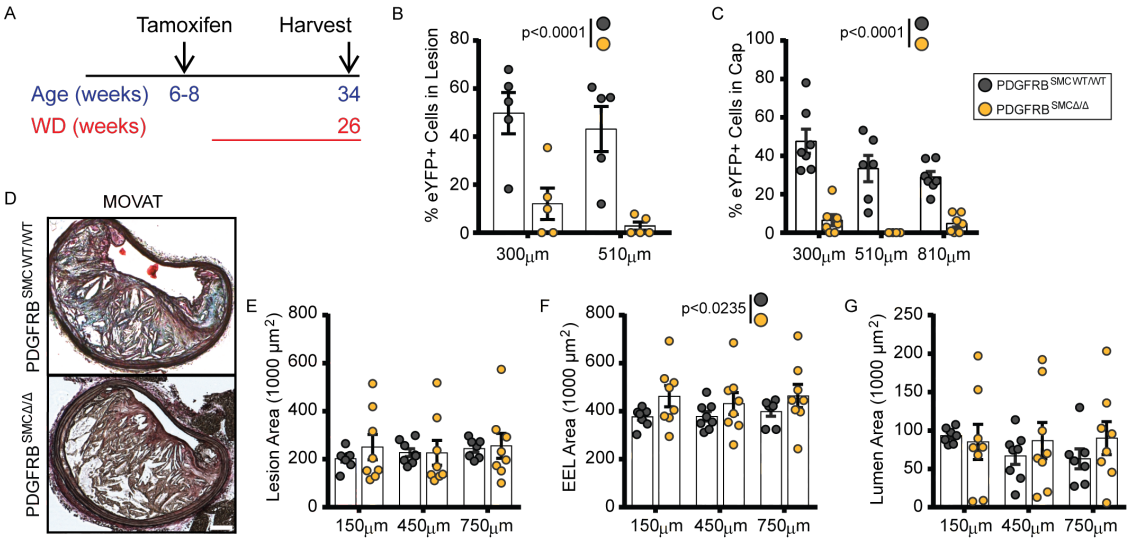

Supplemental Figure 4

SMC-PDGFBR KO also resulted in marked impairment of SMC investment into BCA lesions and the fibrous cap following 26 weeks of WD feeding. Similar to at 18 weeks of WD, at 26 weeks of WD (Schematic in **A**) PDGFBR$^{SMCWT/WT}$ mice exhibited robust SMC accumulation within the lesion (**B**) and fibrous cap (**C**) and this was reduced >90% in PDGFBR$^{SMCΔ/Δ}$ mice. Representative MOVAT images (**D**) and quantification of Lesion (**E**) EEL (**F**) and lumen areas (**G**) Only EEL area is significantly increased between WT and KO animals over the entire BCA. X-axis values represent distance past the aortic arch. Scale bar: 100μm. Graphs were analyzed using two-way ANOVA, error bars represent mean ± SEM.

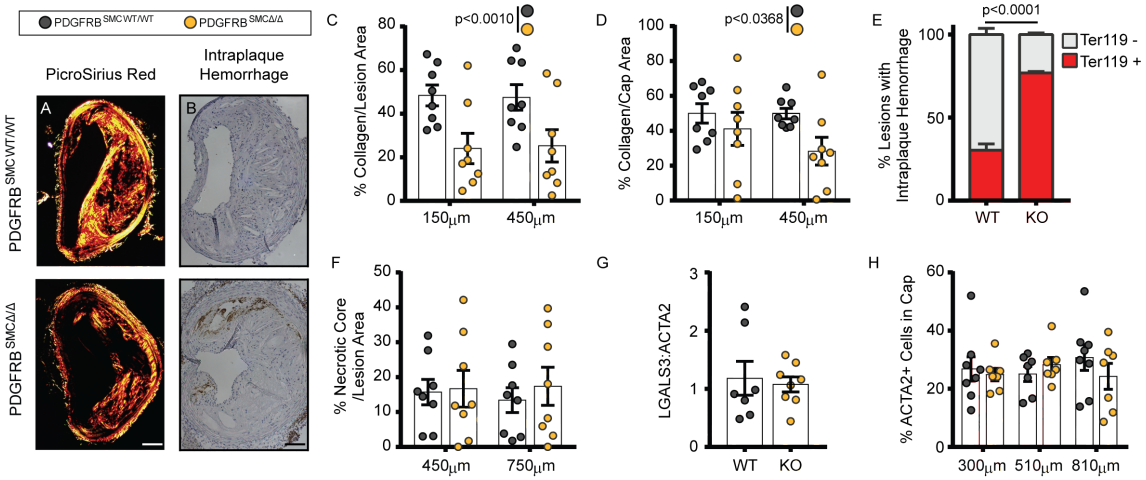

Figure 4

SMC PDGFBR KO was associated with evidence of reduced plaque stability following 26 weeks of WD feeding. (**A**) PicroSirius Red staining representing collagen deposition and TER119 staining for Intraplaque hemorrhage (**B**) within PDGFBR$^{SMCWT/WT}$ and PDGFBR$^{SMCΔ/Δ}$ mice after 26 weeks of WD. Collagen deposition within the lesion (**C**) and fibrous cap (**D**) were both significantly decreased. Percent of lesions with intraplaque hemorrhage (**E**) was significantly increased (3 locations assessed) and necrotic core area (**F**) was unchanged between PDGFBR$^{SMCWT/WT}$ and PDGFBR$^{SMCΔ/Δ}$ mice. (**G**) The ratio of LGALS3:ACTA2 cells was unchanged within the fibrous cap, as was (**H**) the total percentage of ACTA2^{+} cells. Scale bar: 100μm. X-axis values represent distance past the aortic arch. Graphs were analyzed using two-way ANOVA, error bars represent mean ± SEM.

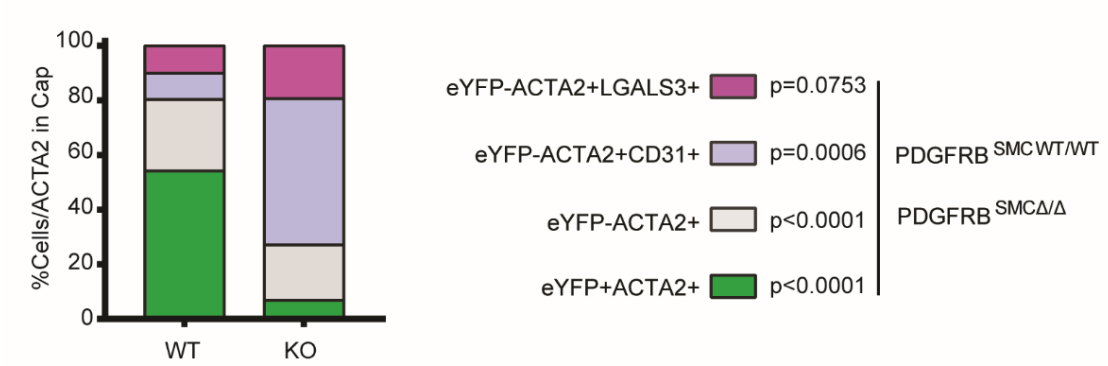

Supplemental Figure 5

At 26 weeks of WD, SMC-PDGFBR KO resulted in similar marked increases in the fraction of ACTA2^{+} fibrous cap cells derived from EndoMT and MMT rather than from pre-existing SMC. Similar to at 18 weeks of WD, at 26 weeks of WD PDGFBR WT mice show about 60% of ACTA2^{+} cells derived from SMC (green) and a basal level of EndoMT (lilac) and MMT (violet), and uncharacterized origin (grey). The percentage of non-SMC derived ACTA2^{+} cells from EndoMT significantly increases after PDGFBR mediated loss of SMC. Graphs were analyzed using Mann-Whitney U test.

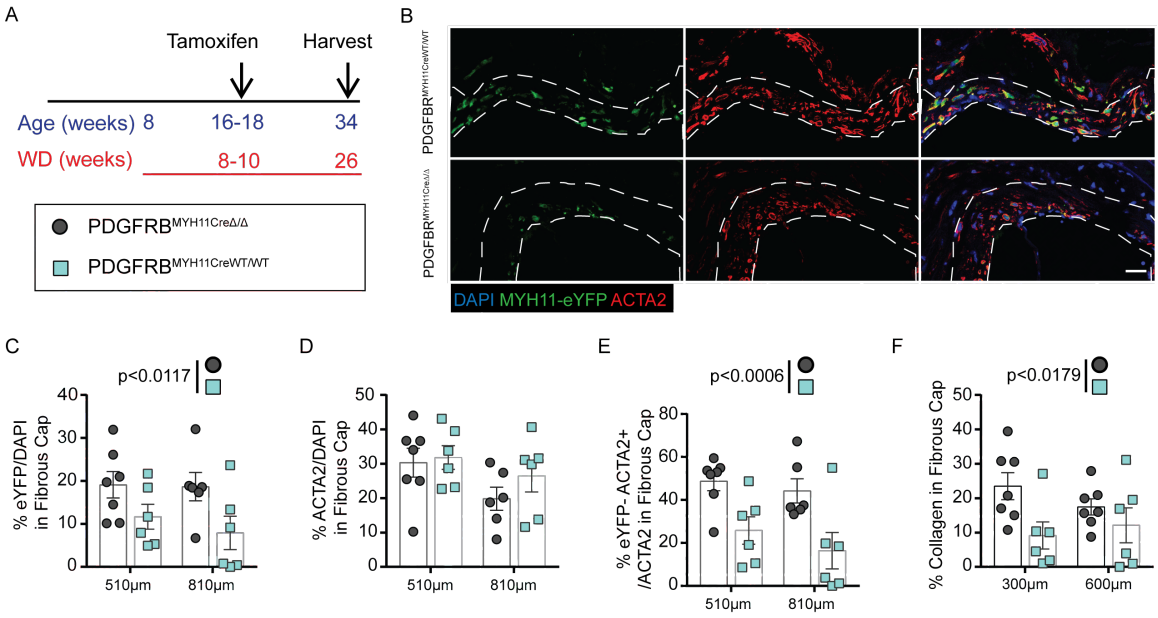

Figure 5

Persistent PDGFBR signaling in MYH11-Cre cells within advanced lesions maintains ACTA2$^+$ expression and collagen deposition in the fibrous cap. (**A**) Schematic of tamoxifen administration in advanced lesions, which results in PDGFBR KO and/or eYFP labelling in the subset of cells expressing MYH11-Cre, located mainly within the media and fibrous cap. Lesions were harvested eight weeks after last tamoxifen injection. Representative images of the fibrous cap of PDGFBR WT (**B**) and KO (**C**) lesions, with the fibrous cap outlined by dashed lines. Single cell counting of the fibrous cap shows: (**D**) KO of PDGFBR in MYH11Cre$^+$ cells results in loss of eYFP$^+$ cells. (**E**) There were no changes in the percentage of ACTA2$^+$ cells. (**F**) PDGFBR KO resulted in decreased eYFP$^+$ ACTA2$^+$ cells per total ACTA2$^+$ cells in the fibrous cap as well. (**G**) Collagen deposition was significantly decreased within the fibrous cap after PDGFBR KO. Scale bar: 20μm. X-axis values represent distance past the aortic arch. Graphs were analyzed using two-way ANOVA, error bars represent mean ± SEM.

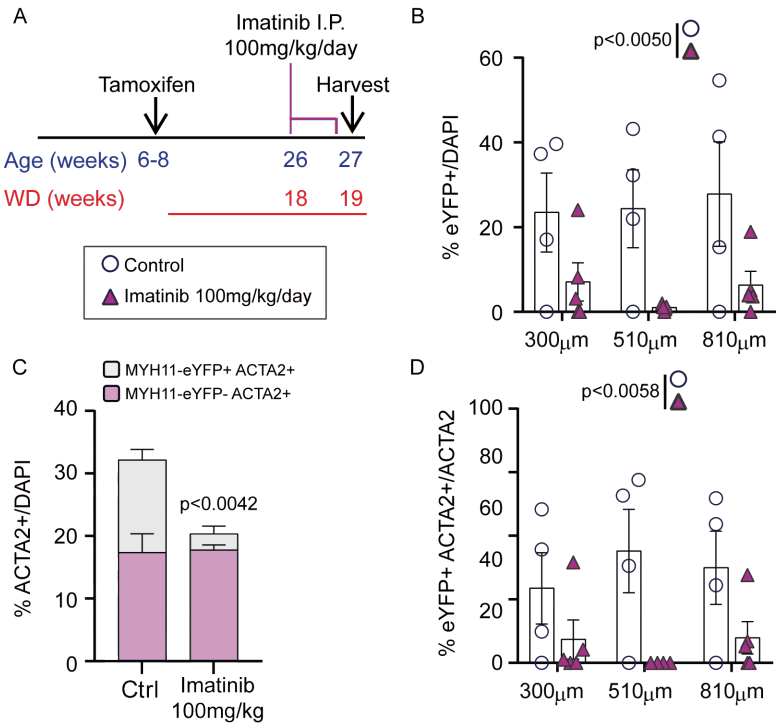

Figure 6

Global PDGFBR antagonism resulted in significantly decreased SMC and total ACTA2$^+$ cell coverage in the lesion and cap. (**A**) Schematic of experimental design detailing once daily injections of Imatinib to mice fed WD for 18 weeks. 100mg/kg/day of Imatinib resulted in significant reductions in eYFP$^+$ cells (**B**), total ACTA2$^+$ cells (**C**), and SMC-derived ACTA2$^+$ cells (**D**) within the fibrous cap. X-axis values represent distance past the aortic arch. Graphs were analyzed using two-way ANOVA, error bars represent mean ± SEM.

Chapter 4

Additional Studies

I. Lessons from Early Lesions

PDGFBR is Required for SMC Investment throughout Atherosclerosis

The bulk of our studies are performed in advanced atherosclerosis in the BCA, as these lesions exhibit multiple characteristics of those found in humans. We performed a time course experiment to determine patterns of SMC accumulation in BCA lesions with and without SMC-PDGFBR KO. SMC investment at 18 and 26 weeks of WD was impaired, which could be because we were sampling late time points. Assessing the 26 week time point suggests that there is not a delayed migratory response. However, was loss of SMC due to early investment into the lesions and subsequent apoptosis meaning we looked too late?

In order to determine if SMC loss is due to loss of initial investment within the lesion, we had to assess an earlier time point. In BCA lesions, 10 weeks of WD seems to mark a turning point from fatty streak to advanced lesions as about 60% of the mice exhibited SMC accumulation and 40% exhibited characteristics of a fatty streak. We found that only one mouse (of seven) showed any SMC investment after SMC-PDGFBR KO, suggesting SMC fail to invest at all stages.

SMC Localize to the Fibrous Cap before Entering the Lesion Core

In Chapter 3, we provide evidence that SMC from the media must migrate, likely toward a chemotactic signal, like PDGF (Grotendorst et al., 1981), and proliferate to populate the lesion. The major local sources of PDGF in the lesion are MΦ and EC (Raines, 2004). The question is, do SMC move toward PDGF-secreting ECs in the fibrous cap and then into the lesion core, or toward PDGF-secreting MΦ in the lesion core before continuing through the lesion to populate the fibrous cap? The route SMC take and the phenotypes they exhibit on the way are particularly important understanding the primary responses of SMC play in the progression and pathology of the lesion.

In early lesions of SMC-lineage tracing mice (after 10 weeks of WD), evidence suggests that SMC first localize to the sub-endothelial space before subsequently accumulating within the lesion (Figure 1). This pattern is consistently observed in the BCA of mice other MYH11-driven lineage tracing models used in the lab,[6] and is similar to published accounts of the initial path SMC take in the aortic root (Misra et al., 2018). However, rigorous time course experiments are necessary to be certain similar to those performed in the aortic root (Misra et al., 2018).

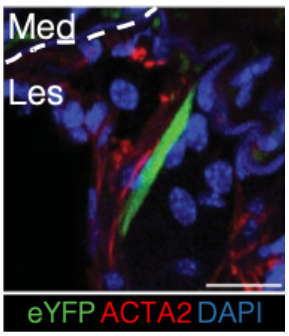

Figure 1

A SMC enters the lesion from the shoulder. Scale bar: 20μm.

Early ACTA2^{+} Cells in the Lesion are Not Derived from SMC

In early SMC-lineage tracing lesions that do not yet have robust SMC accumulation, there are ACTA2^{+} cells that are mostly located in the sub-endothelial space, corresponding to the future site of a fibrous cap (Figure 2). These ACTA2^{+} cells are eYFP^{-}, suggesting they derive from a non-SMC derived source. We have further evidence that these cells are not derived from EC either, as EC-lineage tracing (EC-eYFP) mice show most ACTA2^{+} cells are EC-eYFP^{-} at 10 weeks of WD (Figure 2).[7] We cannot be certain without rigorous lineage tracing, but these results are highly suggestive of MΦ undergoing MMT, as they stain positively for LGALS3 (data not included). In SMC-rich early lesions, SMC have largely replaced the initial investment of non-SMC ACTA2 expression in the lesion, similar to 18 weeks of WD. This is evidence that non-SMC (and likely MΦ) play a direct functional, if underappreciated, role in early fibrous cap development. These early mesenchymal transitions are important to understanding the processes that lead to development of a stable or an unstable atherosclerotic lesion.

[6] Unpublished data from Katie Owsiany
[7] The EC-eYFP mice use a VECadherin-CreER^{T2} promoter (outlined in Methods)

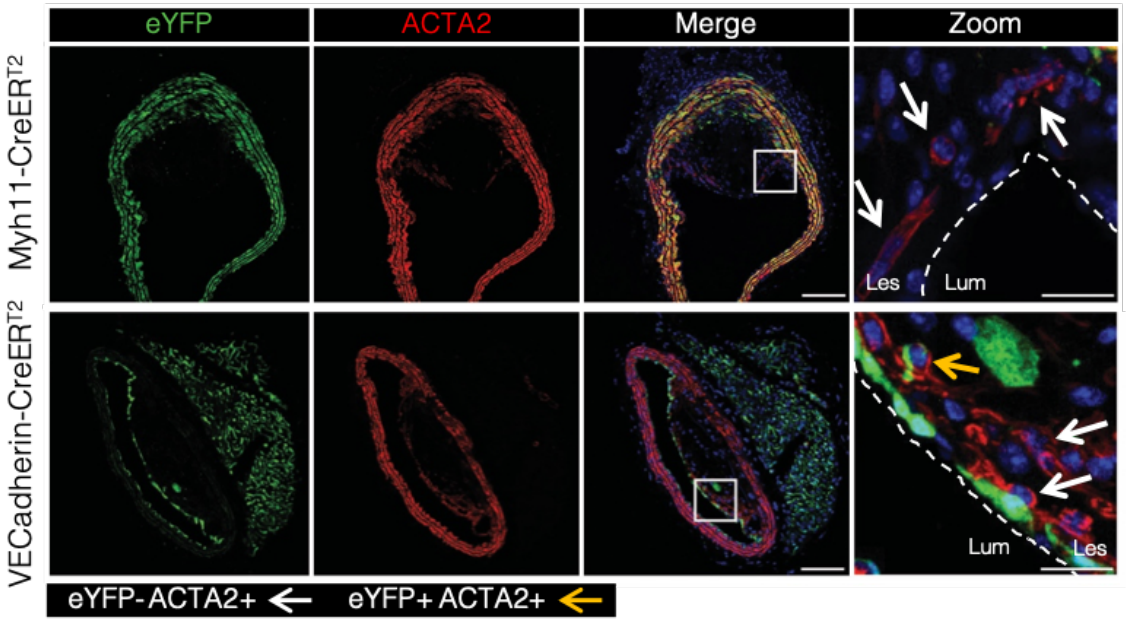

Figure 2

After 10 weeks of WD, lesions demonstrate ACTA2^{+} cells in the sub-endothelial space. The majority of these cells are not derived from SMC (**top**) or EC (**bottom**) based on rigorous lineage tracing. White arrows: eYFP^{-} ACTA2^{+}. Yellow arrows; eYFP^{+} ACTA2^{+}. Scale bar: 100μm or 20μm (zoom).

II. A Method of Dual-Lineage Tracing

Using BMT for BMDC-Lineage Tracing in Atherosclerosis

The thorn in my side throughout the studies in Chapter 3 was that in order to determine the contribution of EC and MΦ to the ACTA2 population in the fibrous cap in our SMC-lineage tracing mice, we had to rely on the very thing we criticized: marker gene staining. We attempted to confirm MMT by performing a series of BMT experiments in SMC-lineage tracing to differentially tag both SMC (eYFP) and BMDCs (tdTomato). However, for faithful BMDC-lineage tracing, ablation of the existing bone marrow with lethal doses of gamma irradiation was required. This resulted in complete loss of SMC in BCA lesions (Chapter 2, Figure 2), which was germane to the studies in Chapter 2 but posed a problem when trying to assess the normal contribution of MMT to the fibrous cap.

With a bit of ingenuity, we realized we could exploit the fact that over four years, three SMC-lineage tracing lines, and careful examination, we never detected a single SMC in any of the BCA lesions we examined after lethal gamma irradiation and BMT. Could we instead demonstrate how EC and BMDCs contribute to the lesion populations and the fibrous cap after SMC loss? Essentially, instead of relying on marker staining to identify the origins of the non-SMC derived ACTA2$^+$ cells in the fibrous cap as done in Chapter 3 (Figure 3), could we use EC-lineage tracing with BMT to directly assess the relative contribution of EndoMT and MMT in lesions that lacked SMC accumulation but had ACTA2$^+$ cells, as in the case after lethal irradiation or SMC-PDGFBR KO (Figure 3)?

EndoMT Comprise the Majority of ACTA2$^+$ Lesion Cells after Irradiation and BMT

We performed BMT experiments in EC-lineage tracing (EC-eYFP) mice with simultaneous BMDC-lineage tracing (tdTomato).[8] After 18 weeks of WD, we observed that of the ACTA2$^+$ cells, 12% were tdTomato$^+$ and 70% were EC-eYFP$^+$. In non-irradiated controls, we observe 20% of ACTA2$^+$ cells are EC-eYFP$^+$ in the fibrous cap, which is

---

[8] Unpublished data from: *"IL1-dependent Endothelial to Mesenchymal Transitions are an Important Source of ACTA2$^+$ Fibrous Cap Cells in Late Stage Atherosclerosis"*, Richard A. Baylis, Xenia Bradley, Alexandra A.C. Newman, Gabriel F. Alencar, Olga A. Cherepanova, Gary K. Owens. Manuscript in preparation for submission to *Circulation Research*, May 2019

representative of the typical contribution of EndoMT (Figure 3). We are not able to assess the contribution of BMDCs to the ACTA2 population in non-irradiated lesions, but we expect their contribution to be between 10 and 20% based on marker staining analysis (see Chapter 3, Figure 3). This data shows that EC, SMC, and MΦ have overlapping roles in atherosclerosis. Recall from Chapters 2 and 3 that these mesenchymal transitions can temporarily contribute to stability, suggesting that increasing mesenchymal transitions as a whole may be a novel therapeutic target.

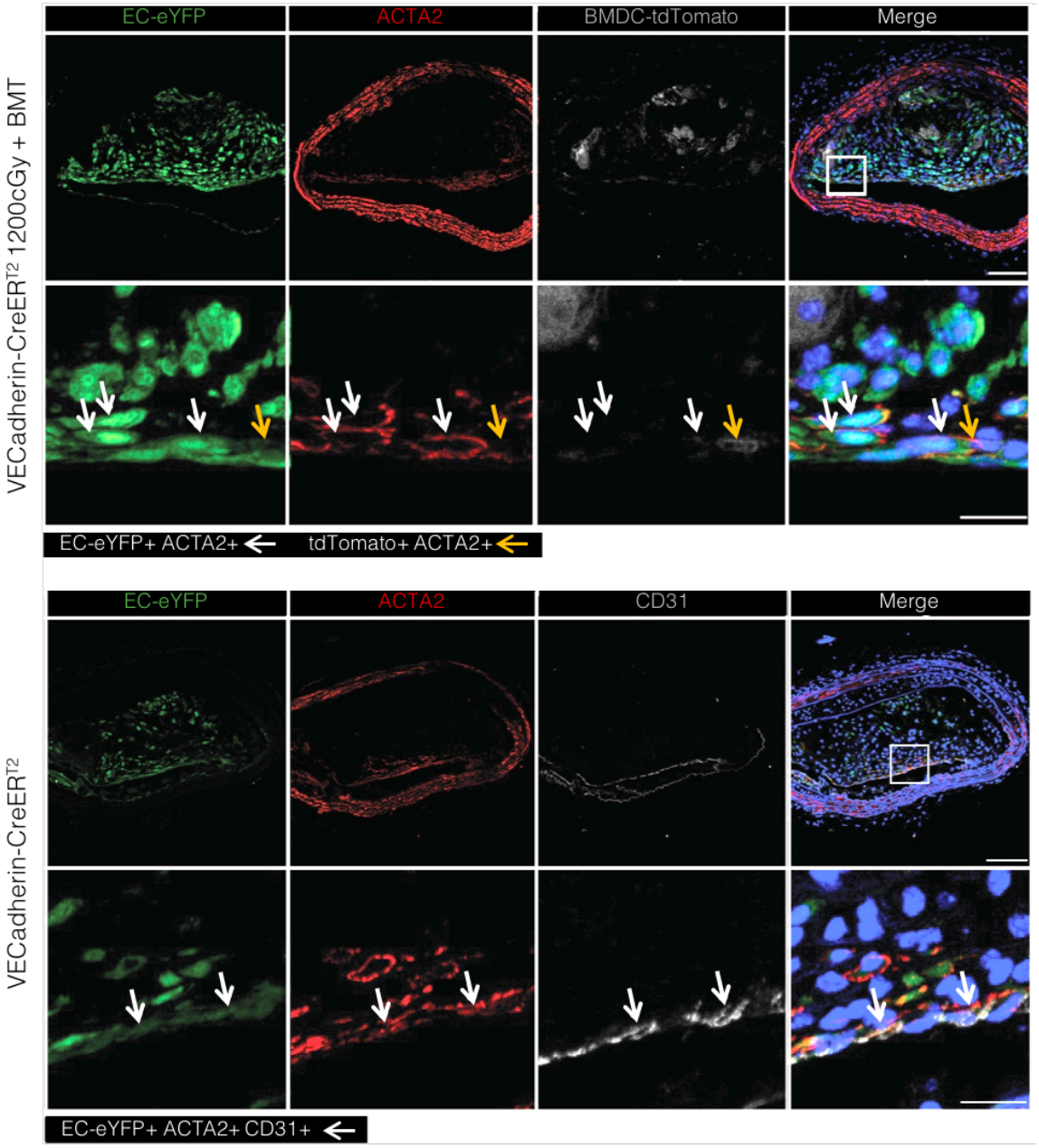

Figure 3

(**Top**) EC-eYFP cells comprise 70% of the ACTA2^{+} cells in the fibrous cap, denoted by white arrows, and BMDCs-tdTomato cells contribute about 12%, denoted by yellow arrows, after lethal irradiation and BMT. (**Bottom**) EC-eYFP^{+} cells normally contribute 20% to the ACTA2^{+} cells in the fibrous cap, white arrows. EC-eYFP^{+} CD31^{+} cells comprise 75% of the total CD31 cells in the fibrous cap. Scale bar: 100μm or 20μm (zoom).

III. Transcriptional Profiles of Atherosclerosis

Bulk RNA-seq Describes the Disease

In order to better understand the effects of SMC-PDGFBR KO on advanced lesion pathology, we performed bulk RNA-seq analyses on the lesion and underlying media of the right and left carotid, BCA, and part of the aortic arch (Figure 4). These bulk RNA-seq analyses on tissue containing many different cell types makes it nearly impossible to ascertain which cells are responsible for any particular change or to determine small effects due to inadequate sensitivity of detection. However, because we assess total differences initiated only by loss of PDGFBR in SMC, we gain powerful insights into the downstream mechanisms and the effects on the lesion as a whole. In essence, these RNA-seq analyses allow us to determine the totality of the differences in transcription of all cells in the lesion and media between WT and KO animals.

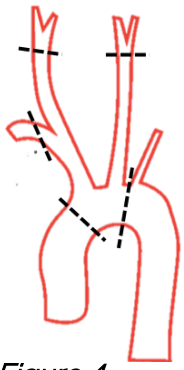

Figure 4

Vessel regions excised for RNA-seq

Metabolic Pathways are Highly Dysregulated

We performed KEGG pathway analysis and were surprised to find that nearly all of the top upregulated pathways in SMC-PDGFBR KO mice were related to metabolism (Table 1). This suggests that one of the direct or indirect effects of SMC-PDGFBR KO is dysregulated metabolism in multiple cell types. This is important in the context of lesion pathology because altered cellular metabolism, especially increased glucose and decreased fatty acid usage correlates with and may be a biomarker of instability in high-risk vs. stable human lesions (Tomas et al., 2018) based on traditional criteria.

We found certain genes associated with high-risk lesions that were upregulated in the KO compared to the WT based on our RNA-seq analysis. These include LDHA, ALDOA, and ENO1, which are all enzymes involved in glycolysis and lactic acid synthesis (see Appendix I for full list of significantly regulated genes). The fact that these pathways and genes are upregulated in SMC-PDGFBR KO compared to the WT lesions suggests

that these changes are occurring in non-SMC, although with the caveat that we include the underlying SMC-rich media in these preparations.

Single Cell RNA-seq Describes the Lesion

In order to better parse out the changes in individual cell populations, we performed single cell RNA-seq analyses on SMC-PDGFBR WT and KO lesions of the BCA, carotid, and aortic arch. This required careful separation of the lesion from the underlying media and flow sorting for $eYFP^+$ and $eYFP^-$ cells. Due to unforeseen technical difficulties, there were low reads in the KO sample and these studies should be repeated.

Using tSNE plots from the $eYFP^+$ and $eYFP^-$ sorted libraries from the WT mice, we determined that cell populations fell into ten distinct clusters (Figure 5, Appendix II for cluster profiles). Cluster 7, comprised mostly of $eYFP^+$ cells, was highly enriched for traditional SMC genes including MYH11 and ACTA2, and likely represents the population of SMC in the fibrous cap. The $eYFP^-$ cells largely contributed to two clusters associated with genes traditionally characteristic of MΦ and monocytes (4 and 5), one of EC (6), one of T-cells (9). The five remaining clusters were highly enriched for multiple ECM genes (COLs, MMPs), chondrocyte and osteocyte markers (DCN, LUM, BMP1, CHAD, SPP1), and stem cell markers like SCA1 (0-3, 8). Of these, cluster 0 is comprised of $eYFP^+$ and $eYFP^-$ cells and 1-3 and 8 are comprised mostly of $eYFP^+$ cells.

Overlaying the KO $eYFP^-$[9] library over the WT tSNE plot, we observed that KO cells were scattered throughout the $eYFP^+$ and $eYFP^-$ clusters from the WT, save cluster 7. This suggests that non-SMC cannot fully differentiate into SMC, however, they do seem to be able to adopt multiple other characteristics of phenotypic states that SMC transition to in the lesion (e.g. ECM synthesis). There is prior evidence that BMDCs do not express $MYH11^+$ in the lesion (Iwata et al., 2010), showing that at least BMDCs cannot fully switch to a SMC-like cell in the lesion. This may help explain why lesions after lethal irradiation and SMC-PDGFBR KO after 26 weeks of WD exhibited multiple indices of lesion instability despite persistent $ACTA2^+$ coverage in the fibrous cap.

---

[9] Because of the lack of SMC in the lesion, we only ran $eYFP^-$ cells from the KO lesions

A particular favorite application of the single cell RNA-seq cluster analysis is the pseudotime function. Provided that multiple different SMC-derived phenotypes are present (as in atherosclerosis), this analysis delineates the potential transitions of SMC based on transcriptional similarities. This paints a picture of how SMC phenotype might change overtime and depending on the local environment. Using pseudotime analysis, it seems that SMC must go through a transition state (exhibited by LGALS3 expression) before becoming chondrocyte-like.[10] To determine stabilizing or destabilizing phenotypes, future studies could selectively ablate cells in a particular cluster (based on transcriptional targets) to determine effects on lesion stability and/or phenotypic modulation.

[10] Unpublished data by Katie Owsiany

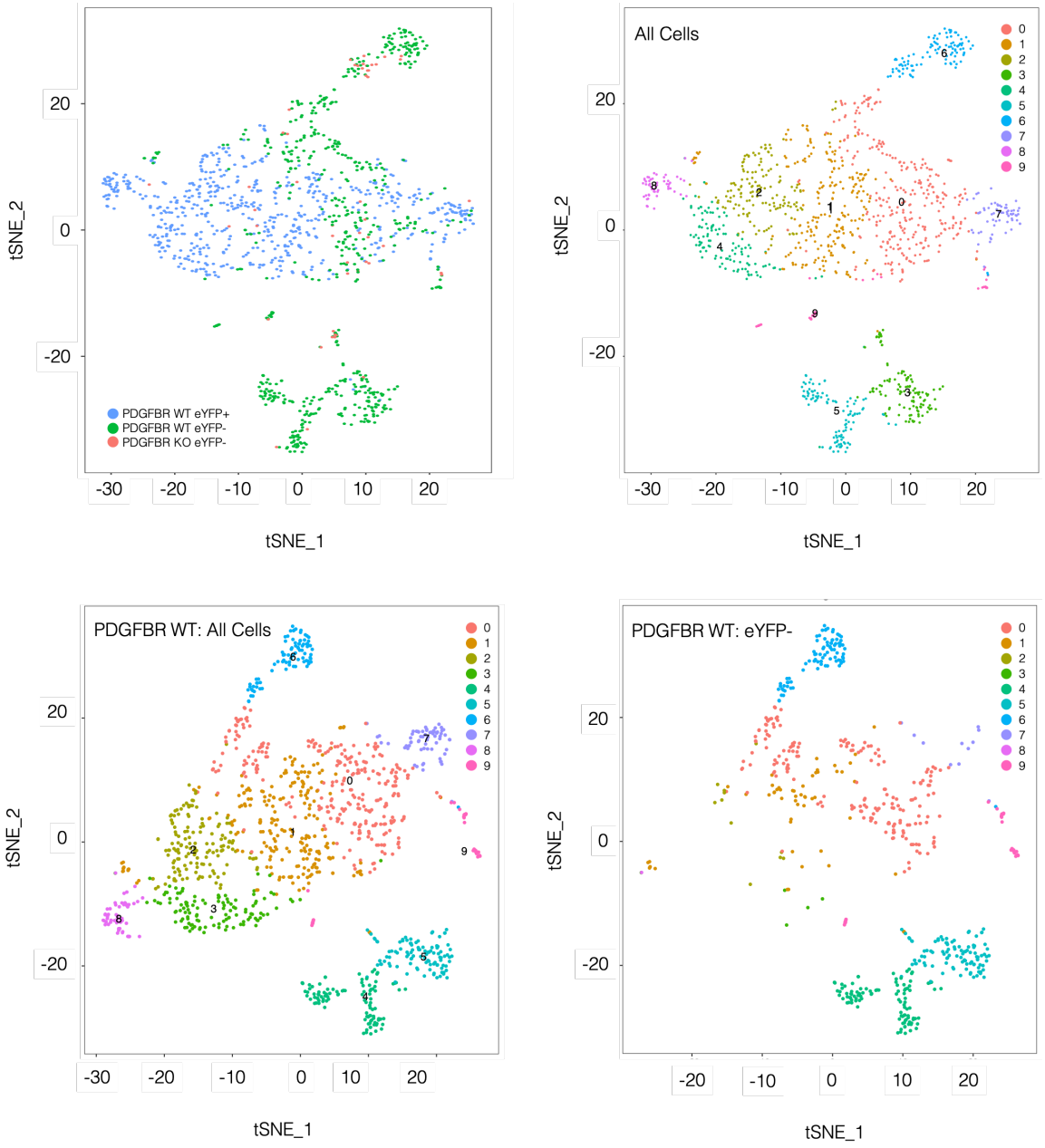

Figure 5

tSNE plots of single cell RNA-seq clusters from SMC-PDGFBR WT and KO lesions. (**Top**) Clustering of all cells. (**Bottom**) Contribution of SMC-PDGFBR WT lesion cells to clusters (**left**) and eYFP^{-} cells to cluster (**right**).

Table 1: Upregulated KEGG pathways in PDGFBR KO vs. WT Mice

KEGG Pathway	P-Value	Benjamini	FDR
Metabolic pathways	1.40E-27	2.60E-25	1.80E-24
Carbon metabolism	4.20E-20	3.90E-18	5.20E-17
Biosynthesis of antibiotics	4.70E-19	2.90E-17	5.80E-16
Citrate cycle (TCA cycle)	3.40E-16	1.50E-14	4.10E-13
Fatty acid metabolism	3.50E-15	1.30E-13	4.40E-12
Oxidative phosphorylation	8.80E-15	2.70E-13	1.10E-11
Pyruvate metabolism	1.30E-14	3.50E-13	1.60E-11
Huntington's disease	1.10E-13	2.50E-12	1.40E-10
Parkinson's disease	4.00E-13	8.10E-12	4.90E-10
Propanoate metabolism	8.00E-13	1.50E-11	9.90E-10
Non-alcoholic fatty liver disease (NAFLD)	1.30E-12	2.20E-11	1.60E-09
Alzheimer's disease	2.70E-12	4.00E-11	3.30E-09
Valine, leucine and isoleucine degradation	8.80E-10	1.20E-08	1.10E-06
Fatty acid degradation	2.60E-09	3.40E-08	3.20E-06
Glycolysis / Gluconeogenesis	9.30E-08	1.10E-06	1.20E-04
Peroxisome	1.70E-07	1.90E-06	2.10E-04
AMPK signaling pathway	5.00E-06	5.30E-05	6.10E-03
PPAR signaling pathway	5.80E-06	5.90E-05	7.20E-03
Cardiac muscle contraction	2.60E-05	2.50E-04	3.20E-02
Fatty acid elongation	4.20E-05	3.80E-04	5.10E-02
Glucagon signaling pathway	5.00E-05	4.30E-04	6.20E-02
Butanoate metabolism	5.20E-05	4.30E-04	6.50E-02
Insulin signaling pathway	6.30E-05	5.00E-04	7.80E-02
Biosynthesis of amino acids	1.40E-04	1.00E-03	1.70E-01
Starch and sucrose metabolism	1.40E-04	1.00E-03	1.80E-01
Regulation of lipolysis in adipocytes	6.20E-04	4.30E-03	7.60E-01
Glycerolipid metabolism	6.90E-04	4.60E-03	8.40E-01
Glyoxylate and dicarboxylate metabolism	7.90E-04	5.10E-03	9.70E-01
2-Oxocarboxylic acid metabolism	1.20E-03	7.80E-03	1.50E+00
Adipocytokine signaling pathway	2.50E-03	1.50E-02	3.00E+00
Biosynthesis of unsaturated fatty acids	4.80E-03	2.80E-02	5.70E+00
Fatty acid biosynthesis	5.00E-03	2.80E-02	6.00E+00
Insulin resistance	7.50E-03	4.10E-02	8.90E+00
beta-Alanine metabolism	9.90E-03	5.20E-02	1.20E+01
Lysine degradation	1.10E-02	5.40E-02	1.20E+01
Glycerophospholipid metabolism	1.10E-02	5.30E-02	1.20E+01
Synthesis and degradation of ketone bodies	3.10E-02	1.50E-01	3.30E+01
Tryptophan metabolism	3.30E-02	1.50E-01	3.40E+01
Pentose phosphate pathway	4.20E-02	1.80E-01	4.10E+01

IV. Metabolism in the Lesion

Dysregulated Metabolic Programing Correlates with Lesion Pathology

Metabolism is necessary for every process a cell undertakes including dedifferentiation, migration, proliferation, phenotypic switching, and ECM deposition. What I am suggesting is that all of the functions SMC carry out to stabilize the lesion requires a metabolic shift, which involves the reallocation of input and output to meet the changing energy needs. The impetus in our lab to study metabolic programming of SMC as it relates to atherosclerosis pathology came about when we analyzed bulk RNA-seq studies from five different mouse models and found metabolism pathways to be the most consistently dysregulated in all cases. The models with similar lesion phenotypes also displayed similar RNA-seq profiles, suggesting that dysregulated metabolic pathways were associated with overall decreased indices of lesion stability.[11]

SMC Phenotype and Function Relies on Metabolic Programing

Preliminary studies in the lab have attempted to better understand the mechanisms by which metabolism affects SMC phenotype and function.[12] By stimulating SMC with various cytokines known to induce different phenotypes, we can assess the metabolic capacity of these phenotypic states, as well as the functional output including ECM synthesis. Furthermore, by blocking key enzymes within the metabolic pathways, we can assess the capacity of a cell to phenotypically modulate. These studies allow us to identify potential pathways for SMC phenotypic switching to multiple lesion populations that we can then test in mouse models of atherosclerosis.

Based on the studies in Chapter 3 and the results of the bulk RNA-seq, these studies have initially primarily focused on the SMC to MF switch and subsequent ECM

---

[11] Unpublished data from: "*scRNAseq and dual lineage tracing define SMC phenotypic transitions behind Klf4-driven CAD risk*", Gabriel F. Alencar, Katie Owsiany, Santosh Karnewar, Anh Nguyen, Gamze Bulut, Molly Kelly-Goss, and Gary K. Owens. In preparation for submission to *Nature Genetics,* February 2019

[12] Unpublished data from Vlad Serbulea, PhD

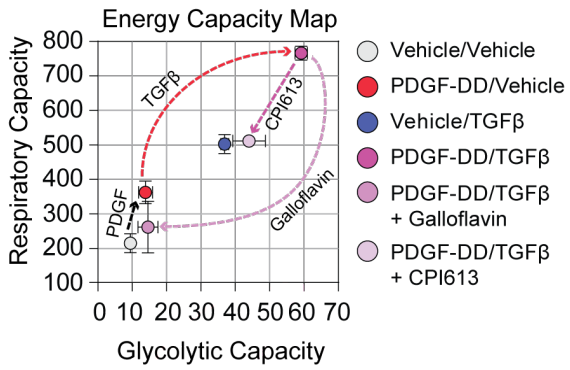

Figure 6

PDGF and TGFβ treatment drives energetic capacity, which can be reversed by treatment.

production. By stimulating SMC with PDGFBB or DD or TGFβ, we have shown that aerobic glycolysis (60% and 200% above vehicle) and respiratory capacity (69% and 134% above vehicle) is highly increased. Sequential stimulation of PDGF followed by TGFβ was performed to first induce dedifferentiation (PDGF) and then phenotypic modulation (TGFβ) to a MF-like state. These studies showed an even greater increase in aerobic glycolysis (529% above vehicle) and respiratory capacity (257% above vehicle). We determined that PDGF and TGFβ-induced collagen mRNA synthesis was dependent on the switching to aerobic glycolysis. These increased respiratory effects were abrogated after chemical inhibition of LDH or PDH.

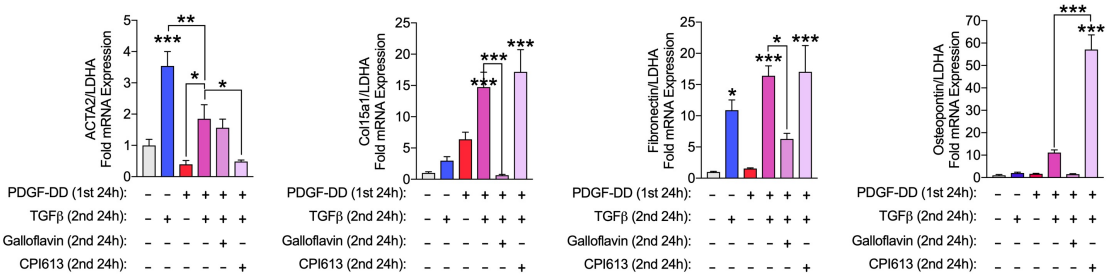

Figure 7

ECM synthesis is regulated by capacity of SMC to perform aerobic glycolysis. ACTA2 expression is induced by TGFβ and repressed by PDGF and by CPI613. Synthesis of multiple ECM mRNA is reduced after inhibiting and increased by augmenting aerobic glycolysis.

Interestingly, chemical inhibition of LDH by Galloflavin (Sigma) not only ablated the increased glycolytic capacity of PDGF and/or TGFβ (Figure 6), but that it also inhibited collagen mRNA synthesis (Figure 7). Furthermore, PDH inhibition by CPI613 (Sigma) decreased the respiratory capacity, increased aerobic glycolysis (Figure 6), and increased ECM mRNA synthesis (Figure 7). Taken together, this suggests that SMC must

switch to a glycolytic state to carry out processes including ECM remodeling and collagen synthesis (Figure 8). How switching metabolic states might relate to SMC content in the fibrous cap and lesion stability is explored in the Future Directions section.

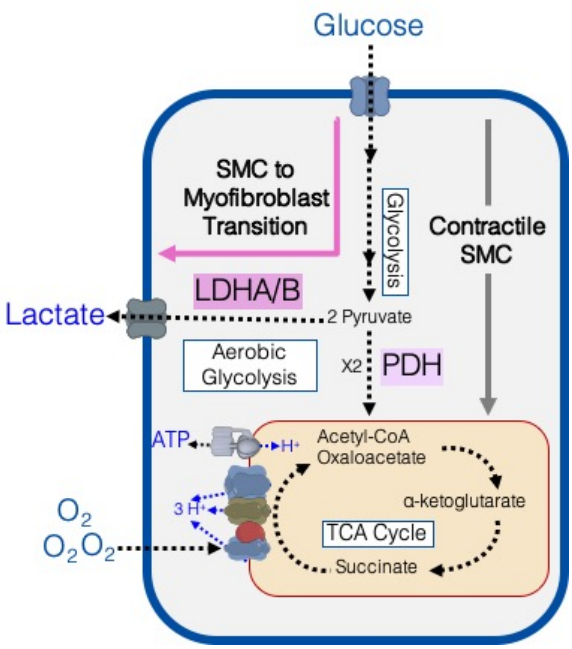

Figure 8

Contractile SMC utilize glucose for oxidative phosphorylation. When SMC transition to a myofibroblast-like state by stimulation with PDGF and TGFβ, the resultant shift to aerobic glycolysis is permissive for ECM synthesis.

Chapter 5

Conclusions and Discussion

I. Summary

The studies in this thesis looked at the role of SMC in atherosclerosis pathogenesis using two major techniques. Chapter 2 demonstrated the effect of lethal radiation and BMT and Chapter 3, the necessity of PDGFBR signaling in SMC response during atherosclerosis and in maintenance of the protective fibrous cap. It came as a surprise that these apparently disparate techniques resulted in such similar phenotypes and I felt compelled to double check my records more than once. It seems all too likely that they are linked molecularly, a fascinating bit of speculation and a study for the future. I will focus this conclusion and discussion section on what these studies have taught us about SMC biology in atherosclerosis and what can be gleaned from them.

Briefly, we demonstrated that radiation or loss of PDGFBR signaling prevented the accumulation of SMC in the lesion during atherogenesis, but did not inhibit their plasticity as they were able to dedifferentiate, proliferate, and modulate within the media. To compensate for SMC loss in the lesion, non-SMC underwent mesenchymal transitions, contributing to the ACTA2^{+} fibrous cap with varying degrees of success maintaining lesion stability. ACTA2 expression of SMC and non-SMC in the fibrous cap seems dependent at least in part on PDGFBR signaling because its chemical inhibition in mice with developed atherosclerosis reduced the total percent of ACTA2^{+} cells in the fibrous cap.

Together, these studies establish the following important points: 1. The presence of SMC-derived cells in lesions is required for long-term lesion stability despite existence of SMC-like cells from other sources, 2. There is a need to reassess plaque composition in light of lineage tracing data, and 3. Stabilizing the fibrous cap may represent a valuable therapeutic target to reduce rupture with subsequent MI or stroke.

A number of interesting questions have yet to be addressed including: 1. What are the downstream effects of PDGFBR and/or irradiation in SMC in atherosclerosis and are they connected? 2. Are mesenchymal transitions of non-SMC beneficial or detrimental and how can we better elucidate the functions of these cells in the lesion? 3. How does this inform human disease and therapies and specifically, what is the future of treatments for cardio-oncology patients?

II. Smooth Muscle Cells are Key Contributors to Lesion Stability

SMC Plasticity is Critical to their Response to Atherosclerosis

For the normal functioning of SMC in the vessel, they must be in a quiescent state, disinclined to proliferate or change phenotype. However, SMC are a distinctive somatic cell type in that they retain a high degree of plasticity (Alexander and Owens, 2012; Owens et al., 2004) that allows them to respond to disease or injury, including conferring stability to the fibrous cap of an atherosclerotic lesion. Mutations preventing normal functioning and plasticity of SMC have drastic and devastating effects during development and throughout the cardiovascular system (Andrae et al., 2008).

This suggests an immense evolutionary selection in favor of regulators of SMC plasticity and mechanisms that control the ability of SMC to respond to and repair vascular insult. This selection pressure cannot be directly translated to atherosclerosis, which manifests beyond one's reproductive years, however, the processes and mechanisms that drive lesion development are similar. The overarching goal of our lab (and others) is to parse out these mechanisms in order to better understand SMC in disease. Future studies related to work in this thesis will aim to determine if all or a specialized subset of SMC respond during atherogenesis, and if this is consistent within lesions across all vascular beds.

PDGFBR Activation is Required for SMC Investment in the Fibrous Cap of the BCA

Our findings indicate that PDGFBR signaling in SMC in atherosclerosis regulates critical processes that make SMC permissive to respond to factors that encourage plaque stabilizing events. This tight regulation of SMC response by PDGFBR underlies the SMC response to atherosclerosis. Results herein suggest that migration not proliferation induces the initial investment of SMC into the atherosclerotic lesion because neither loss of PDGFBR signaling nor lethal radiation impair the modulatory or proliferative capacity of SMC (Chapter 3 Discussion). Our studies suggest that SMC migration is regulated by cell autonomous rather than secondary effects of the PDGFBR signaling (Raines and Ferri, 2005; Raines et al., 2000). While in cultured SMC, PDGF is sufficient for

chemotaxis (Bernstein et al., 1982; Weinstein et al., 1981), it is unclear why other cytokines, which are also shown to induce migration in culture (Gerthoffer, 2007) cannot do so in SMC lacking PDGFBR in atherosclerosis.

Once in the lesion, the interplay of factors found in the distinct microenvironments further direct SMC phenotype and fate, including to a MF-like state in the fibrous cap where they express ACTA2 and can contribute to collagen synthesis (Amento et al., 1991; Ross, 1971; Ross and Klebanoff, 1971). Our studies showed that this process is dependent on PDGFBR signaling (Chapter 3, Figure 1). Furthermore, global PDGFBR antagonism also resulted in decreased SMC and total ACTA2^{+} cells in the fibrous cap (Chapter 3, Figure 6). Taken together, these studies show that PDGFBR signaling is a critical mediator of favorable changes in plaque composition including formation and maintenance of a SMC- and ECM-rich protective fibrous cap. It seems likely that mechanisms regulating SMC investment in atherosclerosis are similar to those regulating nascent vessel development, which both require SMC migration to the endothelium and rely on intact PDGFBR action to do so.

Radiation and SMC-PDGFBR KO have Parallel Phenotypes

It is possible that SMC fail to accumulate in lesion after both SMC-PDGFBR KO and lethal irradiation through unrelated mechanisms that happen to overlap in phenotype. Evidence that this may be the case arises from 1. the fact that SMC in the media stain positively for PDGFBR after radiation (data not included) and, 2. radiation has been shown to induce pro-migratory cytokines including PDGFBB. However, if we speculate that these mechanisms are interconnected, then lethal irradiation may functionally block PDGFBR signaling itself or target a critical mediator.

One possibility is radiation targets the intrinsic mechanisms that are downstream of PDGFBR-mediated migration (De Donatis et al., 2008; Westermark and Heldin, 1985). These include secretion of MMPs (2/9) that degrade the surrounding ECM, and activation of pathways that mobilize its internal actin cytoskeleton through PI3K/AKT, RhoA, Rac1, and CDC42 (including filopodia, lamellipodia formation, actin stress fiber polarization) (Gerthoffer, 2007; Heldin, 1992; Raines, 2000; Westermark et al., 1990). It is likely that

loss of migration is due to the confluence of multiple factors including the reduction of pro-migratory and activation of anti-migratory processes. The anti-migratory events affected could include phosphorylation of tyrosine domains that negatively regulate kinase activity (Kazlauskas and Cooper, 1989), failure to synthesize factors that favorably rearrange the basement membrane (Van Leeuwen, 1996), or increased anti-migratory factors like PDGFAA (Koyama et al., 1994; Koyama et al., 1992) or TGFβ (Gerthoffer, 2007).

This highlights the second possibility, that radiation-induced migration loss is due to cell-extrinsic factors that exert opposing effects to PDGFBR on SMC. For example, TGFβ maintains SMC differentiation, is induced by radiation (Martin et al., 2000), and has previously been shown to reduce SMC accumulation in mouse lesions (Chen et al., 2016). However, increased TGFβ alone is unlikely to be the driver behind the lack of SMC within irradiated lesions. These effects may be mediated by a protein like LRP1, which is a co-receptor for TGFβ and is known to regulate PDGFBR-mediated migration at least in part through endocytosis of MMP2/9 from the extracellular space (Boucher et al., 2003; Boucher et al., 2007; Lillis et al., 2005). This is interesting but speculative as it is unknown if radiation affects LRP1 in our animals.

Finally, radiation may undermine SMC migration through induction of cellular senescence, a state in which cells are metabolically active but persistently in cell cycle arrest in response to DNA damage (Hayflick, 1965; Li et al., 2018). It may also be induced by TGFβ (Acosta et al., 2013; Muñoz-Espín et al., 2013). Senescent cells are resistant to proliferation and apoptosis, which we saw was true of medial SMC after radiation (Chapter 2, Figure 4). While one or a combination of these options might be able to explain the loss of SMC investment in lesions after lethal irradiation (see Chapter 2 Discussion) or SMC-PDGFBR KO, further studies are required to determine the exact mechanisms of their interconnectivity, which is like to be neither trivial nor straightforward.

PDGFBR signaling seems to only be required by SMC in the BCA. For this reason, the bulk of this discussion focuses on the BCA, with speculation in the Future Directions about the same pattern of SMC accumulation in lesions within different vascular beds seen after both SMC-PDGFBR KO (data not included) and lethal radiation.

Why Radiation Might Exhibit Cell-Intrinsic Effects on Medial SMC

To determine how radiation affects SMC accumulation in lesions, one must ask why it might have a cell-intrinsic effect on SMC at all. The paradigm is that radiation targets poorly differentiated and highly proliferative cells, which are not classic characteristics of SMC in the healthy vessel wall (Bergonie and Tribondeau, 1959; Olson et al., 1992; Reidy, 1990). In fact, SMC in the healthy vessel wall are so lowly proliferative (<1%) that they require a sufficiently large stimulus, like vascular injury, to induce a response (Clowes et al., 1983; Clowes and Schwartz, 1985; Jawien et al., 1992). It seems unlikely then, that the effects of radiation are through SMC proliferation.

Let us now visit the next target: "poorly differentiated" cells. SMC in the vessel wall that give rise to cells in the lesion are derived from a SMC that was previously expressing MYH11 at the time of tamoxifen. Supporting evidence of a heterogeneous differentiated medial SMC population comes from studies that observe SMC in a continuum, spanning from contractile to multiple matrix-expressing phenotypes (Drake et al., 1998). These mature SMC have the capacity to clonally expand to populate the lesion (Chappell et al., 2016; Jacobsen et al., 2017), suggesting at least a subset seem to transition to a less differentiated state. For radiation to exert its effect, these less differentiated cells must be present in the healthy vessel. The possibility of SMC contributing to a stem cell-like population has been shown previously by presence of mature-SMC-derived $SCA1^+$ cells (Majesky et al., 2017). $SCA1^+$ progenitor cells demonstrate increased migratory capacity in response to lipids like cholesterol (Kokkinopoulos et al., 2017). The fact that radiation prevents SMC migration to the lesion suggests that SMC are in this less differentiated state, possibly expressing stem cell markers like SCA1 in the healthy media. This might be a "primed" cell population, poised to migrate.

We must also consider the possibility that the effects of radiation on SMC are not intrinsic to SMC themselves (see Chapter 2, Discussion). This would mean that cells like BMDCs lack a pro-migratory signal that is required by BCA SMC. Another possibility is that radiation results in non-permissive changes within the local environment that physically prevents migration of SMC like lack of adequate collagen scaffold (Raines, 2000).

Evidence that Primed SMC Need to Express PDGFBR in Lesions

The literature shows that PDGFBR is a marker of the expansion competent mature medial SMC that clonally expands. This is demonstrated in a mouse model of pulmonary hypertension (PAH) where primed SMC, marked by PDGFBR and localization at the muscular-nonmuscular border, beget the SMC that extend down the normally unmuscuarlized artery. (Sheikh et al., 2015). EC and MΦ-derived PDGFBB, acting through SMC-PDGFBR, regulates KLF4, Hif1α and distal migration (Sheikh et al., 2018). We suggest that similar to PAH, the expansion-competent cells in the BCA media must express PDGFBR. Why then, if nearly all the medial SMC express PDGFBR (Chapter 3, S. Figure 1), does only one (or a very few) give rise to the SMC in the lesion?

Two possibilities are outlined in the Discussion of Chapter 3. Briefly, either most or all PDGFBR^{+} SMC are capable of expansion, possibly cycling between competence and incompetence and the expanding cell negatively regulates migration of the remaining SMC pool, or there are rare PDGFBR^{+} SMC that are uniquely equipped to give rise to the lesion SMC. In support of the latter, recall the previous section describing the heterogeneous medial SMC population, one of which could be “primed” to expand. However, there is evidence in support of the former in that mature medial SMC can be induced to contribute in a polyclonal manner to the lesion, which is dependent on BMDC-derived Itgb3 (Misra et al., 2018).

Finally, an intriguing but highly speculative mechanism for SMC clonal expansion is that the medial SMC, though each with distinct capacities, act in concert to respond to stimuli called quorum sensing (Bentzon and Majesky, 2017; Miller and Bassler, 2001; Widelitz and Chuong, 2016). This is studied in vascular cells as the coordinated total response to acetylcholine of EC with different individual responses (Wilson et al., 2016). Regarding SMC clonal expansion: if the quorum is considered the SMC in the media directly underlying the initial fatty deposit, then the signals that induce SMC migration would be sensed by the group. If there is a higher ratio of anti- to pro-migratory signals, as a group, SMC will want to remain in place. How one SMC is “selected” to enter the lesion may simply be by location, i.e. the cell on the edge or just outside of the quorum,

nearest to the shoulder, which is the purported point of entry into the lesion (Misra et al., 2018; Newby and Zaltsman, 1999). In this way and similar to the model in PAH, most of the medial SMC express the priming protein PDGFBR^{+}, the SMC that underlie the lesion receive a "do not enter" signal, which allows the SMC at the edge to respond to the PDGF gradient and expand into the lesion. Quorum sensing may serve a dual purpose of maintaining vessel contractility and allowing SMC to respond to vascular disease.

III. Mesenchymal Transitions of non-SMC

Evaluating Mesenchymal Transitions of non-SMC in Atherosclerosis

Previous studies have observed that lesion cells from multiple origins express protein markers indicative of SMC and EC or MΦ. What are the origins of and what function does one ascribe to cells expressing ACTA2 and EC or MΦ markers? Is ACTA2 expression representative of a temporary state during a cell's transition to an alternate phenotype? For example, EC might express mesenchymal markers as a means of entering the core of the lesion, similar to the "invasion" phenotype during EMT. Another question is if there are SMC-derived cells within the lesion, what is the need for MΦ or EC to exhibit characteristics and/or functions of SMC?

SMC normally comprise only about 60-70% of the ACTA2^{+} cells in the fibrous cap of advanced BCA lesions (18 or 26 weeks of WD; Chapter 3, Figure 3/S. Figure 5). In fact, this has been previously reported (Albarran-Juarez et al., 2016), although not highlighted by the authors as anti-dogmatic. This means that up to 40% of ACTA2^{+} cells in the fibrous cap are derived from the mesenchymal transition of non-SMC, which was unexpectedly high. As discussed in Chapters 3 and 4, through marker protein staining and EC-lineage tracing, we determined that multiple non-SMC derived cell types normally contribute to the ACTA2^{+} cells in the fibrous cap. Although still a minority of the total ACTA2^{+} fibrous cap, the fact that these non-SMC derived cells are so prevalent in normal lesions suggests they play a direct role in regulating fibrous cap functioning. However, it raises questions as to how well they function in contributing to collagen deposition and strength of the protective fibrous cap over the course of atherosclerosis.

EndoMT and MMT Contribute to Plaque Stability, at Least Temporarily

Longitudinal studies show in SMC-PDGFBR KO mice that EndoMT and MMT can at least temporarily maintain collagen content in the fibrous cap (Chapter 3, Figure 2). To determine if these cells can recapitulate transcriptional profiles of SMC in the lesion, we refer to the results of our single cell RNA-seq analysis. Recall from Chapter 4 that eYFP$^-$ cells in SMC-PDGFBR WT lesions contributed to transcriptional clusters enriched in ECM genes. Furthermore, there is a minority contribution of eYFP$^-$ cells from the SMC-PDGFBR WT lesions to cluster 7, which resembles differentiated SMC seen at the fibrous cap. This evidence suggests that mesenchymal transitions of non-SMC can transcriptionally mimic SMC. Although as addressed earlier, this is not necessarily reflected at the protein level, at least not in BMDCs (Iwata et al., 2010)

This data suggests that augmenting EndoMT and MMT might be beneficial for lesion pathogenesis because not only are these cells present in the lesion normally, but they can contribute to stability. Since we propose that EndoMT and MMT may be stabilizing or destabilizing depending on the lesion environment, it is critical to determine these effects in the context of the lesion as a whole and how to direct these cells to maintain their beneficial functions or inhibit detrimental changes. Since increased fibrotic capacity of EC is generally considered detrimental in disease, we would want EndoMT increased only in the fibrous cap. This may be accomplished similarly to SMC-derived MF-cells at the fibrous cap, which require PDGFBR activation to maintain ACTA2 expression and collagen content (Chapter 3, Figure 5).

Evidence that SMC are the Most Effective Long-term Regulators of Stability

There was only a temporary maintenance of collagen content and indices of lesion stability after SMC-PDGFBR KO, and these effects were not observed after lethal irradiation. This means that lesions require SMC-derived ACTA2$^+$ cells in the fibrous cap for sustained collagen deposition and lesion stability. It is likely that although transcriptionally similar, non-SMC can never fully recapitulate the functions of SMC, reminiscent of the observed faulty cholesterol regulation of SMC-derived MΦ-like cells (Allahverdian et al., 2014; Vengrenyuk et al., 2015). Likely these EndoMT and MMT marker$^+$ cells have a lower

capacity for ECM deposition and regulation, or higher pro-atherogenic inflammatory capacity that negatively contributes to lesion stability. It is also possible that these cells cannot sufficiently maintain a transcriptionally active or proliferative state and/or prematurely undergo cell senescence, leading to instability (Newby and Zaltsman, 1999). Future studies in the lab include cross-referencing different clusters of cells within the lesion with indices of stability to determine their pro- and anti-atherogenic transcriptional signatures and contribution to lesion pathology.

What is the Role of EndoMT and MMT in Human Lesions?

The major question is, how do these mesenchymal transitions impact human disease? If there is a drive toward EndoMT, does that cause a breakdown in the protective anti-thrombotic EC barrier and lead to erosion? (Pasterkamp et al., 2017b; Virmani et al., 1999). Does MMT direct MΦ away from their normal phagocytic functions and result in growth of the pro-atherogenic inflammatory necrotic core? Chapter 3 outlines the possible pro- and anti-atherogenic functions of EndoMT and MMT in the Discussion, but the fact remains that this is speculation based on correlation between evidence of stability and marker protein staining. We must be able to better evaluate the cells within the lesion in order to positively ascribe a function or determine their contribution to stability. This is one of the reasons our lab and others have spent considerable effort and resources identifying unique transcriptional signatures of cells within lesions of lineage traced mice, so that we could apply the insights gained to cell populations in the human lesion.

IV. Considerations for Future Treatments

Novel Therapies Must Clear a High Bar for Market

The current lipid-lowering, anti-hypertensive, and anti-thrombotic drugs are so effective, accessible, and well-tolerated that novel treatments must show significant improvements in these categories to be considered for market. This requires tens of thousands of patients, multi-year follow up, and millions of dollars spent on clinical trials and testing. Recently, PCSK9 monoclonal antibody inhibitors were developed to potently lower LDL and cholesterol levels in patients with adverse side effects or poorly controlled

cholesterol levels after statin treatment (Chaudhary et al., 2017; Sabatine et al., 2017). These biologics were much-anticipated but are cost-prohibitive for many patients, thus rendering their benefit marginal over current statins (Kazi et al., 2017).

The recent CANTOS trial attempted to reduce CVD by blocking systemic inflammation independent of lipid lowering using an anti-IL1β neutralizing antibody canakinumab in patients with a prior MI and residual elevated hsCRP. Results of this trial showed a 15% reduction in major adverse cardiovascular events at one of the three doses tested, but modest benefits with other dosage regimens, and with associated severe side effects including fatal infection (Baylis et al., 2017a; Ridker et al., 2017a; Ridker et al., 2011). The CANTOS results are extremely exciting as they are the first to achieve protection from the adverse clinical complications of advanced atherosclerosis by a therapy that is independent of further lipid lowering. Ultimately, canakinumab is expensive and has major unintended side effects and its use for CVD was rejected by the FDA. We postulate that changing the target of these drugs, namely to stabilizing the fibrous cap, is a viable alternative for more than marginal increases in efficacy.

Augmenting Beneficial SMC Phenotypes as a Therapeutic Target

The counter-intuitive idea to reduce the number of SMC in the lesion, despite the fact that general consensus is increased ACTA2^{+} cells in the fibrous cap is beneficial and would be associated with increased indices of lesion stability, has been attempted by numerous studies that have previously been outlined in this thesis. While limiting the SMC transitions to a detrimental phenotype may have merit, these studies generally result in either a MΦ-rich collagen-poor phenotype, or show evidence of decreases in multiple indices of lesion stability. Furthermore, many studies that antagonize PDGFBR signaling are designed as preventions (Boucher et al., 2003; Kozaki et al., 2002; Lassila et al., 2004; Pouwer et al., 2018), which is analogous to starting a life-long treatment in infancy (Baylis et al., 2017b). One must take caution not to misattribute the effects of a drug administered throughout atherogenesis to its possible action as an intervention.

A Case for a PDGFBR Agonist

Understanding the mechanisms of how a potential therapy might act is first priority. The fibrous cap functions to protect the pro-thrombotic factors in the necrotic core from coming into contact with the blood. When this system is overwhelmed by the buildup of ROS or pro-atherogenic factors, coupled with the high proliferation rate of fibrous cap SMC (Misra et al., 2018), senescence occurs, which destabilizes the lesion (Childs et al., 2016; Newby and Zaltsman, 1999; Uryga and Bennett, 2016; Wang et al., 2016a). It is suggested that fibrous cap cell senescence may be rescued by a sufficiently large stimulus, like PDGF acting on PDGFBR as is seen in vascular injury (Jawien et al., 1992; Newby and Zaltsman, 1999). Thus, exogenous therapies that coax these beneficial SMC phenotypes at the fibrous cap represents a strategic therapeutic target. We argue that an intervention study that results in maintenance of SMC in a MF-like state with increased collagen synthesis, as occurs at the fibrous cap, would be a valuable future study. We are aware of the caveat that one cannot necessarily assume that agonism will have the intended effect of increasing lesion stability just because antagonism does the opposite.

PDGFBR Action Must be Tightly Regulated

As mentioned briefly in the Introduction, uncontrolled PDGFBR overexpression in SM22α cells results in multiple detrimental effects on the cardiovascular system as a whole (He et al., 2015). Further, studies of LRP1 in mice resulted in near occlusion of mesenteric arteries in a PDGFBR-dependent manner in SM22α-Cre LRP1 KO mice (Boucher and Gotthardt, 2004; Boucher et al., 2003). This is not representative of the normally tightly regulated SMC response mechanism and is the opposite of our intended effect of increasing PDGFBR signaling to stabilize lesions and highlights the necessity of controlling PDGFBR and SMC response.

PDGFBB Accelerates Wound Healing

If one considers the formation, maintenance, and repair of the fibrous cap akin to a wound, then the critical role PDGFBR plays becomes even more evident. Exogenous PDGFBB has a well-documented effect of accelerating wound healing in cases of pronounced hypoxia like diabetic ulcers, which led to the production of exogenous PDGFBB

gel Becaplermin (Regranex, Smith and Nephew, UK) (Steed, 1995; Wieman et al., 1998). PDGFBB does not indiscriminately increase ECM synthesis and fibrosis in the wound healing process, but also contributes to collagen turnover and cross-linking and proper wound resolution (Fang and Galiano, 2008). This is a key point when considering plaque rupture as a wound; the effects of PDGFBR activation must be controllable to prevent vessel stenosis or pathological fibrosis.

V. Links between CVD and Cancer Treatments

Cancer Treatments Exacerbate Atherosclerosis

While canakinumab may not be the next blockbuster drug for reducing atherosclerosis and MI, it did reveal an unintended protection against lung cancer (Ridker et al., 2017b), further suggesting commonalities between pathology of CVD and cancer. In Chapter 2, we discuss that radiation is an independent risk factor for developing CVD, and a substantial portion of this discussion proffers possible mechanistic links.

Evidence suggests that other drugs that demonstrate potent anti-cancer benefits seem to exacerbate atherosclerosis (Giles et al., 2013; Kim et al., 2013). In the clinic, Imatinib is associated with adverse vascular events related to atherosclerosis, which are outlined in the Discussion of Chapter 3. In light of our data, we suggest that this is due at least in part to a destabilization of the $ACTA2^{+}$ SMC-rich fibrous cap, which we show requires sustained PDGFBR signaling. In light of our data, we suggest that Imatinib users be screened longitudinally for evidence of lesion destabilization, especially considering the decades-long process that is lesion development, and the relatively short (17 year) time frame since FDA approval.

Mesenchymal-like Cells in Tumors and Atherosclerosis

While Imatinib is usually the first-line treatment for certain leukemias like CML and AML and stromal cancers like GIST, tumor cells can become refractory, requiring use of newer RTK inhibitors. These, in contrast to Imatinib, are much more frequently associated with atherosclerosis-related vascular events, and caution is advised when treating for patients at risk for heart disease (Giles et al., 2013; Kim et al., 2013; Larson et al., 2014).

Of major significance, recent seminal studies on drug-tolerant “persister” cells in multiple cancer lines have shown acquired drug resistance in cells with mesenchymal properties including being derived from sarcomas or having undergone EMT (Gröger et al., 2012; Hangauer et al., 2017; Viswanathan et al., 2017). This refractory state is dependent on the lipid peroxidase GPX4, which protects against ferroptosis mediated cell death (Yang et al., 2014b). In these cells, ferroptosis is one of the proposed mechanisms to target the mesenchymal persister cells. Interestingly, a second generation PDGFBR antagonist, Sorafenib, has been shown to induce ferroptosis mediated death, which may in part explain the increased vascular adverse events seen after its use (Dixon et al., 2014; Louandre et al., 2013).

This is not the first time SMC accumulation in atherosclerosis has been compared to tumor cell growth. In fact, it is supposed that SMC investment in the human arterial intima mimics neoplasm formation similar to the leiomyomas on the uterus (Moss and Benditt, 1975; Wainscoat and Fey, 1990). If SMC clonal expansion is due to a selective growth advantage of a single medial SMC and if this advantage is dependent on a mesenchymal phenotype (not dissimilar to the mesenchymal properties required for tumor cell invasion), then it is likely that these drugs would have multiple detrimental effects on the SMC in the lesion and thus, the lesion as a whole.

Chapter 6

Future Directions

During my graduate studies, I most lamented the lack of two technologies that would have clarified many of the unknowns in this thesis. The first being a method of tracking the path of SMC from the media to the lesion. While intravital microscopy of vessels is possible (McArdle et al., 2015), doing so over weeks would cause undue suffering on the mice involved. The second would be multi-cell lineage tracing with simultaneous KO of PDGFBR specifically in SMC. No doubt, these technologies will exist one day so that another graduate student can lament something new.

Given the choice, I would have performed these studies in both male and female mice, as the presentation and effects of atherosclerosis and CVD can be wildly different depending on sex and CVD in females is woefully understudied (Mautner et al., 1993; Nicholls et al., 2007; Sanghavi and Gulati, 2015; Thomas and Smart, 2007; Virmani et al., 1999; Vitale et al., 2007). It should be stated here that all studies should be performed on both male and female mice and a case can even be made for repeating many of the studies in this thesis in female mice. Luckily, this can be accomplished using new MYH11-driven mouse models (including the dual-lineage tracing mouse below) that do not have MYH11-Cre in the Y chromosome. The future studies outlined below are a mix of ideas that are feasible with current technologies in the lab and those that would require significant investments in thought and development. Ultimately, they all attempt to determine how to augment the beneficial cell phenotypes within the fibrous cap in order to address the major cause of death from atherosclerosis: unstable plaque rupture.

I. Out of the Media: SMC Migration and Expansion

Elucidating Mechanisms of SMC Migration

While there is abundant evidence of SMC clonality within lesions, the mechanisms that underlie SMC accumulation in atherosclerosis are poorly understood. Studies herein suggest that both PDGFBR signaling and radiation are upstream of SMC expansion into the lesion in the BCA. It is of great interest to determine the subset of primed SMC that populate the lesion. The previous section outlined several possible mechanisms

including a rare uniquely primed cell, stochastic cycling of permissive factors, and quorum sensing regulating SMC accumulation, which all rely on a unique SMC signature.

One way to determine the permissive factors for SMC accumulation within the lesion downstream of PDGFBR or radiation is to perform a series of transcriptomic and proteomic studies to compare and contrast the changes within individual SMC. This would require precise microdissection of the media underlying a fatty streak and the SMC within the lesion. Sequencing these two populations will require a lot of input because we are looking for a rare change within a small population (a technical limitation of these methods). Another option, although not unbiased, is MS-CyTOF, a multiplex epitope-based method of imaging up to 135 antibodies in tissue sections (Giesen et al., 2014).

Assessing Clonal Expansion

One potential mechanism to understand clonality in SMC is through BMDC-loss of Itgb3 (Misra et al., 2018). Itgb3 mediates cell surface signaling and has been shown to induce SMC migration (Slepian et al., 1998). It is itself part of the PDGFBB-dependent migratory machinery (Woodard et al., 1998), suggesting that this effect might be downstream of PDGFBR. Why loss of an integrin in a BMDC might affect SMC clonality is unclear, but one explanation is that it causes secondary changes within the ECM scaffold that is permissive for SMC migration (Cherepanova et al., 2016; Durgin et al., 2017; Gerthoffer, 2007). To test this, we could use MS-CYTOF to carefully assess of ECM synthesis by Itgb3-deficient BMDCs and the ECM content of the lesion. If there is dysregulated ECM organization present, we would perform in vitro assays where SMC are plated on different ECM matrices and induced to migrate or proliferate given stimuli like PDGF.

One consideration when translating these studies to ours is that Itgb3-mediated polyclonality was demonstrated in the aortic root, not the BCA. In the aortic root, SMC accumulate independently of PDGFBR activation, as they are present even after SMC-PDGFBR KO. It is of great interest to our lab and the field to determine if there are similar effects in the BCA tissue within the BMDC-Itgb3 null mice and to identify additional mechanisms of regulating SMC accumulation into lesions. The studies above should be tested in multiple vascular beds where the SMC derive from different embryonic origins.

II. Brave New World: Transcriptional Signatures of SMC

We and others provide evidence that mesenchymal transitions of non-SMC directly contribute to lesion stability, but that beneficial SMC populations most effectively modulate stability. Since these transitions are normally found within lesions, major unanswered questions include why do these transitions occur, and how well do they function in contributing to collagen deposition and lesion strength?

In order to understand how cells contributes to atherosclerosis, one must first be able to identify each cell. This is an important consideration when attempting to simultaneously assess the role of ACTA2^{+} cells of multiple origins. To unequivocally identify a cell's origin, we would need to develop a method of whole organism lineage tracing. This could be achieved by using a novel method called GESTALT that tags each cell with an individual bar code (McKenna et al., 2016). This barcoding system, which is the result of unique patterns of CRISPR/Cas9 insertions and deletions, was pioneered in zebrafish to show cell lineage relationships beginning in the embryo. In this manner, one could trace the origin of a cell that is actively expressing ACTA2 protein to its embryonic origin. This would be highly informative and answer multiple questions raised in this thesis including those related to the embryonic origin of SMC in different vascular beds or the origin of the clonally competent SMC.

Coupling unique barcode tagging with SMC-lineage tracing and single cell RNA-seq would provide information about the localization of MF-cells in the lesion and relationship of individual cells with similar transcriptional profiles. The next step would be to perform unbiased ECM-proteomics – the current focus of our collaborators who have identified a signature of symptomatic human lesions and potential biomarkers (Langley et al., 2017) – to determine the transcription and expression of multiple different ECM molecules by SMC on a single cell level. Using an EC or MΦ-driven promoter, one can similarly assess alternate lineages of the ACTA2^{+} fibrous cap cells and if origin impacts their ability to contribute to ECM content normally.

III. A Tale of Dual-Lineage Tracing Mice

Identifying Subpopulations of SMC in the Lesion

To gain further insights into the phenotypic profile of SMC, we developed a method of stable sequential lineage tracing to identify subpopulations of SMC that have transitioned to alternate states (Figure 1).[13] For example, using this system we observe the subset of SMC (using the MYH11 promoter) that have activated LGALS3 in the lesion (which in itself is not surprising). The novelty of this mouse lies in its complex genetics that sequentially expresses tdTomato (upon activation of the Myh11 promoter) and then

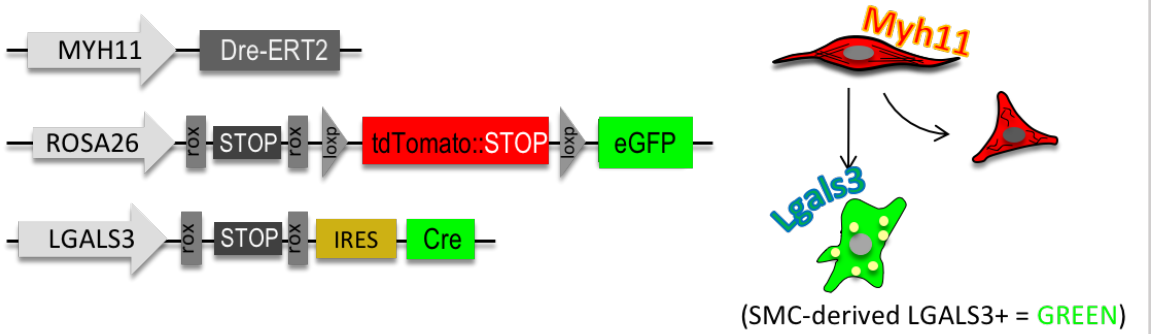

Figure 1

Sequential dual-lineage tracing. SMC that express MYH11 ahead of a Dre reporter activate tdTomato by excision of rox sites around the STOP sequence. If SMC subsequently activate LGALS3, they express Cre, which excises lox sites and removes the tdTomato and an internal STOP sequence. These cells then transition to express eGFP. LGALS3-Cre will also excise lox sites around genes for selective KO in eGFP^{+} cells.

eGFP, which is stably expressed only in cells that have subsequentl activated the LGALS3 promoter. Coupling this dual-lineage tracing mouse with single cell RNA-seq, we have determined that SMC that have activated LGALS3 (eGFP) comprise clusters that are distinct from tdTomato^{+} SMC in that they no longer express characteristic markers like MYH11 and are instead enriched in chondrocyte markers.

Unfortunately, we cannot use this SMC dual-lineage tracing model with an ACTA2 promoter to assess the subset of lesion SMC that have activated ACTA2 in the lesion.

---

[13] Designed by Anh Nguyen, PhD

Since ACTA2 co-stains with MYH11 in medial SMC, likely every cell would immediately transition to express eGFP, rendering the attempt wasted. However, using an EC or MΦ-driven lineage tracing model crossed to the sequential ACTA2 promoter may provide valuable insight into the populations of EC or MΦ that undergo mesenchymal transitions, as well as inform their potential functions.

To circle back to how to assess mechanisms of SMC accumulation in lesions, we could use this dual mouse model to help identify the subset of SMC that are capable of clonal expansion. We would employ a MYH11-driven promoter with a sequentially activated SCA1-promoter dual-lineage tracing mouse, expression of which is associated with SMC in a progenitor state (Majesky et al., 2017). If SCA1 activation is upstream of clonal expansion, then all of the lesion cells will express eGFP. Coupling the SMC to SCA1 dual-lineage mouse with simultaneous PDGFBR KO specifically in the SCA1$^+$ SMC population would be an effective way of elucidating if PDGFBR is required for clonality.

Methods of Elucidating SMC Function

The ingenuity behind the design of this dual-lineage tracing model, as I just mentioned, is that we can selectively KO genes of interest specifically in the subpopulation of eGFP$^+$ cells. This allows us to directly ascertain the function of these cells in atherosclerosis. We can also ascertain the role of an entire subpopulation of SMC within the lesion by crossing this dual-lineage tracing mouse with a diphtheria toxin (DT) receptor mouse (Saito et al., 2001) to selectively ablate the eGFP$^+$ cell subset itself. One can then determine if DT-mediated suicide of this subset of SMC has overall beneficial or detrimental effects on the lesion.

To date, no one has determined the effects of endogenous EndoMT or MMT on indices of lesion stability. To assess the role of EC or MΦ mesenchymal transitions on lesion pathogenesis, we would use an EC or MΦ-lineage tracing mouse with a sequentially activated ACTA2-promoter. We can selectively ablate the EC or MΦ population that has expressed ACTA2 (eGFP) in advanced atherosclerosis. If loss of the eGFP subset results in increased lesion stability, then these mesenchymal transitions have a detrimental role in stability, and vice versa. We would also have temporal control, as ablation

can occur at any point during atherogenesis allowing us to determine these effects in a longitudinal way during atherogenesis, and even during animal development.

IV. Of Mice and Men: Translating Cell Functions to Human Lesions

A major question is, how do these mesenchymal transitions impact human disease? Neither the dual-lineage tracing nor this CRISPR/Cas9 system can be used on humans for obvious ethical reasons, and the chance of fortuitous accidental barcoding in humans who received CRISPR/Cas therapy is reduced by careful design of the CRISPR/Cas system used (Zhang et al., 2015). We previously developed the ISH-PLA method of detecting histone modifications on a specific genetic locus, but while this method can be applied to cells with stable unique histone modifications, it does not indicate a cell's function. However, we can still use mouse models to inform human disease by showing at least the potential of a cell population in the human with shared characteristics in the mouse like localization or transcriptional and protein phenotypes.

Single cell RNA-seq was outlined previously as a way to determine the transcription profiles of SMC and non-SMC within mouse lesions. We would first want to correlate the transcriptional profile of lesion cells with indices of stability to develop a signature of a stable lesion. If we start by cross-referencing our -omics analysis with gene variants known to play a role in CAD (van der Harst and Verweij, 2018), we can assess their direct function in subpopulations of SMC using the dual-lineage tracing KO mouse. This will give us directly translatable data about the characteristics of the cells within the lesion as a function of the specific gene in SMC that can then be applied to human lesions.

Evidence that SMC can be identified based on unique transcription signatures is seen in SMC and non-SMC MF that ACTA2 gene expression is differentially modulated through binding of transcription factors (TEF-1 or RTEF-1, respectively) to specific sequences in the promoter called MCAT elements (Gan et al., 2007; Swartz et al., 1998; Yoshida, 2008). This is one example of SMC transcriptional diversity (Kim et al., 1997; Li et al., 1996; Manabe and Owens, 2001) indicative of alternate regulation of genes by SMC and non-SMC, which may result in the increased ability of SMC to regulate ECM content over non-SMC derived MF-like cells. Recall data in Chapters 2 and 3 that show

ACTA2 expression in the fibrous cap does not does not itself correlate with stability but rather, sustained SMC-derived ACTA2^{+} cells seemed to be necessary to maintain collagen content. It is important here to note that ACTA2 is a marker of all MF-like cells in the fibrous cap, not itself a marker of ECM synthesis, which is dependent on its transcriptome and proteome. This understanding of the function and capacity of cells of different origins to synthesize beneficial ECM can then be applied to human disease to better characterize human lesion. A major consideration moving forward is integrating the -omics data amassed in mouse models for novel drug targets and better understanding of disease.

V. Zen and the Art of Lesion Stability Maintenance

Enhancing MF-like Cells

The one question I continually return to is how to manipulate the cells in the fibrous cap to exhibit a beneficial MF phenotype that contributes to collagen content and lesion stability. We demonstrate that PDGFBR signaling in SMC is required for accumulation, ACTA2 expression, and maintenance of the collagen rich fibrous cap in the BCA but not in SMC in various other vascular beds (e.g. the abdominal aorta and aortic root). Can we exploit mechanisms that govern mesoderm-derived SMC accumulation and ACTA2 expression in order recruit additional beneficial SMC into SMC-poor lesions that do rely on PDGFBR signaling or that are affected by radiation? The ultimate goal of the -omics analyses on the lesions is to understand the mechanisms by which SMC respond to disease.

One way to do this is to cross reference the single cell RNA-seq cluster data with the aforementioned risk loci or symptomatic plaque signature to find commonalities associated with beneficial CAD outcomes. For example, can we knock out inhibitors of ECM synthesis to strengthen the fibrous cap? An important consideration is that many human diseases are due to excess fibrosis (Rosenbloom et al., 2017). This means that careful consideration must be given to how to achieve enhancement of MF-like cells. In fibrotic disease, a buildup of ECM scar tissue leads to eventual organ failure. We see, in cases like wound healing, that fibrosis is a necessary part of the process, but just as important is ECM clearing and organization. The fibrous cap may be the only location where we

would want to promote fibrosis, although, we are not suggesting uncontrolled ECM accumulation within the cap as that can lead to vessel stenosis (Glagov et al., 1987). For this to work, we need to be able to directly target the SMC in the fibrous cap, which requires an understanding of the genetic underpinnings and tissue specific feature of fibrosis (Friedman et al., 2013) and refinement of precision medicine.

Exogenous Agonism

To determine if increasing PDGFBR activation results in beneficial changes in the fibrous cap cells, we can administer recombinant PDGFBB to atherosclerotic mice. This has previously been shown to be sufficient to induce responses in SMC to vascular injury through PDGFBR (Jawien et al., 1992). However, an alternative method is to augment specific downstream functions of PDGFBR like migration or collagen synthesis. This would require development of, to the best of our knowledge, an as yet undeveloped small molecule agonist. The key challenge would be selectivity for the PDGFBR or a non-redundant mediator. This may be feasible based on previous studies that identify discrete downstream events of differential phosphorylation sites including activating specific inositol phosphate second messengers (Williams, 1989). Again, understanding the differences in SMC based on embryonic origin would bolster these studies.

Another potential target is TGFβ, a critical mediator of mesenchymal transitions and collagen synthesis (Amento et al., 1991; Goel et al., 2013) and a cytokine known to differentially modulate SMC response based on embryonic origin. TGFβ inhibition has multiple detrimental effects on the lesion (Lutgens et al., 2002; Mallat et al., 2001). Testing if increased TGFβ results in beneficial mesenchymal transitions in the fibrous cap cells would require intervention studies similar to those outlined in Chapter 3 (Figures 5,6) to assess agonism on the lesion. It would also be necessary to determine off target effects of exogenous treatment with PDGFBR or TGFβ by looking at disease or repair mechanisms like angiogenesis, or tumor growth.

SMC-derived Persister Cells

Of particular interest, both radiotherapy and PDGFBR inhibition are widely-used anti-cancer therapies that have parallel effects on lesion composition and vascular

patterning. Recall the persister cells in refractory tumors that are characterized as having transitioned to a mesenchymal phenotype and are resistant to apoptosis. Targeting these mesenchymal cells (for example with PDGFBR inhibitors) may in part explain the associated vascular adverse events. Ferroptosis is mediated by high levels of oxidized lipids and the survival of perister cells is dependent on GPX4-mediated evasion of ferroptosis. If MF in the fibrous cap (SMC or otherwise) express GPX4, then do these cells act in a similar manner? GPX4 presence in MF-like cells in the fibrous cap can be assessed with a simple stain. To determine if GPX4 is necessary for SMC to maintain a MF-like state, one can test this using knock down assays in cultured SMC and then assessing their ability to synthesize ECM. SMC in the fibrous cap undergo apoptosis due to the high inflammatory and ROS-ridden environment, which leads to lesion destabilization (Newby and Zaltsman, 1999). To determine if activating a persister phenotype can prevent SMC loss at the fibrous cap even in the presence of detrimental cytokines and factors, we could induce GPX4 in mice with advanced atherosclerosis and assess the effects on the SMC and the lesion as a whole.

VI. A Moveable Feast: Defining Metabolic Targets

Current and future studies in our lab are attempting to understand the metabolic programing that regulates stabilizing events like ECM synthesis, or migration and proliferation in SMC to occur. Understanding the differences in metabolic programing that govern SMC transitions to a beneficial or detrimental phenotype can then be exploited as future therapeutic targets. Metabolic pathways are upregulated in SMC-PDGFBR KO animals, meaning they are downstream of PDGFBR-mediated loss of SMC investment into the lesion. To determine a metabolic signature in specific cell populations, we can mine our single cell RNA-seq data. For example, cluster 2 is enriched for LDHA and B and is mostly comprised of $eYFP^{+}$ cells, suggesting that SMC play an integral role in differentially-regulated metabolism in the lesion.

Recall that we have determined that aerobic glycolysis regulates SMC phenotypic transitions to MF-like cells and collagen mRNA synthesis. Assessing these targets in vivo has various limitations and requires use of surrogate markers of metabolic changes in

tissue sections. For example, we can measure metabolic substrate or product levels in tissues or specific cells at any given time point by mass spectrometry, which we can correlate with overall stability. By staining enzymes involved in aerobic glycolysis, we can assess differences between MF-like and differentiated SMC. However, it is difficult to determine activity of inhibition based on these techniques, and directly assessing metabolic flux in vivo requires technology that does not currently exist.

In order to better understand the metabolic flux within the lesion, we are developing an ex vivo technique to measure flux in dissected lesions from the mouse in response to stimuli.[14] Once standardized, we can assess metabolic shifts between lesions and healthy vessels, between SMC-PDGFBR WT and KO lesions, between lesions in different vascular beds, or after selective KO of a target gene in the dual-lineage tracing mouse, among others. This will help predict and elucidate the metabolic states of cells in vivo in disease. This understanding can inform future therapies to target pathways to boost or inhibit metabolic pathways to achieve a particular function.

To directly test the energy capacity of SMC in the lesion, we are currently developing a mouse model to inhibit aerobic glycolysis in SMC in atherosclerotic lesions (through exogenous or genetic LDH inhibition). We expect that this will result in destabilization of the lesion including reduced numbers of SMC-derived MF-like cells and detrimental rearrangement of the ECM in the fibrous cap. An alternate treatment would be to inhibit oxidative respiration and boost aerobic glycolysis through PDH inhibition, which we predict would augment the beneficial ECM synthesizing capacity of SMC-derived MF-like cells in the fibrous cap, independent of cytokine or growth factor action. Understanding the link between SMC metabolic capacity and phenotype and function is highly interesting considering the increase in metabolic disorders and type II diabetes worldwide.

---

[14] In collaboration with Vlad Serbulea, PhD

Afterword

I hope you find this thesis both informative and comprehensive, at least, as comprehensive as I could make it considering the decades of research that came before me. For myself, I found this process to be more enjoyable than I had previously anticipated, which is not to say that it was easy. Rather, for the first time since I joined graduate school, I could really appreciate the breadth and depth of knowledge that had been elucidated prior to me sitting down and writing. I applied to graduate school because I like thinking and doing experiments, I found science interesting, and I was a good biology student and I knew I needed a PhD to continue to do these things at a higher level. Most of my frustration during my tenure as a graduate student was that I could not glean what I needed to know by reading it in a book. It took me longer than I liked to admit to realize that I was creating knowledge. I cannot even take credit for realizing this point myself. It was explained to me by a dear friend, which upon hearing, knocked something into place in my brain. This made process of getting my PhD special and important. To me, at least.

-AACN

Charlottesville, VA

January 2019

Appendix

I. Bulk RNA-seq

Table 1: Significantly upregulated genes in SMC-PDGFBR KO vs. WT

Gene	Log2 FC	P-Value	Adj P-Val	Gene	Log2 FC	P-Value	Adj P-Val
Sema3e	1.06	1.59E-10	1.00E-06	Atp5b	0.538	0.000162	0.012
Gm10800	1.01	1.53E-10	1.00E-06	Dnajc28	0.528	0.000161	0.012
Fabp3-ps1	1.17	2.75E-10	1.30E-06	Gk	0.536	0.000163	0.0121
Ptger3	1.08	5.59E-10	1.76E-06	Atp5o	0.421	0.000164	0.0121
Sec14l4	1.13	1.20E-09	2.84E-06	Pm20d1	0.693	0.000168	0.0123
Gm21738	0.963	1.05E-09	2.84E-06	Narf	0.375	0.000168	0.0123
Gm10718	0.962	1.81E-09	3.81E-06	Lgi2	0.574	0.000171	0.0124
1500015A07Rik	0.934	3.35E-09	6.34E-06	Lyve1	0.531	0.000175	0.0127
Fabp3	1.08	6.14E-09	1.06E-05	Igfbp6	0.508	0.000177	0.0127
Kng2	1.06	8.08E-09	1.28E-05	Letmd1	0.591	0.000178	0.0128
Pdha1	0.704	1.60E-08	2.16E-05	Ntrk2	0.588	0.00018	0.0128
Aldh1a7	1.03	2.19E-08	2.76E-05	Cxadr	0.604	0.000184	0.013
Rnf152	0.787	2.47E-08	2.92E-05	Eno1	0.46	0.000187	0.0131
Gm10722	0.933	2.71E-08	3.02E-05	Tuba8	0.684	0.000193	0.0132
Gm10717	0.931	2.92E-08	3.07E-05	Pdk4	0.675	0.000193	0.0132
Acadm	0.848	3.85E-08	3.84E-05	Cd1d1	0.661	0.000191	0.0132
Slc25a20	0.795	4.11E-08	3.89E-05	Aco2	0.678	0.000204	0.0137
Sucla2	0.834	4.84E-08	4.36E-05	Nrg4	0.657	0.000208	0.0139
Tmem45b	0.995	7.17E-08	5.90E-05	Fst	0.576	0.000219	0.0145
Slc25a42	0.887	6.85E-08	5.90E-05	Ndufb9	0.444	0.000221	0.0146
Fitm2	0.752	8.99E-08	7.09E-05	Adhfe1	0.637	0.000223	0.0147
Idh3a	0.835	1.90E-07	0.000144	Fibin	0.459	0.000227	0.0149
Slc16a1	0.816	2.15E-07	0.000156	Cyp2u1	0.467	0.000238	0.0156
Scd1	0.947	3.21E-07	0.000214	Dgat2	0.644	0.000264	0.0169
A530053G22Rik	0.944	3.50E-07	0.000214	Pcsk6	0.617	0.000259	0.0169
Fabp4	0.81	3.41E-07	0.000214	Gm6123	0.538	0.00026	0.0169
Ebf3	0.775	3.34E-07	0.000214	Uqcrc1	0.526	0.000267	0.0169
Dusp4	0.553	3.61E-07	0.000214	mt-Cytb	0.51	0.000263	0.0169
Cpt2	0.812	3.83E-07	0.000215	Dlat	0.443	0.000267	0.0169
Tspan12	0.778	3.86E-07	0.000215	Apmap	0.427	0.000266	0.0169
Trpc3	0.937	4.26E-07	0.00022	Gpd1	0.634	0.000279	0.0172
Gm11168	0.855	4.42E-07	0.00022	Elovl3	0.591	0.000275	0.0172
Hacd2	0.656	4.37E-07	0.00022	Ppp1r3b	0.564	0.000274	0.0172
Pde3b	0.531	4.40E-07	0.00022	Uqcrc2	0.513	0.000278	0.0172
Rgcc	0.85	4.86E-07	0.000231	Pdk1	0.375	0.000277	0.0172
Gpd2	0.724	4.88E-07	0.000231	RP23-137N6.2	0.669	0.000282	0.0173

Chpt1	0.678	5.47E-07	0.000253	Enpp3	0.35	0.000283	0.0174
Uqcrfs1	0.654	5.67E-07	0.000255	Pnpla8	0.264	0.00029	0.0177
Mme	0.847	6.21E-07	0.000261	Npr3	0.444	0.000295	0.0179
Hadh	0.756	6.41E-07	0.000264	Tmem176b	0.325	0.000299	0.0181
Ehhadh	0.871	7.03E-07	0.000272	Phyh	0.443	0.000317	0.019
Acadl	0.763	6.78E-07	0.000272	Ptgr2	0.334	0.000318	0.019
Etfa	0.709	6.97E-07	0.000272	Bckdha	0.538	0.000321	0.0191
Gm26870	0.829	7.22E-07	0.000273	Srpx	0.557	0.000331	0.0193
Chdh	0.806	7.76E-07	0.000283	Serping1	0.473	0.000328	0.0193
Slc22a23	0.723	7.75E-07	0.000283	Maf	0.457	0.000328	0.0193
Cdo1	0.795	8.52E-07	0.000305	Kif21a	0.608	0.000337	0.0195
Arxes2	0.908	9.40E-07	0.00033	AI464131	0.511	0.000337	0.0195
Insig1	0.663	1.02E-06	0.000351	Rasgrp4	0.468	0.000339	0.0195
Nat8l	0.843	1.29E-06	0.000417	Aldh1a2	0.655	0.000341	0.0196
H2-Q10	0.821	1.32E-06	0.000417	Nid2	0.392	0.000342	0.0196
Fh1	0.71	1.30E-06	0.000417	Uqcr11	0.503	0.000348	0.0197
Dbi	0.692	1.24E-06	0.000417	Trib2	0.42	0.000354	0.0199
Pank1	0.836	1.35E-06	0.000419	Gm15285	0.661	0.00036	0.0202
Gprin3	0.497	1.41E-06	0.000431	Gm37058	0.492	0.000359	0.0202
Ormdl3	0.511	1.48E-06	0.000444	Nudt12	0.536	0.000363	0.0203
Bnip3	0.598	1.53E-06	0.000453	Clpx	0.347	0.000365	0.0203
Decr1	0.732	1.56E-06	0.000455	Il1rl1	0.594	0.00038	0.0206
C1qtnf9	0.889	1.60E-06	0.000458	Fmod	0.523	0.000379	0.0206
Prkar2b	0.888	1.64E-06	0.000463	Coq9	0.495	0.000375	0.0206
Agpat2	0.811	1.68E-06	0.000467	Mtch2	0.293	0.000379	0.0206
Cs	0.609	1.74E-06	0.000471	Trp53inp2	0.267	0.00038	0.0206
Gpam	0.724	1.97E-06	0.000526	Ybx2	0.658	0.000384	0.0208
Gm10719	0.802	2.53E-06	0.000655	mt-Te	0.632	0.000394	0.0211
Hsdl2	0.612	2.52E-06	0.000655	Cox7a1	0.605	0.000392	0.0211
Slc5a3	0.478	2.88E-06	0.000738	Pdhb	0.444	4.00E-04	0.0213
Dhcr24	0.776	3.13E-06	0.000784	Dgat1	0.427	0.000403	0.0214
Mpzl2	0.861	3.25E-06	0.000799	Plin5	0.632	0.000408	0.0215
Arl4a	0.639	3.38E-06	0.00081	Prkaa2	0.445	0.000406	0.0215
Fam213a	0.711	3.81E-06	0.000902	Gm5421	0.629	0.000413	0.0217
Crls1	0.562	3.93E-06	0.000918	Fgf10	0.654	0.000418	0.0218
Ms4a4d	0.728	4.04E-06	0.000924	Ppa1	0.507	0.000422	0.0218
Figf	0.577	4.05E-06	0.000924	Mdh2	0.434	0.00042	0.0218
Gbe1	0.579	4.17E-06	0.00094	Siglece	0.568	0.000439	0.0225
Klb	0.837	4.71E-06	0.00104	Eno1b	0.432	0.000443	0.0227
Gm13910	0.768	4.89E-06	0.00107	BB365896	0.638	0.000459	0.0232

Me1	0.621	5.21E-06	0.00112	Slc24a3	0.53	0.000461	0.0232
Lilra5	0.655	5.47E-06	0.00116	Ndufb8	0.445	0.000461	0.0232
Gm10801	0.825	5.98E-06	0.00123	Cycs	0.542	0.000465	0.0233
Uck1	0.631	5.96E-06	0.00123	Gpx3	0.54	0.000475	0.0236
Adora1	0.816	6.10E-06	0.00124	Ccbe1	0.528	0.000478	0.0236
Mpc2	0.519	6.97E-06	0.00139	Serpinf1	0.459	0.000476	0.0236
Xrcc6	0.546	7.41E-06	0.00146	Car4	0.64	0.000484	0.0239
Slc4a4	0.727	7.93E-06	0.00154	G0s2	0.637	0.000487	0.024
Abcd3	0.341	7.95E-06	0.00154	Oplah	0.544	0.000492	0.024
Pfkl	0.601	8.41E-06	0.00161	Crat	0.488	0.000489	0.024
Hibch	0.649	9.12E-06	0.00173	Fzd4	0.389	0.000493	0.024
Etfb	0.61	9.94E-06	0.00184	Fmo1	0.435	0.000506	0.0243
Adipor2	0.485	1.36E-05	0.00243	Igkc	0.637	0.000524	0.0248
Hadhb	0.581	1.48E-05	0.00257	Dpyd	0.574	0.000523	0.0248
Uqcrh	0.396	1.47E-05	0.00257	Ndufa9	0.396	0.000519	0.0248
Nudt7	0.646	1.60E-05	0.00273	Slc25a51	0.314	0.000521	0.0248
Acad11	0.654	1.63E-05	0.00276	Pcdh19	0.543	0.000529	0.0249
Suclg1	0.63	1.92E-05	0.00319	Atp5a1	0.413	0.000531	0.0249
Epha3	0.473	2.05E-05	0.00337	Hspa9	0.352	0.000549	0.0255
Acsl1	0.774	2.10E-05	0.00339	Aspa	0.563	0.000557	0.0258
Dhdh	0.483	2.13E-05	0.00341	Sod2	0.435	0.00057	0.0263
Rnase4	0.344	2.15E-05	0.00341	Slc1a1	0.631	0.000577	0.0265
Aplnr	0.766	2.18E-05	0.00345	Cpxm2	0.572	0.000578	0.0265
Snrk	0.368	2.24E-05	0.00351	D10Jhu81e	0.495	0.000593	0.027
Elovl6	0.777	2.49E-05	0.00371	D10Jhu81e	0.495	0.000593	0.027
Ppargc1a	0.765	2.48E-05	0.00371	Gsta4	0.633	0.000604	0.0275
Pnpla2	0.668	2.48E-05	0.00371	Adgre4	0.583	0.00062	0.028
Naalad2	0.632	2.46E-05	0.00371	Bche	0.595	0.000628	0.0282
Adtrp	0.775	2.58E-05	0.00379	Adrb1	0.625	0.000636	0.0285
Prkcq	0.632	2.56E-05	0.00379	Omd	0.529	0.000667	0.0294
Acat2	0.649	2.72E-05	0.00397	Acvr1c	0.621	0.000675	0.0297
Etfdh	0.641	2.76E-05	0.00399	Hist1h2bl	0.579	0.000689	0.0302
Ffar4	0.771	2.83E-05	0.00403	Mmd	0.314	0.000693	0.0302
Cmtm4	0.292	2.83E-05	0.00403	D5Ertd579e	0.212	0.000692	0.0302
Lbh	0.342	2.91E-05	0.00411	Nckap1	0.19	0.00071	0.0308
Atp1a2	0.695	2.96E-05	0.00415	Tmem182	0.612	0.00073	0.0313
Sdha	0.585	3.13E-05	0.00435	Bckdhb	0.426	0.000733	0.0313
Ebf2	0.678	3.22E-05	0.00445	Ginm1	0.273	0.000731	0.0313
Ppp1r3c	0.752	3.28E-05	0.00449	Cox6a1	0.418	0.000739	0.0315
Chrdl1	0.63	3.32E-05	0.00452	Cox17	0.366	0.000748	0.0318

Clec4a1	0.536	3.36E-05	0.00452	Mcpt4	0.62	0.000785	0.0331
Hmgcs1	0.459	3.36E-05	0.00452	Acadvl	0.614	0.000786	0.0331
AI317395	0.766	3.50E-05	0.00457	Ndufa12	0.416	0.000799	0.0335
Gm10053	0.68	3.50E-05	0.00457	Gm17535	0.616	0.000807	0.0337
Ccl11	0.717	3.57E-05	0.0046	Cisd3	0.557	0.000818	0.034
mt-Nd2	0.603	3.75E-05	0.0048	Pds5b	0.197	0.000817	0.034
Akap1	0.553	3.80E-05	0.00483	Cnst	0.344	0.000829	0.0343
Tob1	0.451	3.87E-05	0.00489	Ces1f	0.606	0.00084	0.0346
Meox2	0.609	4.19E-05	0.00521	Ech1	0.535	0.000853	0.035
Cxcl12	0.432	4.19E-05	0.00521	Chp2	0.577	0.000863	0.0354
Rasd1	0.646	4.57E-05	0.00551	Trdn	0.522	0.00087	0.0355
Acss2	0.643	4.55E-05	0.00551	Hemk1	0.446	0.000872	0.0355
Egln3	0.631	4.50E-05	0.00551	Oxnad1	0.453	0.000879	0.0356
Ppp2r5a	0.439	4.53E-05	0.00551	Ndrg4	0.296	0.000885	0.0358
Cib2	0.654	4.64E-05	0.00556	Clec10a	0.538	0.000894	0.0361
Pgm2	0.486	4.81E-05	0.00572	Gpihbp1	0.607	0.000921	0.037
Esrrg	0.686	5.00E-05	0.00592	Ces1d	0.586	0.00093	0.0371
Fam195a	0.707	5.14E-05	0.006	Ndufs3	0.361	0.000936	0.0373
1810011O 10Rik	0.663	5.16E-05	0.006	Trim67	0.605	0.000951	0.0376
Clec4b1	0.732	5.41E-05	0.0062	Cd226	0.555	0.000953	0.0376
Fasn	0.731	5.38E-05	0.0062	Cidea	0.534	0.000946	0.0376
Tppp	0.707	5.67E-05	0.0063	RP23-354G14.1	0.611	0.000959	0.0377
Gys1	0.618	5.70E-05	0.0063	Tpsb2	0.61	0.000964	0.0378
Cyc1	0.58	5.76E-05	0.0063	Aldoa	0.31	0.000965	0.0378
Ndufb3	0.447	5.73E-05	0.0063	Gm38178	0.55	0.000991	0.0386
Itih5	0.526	5.86E-05	0.00634	Pcdh18	0.454	0.000996	0.0386
Lyrm5	0.406	5.93E-05	0.00638	Cox6c	0.405	0.00101	0.0391
Clybl	0.635	5.99E-05	0.0064	Rgs7	0.556	0.00102	0.0393
Pparg	0.557	6.08E-05	0.00643	Adrb3	0.565	0.00105	0.0398
Ndufs1	0.44	6.25E-05	0.00654	Gys2	0.543	0.00104	0.0398
Gm10720	0.715	6.47E-05	0.0067	Tspan15	0.508	0.00104	0.0398
Acaca	0.576	6.48E-05	0.0067	Gm7895	0.417	0.00105	0.0398
Cd300lg	0.721	6.58E-05	0.00671	Fam13a	0.606	0.00108	0.0406
Lvrn	0.687	6.59E-05	0.00671	Pde4c	0.605	0.00109	0.0406
Aifm2	0.59	6.63E-05	0.00671	L2hgdh	0.458	0.00107	0.0406
Dbt	0.364	6.52E-05	0.00671	Gdf10	0.443	0.00108	0.0406
RP23-119D13.4	0.715	6.73E-05	0.00675	Lpin1	0.373	0.00108	0.0406
Dcn	0.336	6.80E-05	0.00675	Sfrp2	0.353	0.00108	0.0406
Ctcfl	0.736	7.05E-05	0.00696	Mrpl12	0.379	0.0011	0.0409
C3	0.559	7.09E-05	0.00696	Acacb	0.603	0.00113	0.0416

A530016L24Rik	0.734	7.24E-05	0.00706	Chchd3	0.331	0.00113	0.0416
Gm10032	0.684	7.30E-05	0.00707	Ldha	0.274	0.00117	0.0426
Deptor	0.44	7.32E-05	0.00707	Ldhb	0.534	0.00117	0.0427
Ddo	0.721	7.59E-05	0.00725	Plbd1	0.422	0.00118	0.0427
Tmem79	0.726	7.97E-05	0.00755	Colec11	0.572	0.0012	0.0432
Dhrs4	0.405	7.97E-05	0.00755	Agpat9	0.521	0.0012	0.0432
Lep	0.694	8.23E-05	0.00776	Pon1	0.6	0.00121	0.0433
Kbtbd11	0.563	8.43E-05	0.00786	Pcx	0.595	0.00121	0.0433
Ndufa10	0.532	9.38E-05	0.00854	Dnah3	0.594	0.00121	0.0433
Ndufv1	0.549	9.58E-05	0.00863	BC023105	0.585	0.00121	0.0433
Ncan	0.64	9.73E-05	0.00869	P2rx5	0.507	0.00121	0.0433
Tnfrsf11b	0.472	1.00E-04	0.00886	Cidec	0.575	0.00122	0.0434
Acaa2	0.713	0.000101	0.00889	Cox5b	0.407	0.00123	0.0434
Mrc1	0.444	0.000102	0.00893	Ephx2	0.414	0.00124	0.0436
F13a1	0.588	0.000106	0.00913	Kcnk3	0.556	0.00124	0.0437
Spta1	0.718	0.000107	0.00914	mt-Nd5	0.424	0.00126	0.0442
RP24-492L15.5	0.713	0.000107	0.00914	Scp2-ps2	0.368	0.00126	0.0442
Mipep	0.407	0.00011	0.00926	Anapc13	0.4	0.00127	0.0446
Steap4	0.635	0.000115	0.00971	Pdp2	0.424	0.0013	0.0453
Hadha	0.508	0.000116	0.00971	Pygl	0.387	0.00131	0.0456
Idh3b	0.562	0.000118	0.00979	Adamtsl3	0.322	0.00135	0.0463
Tmem204	0.492	0.000118	0.00979	Fbp2	0.558	0.00136	0.0465
mt-Nd4	0.54	0.000126	0.0102	Poldip2	0.297	0.00136	0.0465
Acat1	0.538	0.000125	0.0102	Adck3	0.588	0.00137	0.0468
Prdx3	0.396	0.000125	0.0102	1700037H04Rik	0.441	0.00138	0.0468
Negr1	0.645	0.000128	0.0103	Vwa8	0.354	0.00138	0.0468
Gmpr	0.709	0.00013	0.0104	Echdc3	0.555	0.00139	0.0471
Ldhd	0.644	0.000132	0.0104	Gm13169	0.574	0.00139	0.0472
Slc25a19	0.581	0.000132	0.0104	Gm9899	0.577	0.00142	0.0477
Pex11a	0.511	0.000129	0.0104	Otop1	0.529	0.00142	0.0477
Dld	0.462	0.000131	0.0104	Gm7666	0.43	0.00142	0.0477
Vtn	0.671	0.000135	0.0105	Acox1	0.43	0.00145	0.0484
Dlst	0.439	0.000135	0.0105	Csad	0.374	0.00145	0.0485
Myh14	0.699	0.000141	0.0108	Irs3	0.59	0.00146	0.0486
Slc25a1	0.401	0.00014	0.0108	Timp4	0.559	0.00148	0.0489
Idh3g	0.593	0.000143	0.0109	Ndufab1	0.347	0.00149	0.0492
Art3	0.562	0.000146	0.0111	Scn4a	0.546	0.00151	0.0496
Fcor	0.703	0.000148	0.0112	RP23-385G21.3	0.563	0.00152	0.0498
Amy1	0.684	0.000157	0.0118	Slc25a48	0.503	0.00153	0.0499
Hsd11b1	0.64	0.000162	0.012	Lrrc24	0.462	0.00153	0.05

Table 2: Significantly downregulated genes in SMC-PDGFBR KO vs. WT

Gene	Log2 FC	P-Value	Adj P-Val	Gene	Log2 FC	P-Value	Adj P-Val
Pdgfrb	-0.488	3.33E-11	6.31E-07	Cic	-0.18	0.000417	0.0218
F830016B08Rik	-1.15	3.60E-10	1.36E-06	Slamf7	-0.458	0.000418	0.0218
Pianp	-0.634	9.63E-09	1.40E-05	Kif1a	-0.385	0.000431	0.0222
Plekhm2	-0.386	2.41E-07	0.000169	Pdlim4	-0.309	0.000435	0.0224
Vipr1	-0.556	5.89E-07	0.000255	Unc93b1	-0.263	0.000453	0.0231
Tmem82	-0.674	5.94E-07	0.000255	St18	-0.498	0.000454	0.0231
Cd22	-0.478	1.29E-06	0.000417	Fjx1	-0.422	0.000458	0.0232
Mical1	-0.38	1.72E-06	0.000471	Cd4	-0.487	0.000461	0.0232
Dock3	-0.695	3.15E-06	0.000784	Tanc2	-0.218	0.000469	0.0234
Cd37	-0.466	3.31E-06	0.000803	Kirrel3	-0.467	0.000478	0.0236
Coro2a	-0.491	4.49E-06	0.000999	Fmn1	-0.371	0.000491	0.024
Syt15	-0.399	5.51E-06	0.00116	Zfp516	-0.22	0.000497	0.0241
G530011O06Rik	-0.771	6.79E-06	0.00137	Nckap5l	-0.308	0.000496	0.0241
Treml2	-0.543	9.38E-06	0.00176	Nipal3	-0.333	0.000501	0.0242
Sep9	-0.21	1.14E-05	0.00209	Ppap2c	-0.356	0.000504	0.0243
Pitpnm1	-0.269	1.15E-05	0.00209	Ptpn1	-0.36	0.000519	0.0248
Il10ra	-0.396	1.18E-05	0.00212	Il12rb2	-0.429	0.00052	0.0248
Cerk	-0.356	1.47E-05	0.00257	Aatk	-0.336	0.000527	0.0249
Hpse	-0.611	1.60E-05	0.00273	Lrp12	-0.426	0.000529	0.0249
Tpcn2	-0.368	1.92E-05	0.00319	Gm4951	-0.642	0.000534	0.025
C77080	-0.436	2.07E-05	0.00338	Hook2	-0.418	0.000544	0.0254
Slc8b1	-0.41	2.27E-05	0.00353	Vasp	-0.244	0.000552	0.0256
Src	-0.312	2.33E-05	0.00359	Il4ra	-0.281	0.000571	0.0263
Ttyh3	-0.243	3.39E-05	0.00452	Bcl11a	-0.461	0.000586	0.0268
Gm13889	-0.602	3.42E-05	0.00452	Tbc1d22a	-0.27	0.000611	0.0277
Eepd1	-0.388	3.53E-05	0.00458	Acpp	-0.479	0.00061	0.0277
Unk	-0.338	4.54E-05	0.00551	Slc6a8	-0.394	0.000623	0.0281
Aldh1b1	-0.571	5.17E-05	0.006	6330416G13Rik	-0.363	0.000637	0.0285
Ssh3	-0.294	5.70E-05	0.0063	Wdr81	-0.225	0.00065	0.0289
Adgre5	-0.373	5.71E-05	0.0063	Pip5k1c	-0.251	0.000648	0.0289
H2-D1	-0.379	5.53E-05	0.0063	Jade2	-0.275	0.000651	0.0289
H2-M2	-0.738	5.56E-05	0.0063	Apoe	-0.569	0.000657	0.0291
Ahnak2	-0.295	5.80E-05	0.00631	Hal	-0.578	0.000661	0.0293
Lyz1	-0.604	6.03E-05	0.00641	Cmip	-0.262	0.000666	0.0294
Apobec1	-0.432	6.18E-05	0.0065	Pld3	-0.436	0.000706	0.0307
Sash1	-0.31	6.66E-05	0.00671	Zyx	-0.262	0.000721	0.0312

Sdc1	-0.328	6.81E-05	0.00675
Slco2a1	-0.218	7.58E-05	0.00725
Sbno2	-0.262	8.30E-05	0.00778
Sipa1l2	-0.282	8.60E-05	0.00798
Pik3r5	-0.395	8.77E-05	0.0081
Mir143	-0.667	9.00E-05	0.00827
Itga5	-0.326	9.07E-05	0.0083
Best1	-0.592	9.46E-05	0.00857
Ssbp4	-0.284	9.63E-05	0.00864
Rin3	-0.323	9.96E-05	0.00885
Eno2	-0.396	0.000102	0.00893
Abr	-0.291	0.000105	0.00913
Rasa3	-0.201	0.000106	0.00914
Entpd1	-0.377	0.000108	0.00919
Tcirg1	-0.399	0.000121	0.00999
P2rx4	-0.347	0.000124	0.0102
Gm25099	-0.693	0.000128	0.0103
Syk	-0.344	0.00013	0.0104
Cd300lf	-0.462	0.00014	0.0108
Sprn	-0.694	0.000146	0.0111
Mvb12b	-0.27	0.000159	0.0119
Ppp1r15a	-0.303	0.000176	0.0127
Stra6l	-0.501	0.00018	0.0128
Cd244	-0.524	0.000179	0.0128
Snord89	-0.636	0.000183	0.0129
Apba1	-0.329	0.000185	0.013
Acox3	-0.36	0.000192	0.0132
Mertk	-0.414	0.000193	0.0132
Ccdc148	-0.594	0.000192	0.0132
Rn7s2	-0.563	2.00E-04	0.0136
Coro7	-0.264	0.000203	0.0137
Tpra1	-0.335	0.000204	0.0137
Arid3a	-0.404	0.000204	0.0137
Akt1	-0.189	0.000212	0.0141
Gab2	-0.255	0.000251	0.0164
Dnase2a	-0.385	0.000268	0.0169
Gm28154	-0.583	0.000265	0.0169
Sh3pxd2b	-0.263	0.000275	0.0172
St6gal-nac4	-0.401	0.000275	0.0172
Lrp10	-0.181	0.000282	0.0173
5033426O07Rik	-0.624	0.000721	0.0312
Mgat5	-0.247	0.00073	0.0313
Tmem144	-0.464	0.000727	0.0313
Slc23a2	-0.286	0.000746	0.0317
Speg	-0.448	0.000768	0.0325
Camk2g	-0.233	0.000781	0.033
Hps1	-0.295	0.000806	0.0337
Ttyh2	-0.397	0.000806	0.0337
Galns	-0.416	0.000826	0.0342
Snx29	-0.219	0.000843	0.0347
Sirpa	-0.401	0.000866	0.0354
Evl	-0.389	0.000874	0.0355
Rpl10a	-0.337	0.000915	0.0369
Lyz2	-0.443	0.000922	0.037
Col18a1	-0.263	0.000927	0.0371
Abcg1	-0.37	0.000938	0.0373
Daglb	-0.351	0.000955	0.0376
Nceh1	-0.439	0.000948	0.0376
Dna2	-0.367	0.000974	0.038
Gns	-0.362	0.000994	0.0386
Coro1c	-0.278	0.00101	0.0389
Csf2rb	-0.341	0.00102	0.0393
Arhgap6	-0.257	0.00104	0.0398
Parvg	-0.352	0.00104	0.0398
Gm26165	-0.602	0.00106	0.0401
Bex1	-0.574	0.00106	0.0403
Plekhm3	-0.201	0.00108	0.0406
Plekho2	-0.358	0.00109	0.0407
Tmem132a	-0.281	0.00112	0.0415
Mlph	-0.325	0.00112	0.0415
Pi4k2a	-0.347	0.00112	0.0415
Galnt7	-0.363	0.00114	0.0417
Gm15247	-0.573	0.00114	0.0417
Trim29	-0.516	0.00116	0.0425
Ndst1	-0.174	0.00117	0.0426
Klhl3	-0.453	0.00117	0.0426
Stac2	-0.323	0.00119	0.0431
Slc4a8	-0.317	0.0012	0.0432
Accs	-0.324	0.00122	0.0434
Grb2	-0.33	0.00122	0.0434

Mcoln2	-0.501	0.000296	0.0179	Lemd2	-0.23	0.00127	0.0446
Iqsec1	-0.257	3.00E-04	0.0181	Dnase1l1	-0.36	0.00128	0.0449
Furin	-0.188	0.000312	0.0188	Itgb3	-0.327	0.00129	0.0451
Cd300a	-0.442	0.000323	0.0191	Gdf15	-0.504	0.00132	0.0457
Tnfaip2	-0.419	0.000324	0.0192	Prkcd	-0.283	0.00132	0.0458
Gdpd1	-0.385	0.000329	0.0193	Gltp	-0.317	0.00135	0.0463
Pltp	-0.425	0.000329	0.0193	Polm	-0.406	0.00134	0.0463
Fam83f	-0.533	0.000343	0.0196	5031414D 18Rik	-0.423	0.00135	0.0463
Tnfrsf1b	-0.351	0.000348	0.0197	Adgrg3	-0.465	0.00136	0.0465
Slc35f6	-0.409	0.000347	0.0197	Syngr1	-0.471	0.00138	0.0468
Sorbs3	-0.311	0.000353	0.0199	Zmiz1	-0.181	0.00142	0.0477
Dmxl2	-0.328	0.000365	0.0203	Fam84a	-0.442	0.00141	0.0477
Mroh1	-0.243	0.000371	0.0205	Clcn7	-0.335	0.00146	0.0487
Ralgds	-0.281	0.00037	0.0205	Rasa4	-0.342	0.00147	0.0489
Atp13a2	-0.342	0.000373	0.0205	Atp6v0d2	-0.461	0.00148	0.0489
Arap1	-0.263	0.000393	0.0211	Zdhhc18	-0.294	0.0015	0.0494
Rab11fip5	-0.233	0.000397	0.0212	Slc11a1	-0.359	0.00151	0.0496
5031439G 07Rik	-0.386	0.000399	0.0213	Cxcr1	-0.587	0.00152	0.0498
Xylt1	-0.386	0.000415	0.0217	Mefv	-0.455	0.00153	0.0499

II. Single Cell RNA-seq

Table 3: Top 100 enriched genes in each cluster

Cluster	Gene	Adj P-Value	Cluster	Gene	Adj P-Value
0	Ltbp2	2.89E-71	1	1500015O10Rik	3.60E-61
0	Crlf1	3.61E-64	1	Fibin	2.87E-45
0	Ly6a	6.38E-59	1	Cst6	1.97E-42
0	Cald1	9.85E-57	1	Col6a1	8.42E-40
0	Vcam1	9.61E-53	1	Col1a1	3.44E-39
0	Timp1	1.15E-47	1	Sparc	5.83E-39
0	Nbl1	1.24E-47	1	Col6a2	4.00E-37
0	Pcolce	3.67E-47	1	Tnc	6.16E-36
0	Sod3	1.27E-46	1	Cilp2	4.29E-35
0	Lgals1	5.09E-46	1	Col1a2	7.50E-35
0	Fbln2	3.98E-44	1	Bgn	3.39E-33
0	Fstl1	4.23E-44	1	Acan	5.13E-33
0	Ecm1	6.91E-44	1	Lum	5.85E-33
0	Loxl3	8.12E-43	1	C1qtnf2	5.01E-31
0	Mmp2	2.83E-40	1	Gsn	2.91E-30
0	Col3a1	1.16E-38	1	Vkorc1	6.86E-30
0	Fbn1	1.32E-38	1	Prelp	1.47E-29
0	Ptgis	4.84E-38	1	Col6a3	2.40E-29
0	Serpinf1	9.40E-38	1	Gm17455	1.86E-28
0	Fat1	1.28E-37	1	Fkbp7	5.03E-28
0	Fzd1	1.37E-37	1	Col3a1	2.41E-27
0	Adamts2	2.08E-37	1	Pcolce	6.85E-27
0	Lum	5.60E-37	1	Mxra8	9.75E-27
0	Col8a1	7.46E-37	1	Wwp2	1.72E-26
0	Bgn	1.90E-36	1	Tnfrsf11b	1.85E-25
0	Fst	3.63E-36	1	Frzb	4.25E-25
0	Fbln5	6.60E-36	1	Cryab	2.24E-24
0	Rbp1	1.06E-35	1	Dap	6.69E-24
0	Lmna	3.62E-35	1	Pkd1	2.88E-23
0	Angptl2	7.39E-35	1	Gdf10	1.13E-22
0	Aebp1	7.69E-34	1	Susd5	1.81E-22
0	Sdc2	5.14E-33	1	Copz2	4.65E-22
0	Igfbp7	5.84E-33	1	Slc29a1	5.12E-22
0	Pde1a	5.85E-33	1	Rcn3	6.33E-22
0	Mrc2	2.84E-32	1	S100b	9.30E-22
0	Kcnj15	4.69E-32	1	Nupr1	9.58E-22
0	Phlda3	8.86E-32	1	Fzd9	1.18E-21
0	Inhba	2.20E-31	1	Crispld1	2.04E-21
0	Vcan	1.30E-30	1	Igfbp7	2.08E-21
0	Ak1	1.63E-30	1	Serpine2	2.19E-21

0	Sfrp4	1.81E-30	1	Ppic	3.20E-21
0	Sdc1	2.30E-30	1	Fn1	4.26E-21
0	Nrn1	3.81E-29	1	Rarres1	5.27E-21
0	Dkk3	6.72E-29	1	Aspn	8.68E-21
0	Lhfp	2.28E-28	1	Matn2	1.01E-20
0	Ly6c1	7.58E-28	1	Spp1	6.05E-20
0	Mmp23	1.94E-27	1	Serpinh1	4.34E-19
0	Wisp2	4.04E-26	1	Selm	4.62E-19
0	Tnfrsf12a	1.63E-25	1	B3gnt9	7.44E-19
0	Rnase4	2.86E-25	1	Abi3bp	9.42E-19
0	Plpp3	3.19E-25	1	Col15a1	1.77E-18
0	2200002D01Rik	2.20E-24	1	Gas1	2.14E-18
0	S100a4	2.32E-24	1	Cdo1	2.35E-18
0	Bmp1	2.36E-24	1	Tspan3	2.54E-18
0	Gja1	2.40E-24	1	Dcn	3.05E-18
0	Ank	3.47E-24	1	Cox4i2	4.35E-18
0	Chpf	3.50E-24	1	Slc7a2	4.86E-18
0	Selp	3.58E-24	1	Clu	1.10E-17
0	Thbs1	4.07E-24	1	Scara3	1.16E-17
0	Mgp	2.45E-23	1	Enpp1	1.50E-17
0	Nupr1	4.09E-23	1	Fmod	1.54E-17
0	Id3	4.76E-23	1	Mmp2	1.86E-17
0	Gas6	7.48E-23	1	Cgref1	5.73E-17
0	Cthrc1	1.34E-22	1	Erg	9.94E-17
0	Sulf1	1.78E-22	1	Dkk3	1.36E-16
0	Col12a1	5.85E-22	1	Cspg4	2.74E-16
0	Efemp2	8.92E-22	1	Dbp	5.36E-16
0	Rcn3	2.73E-21	1	Col12a1	1.13E-15
0	Col5a1	3.90E-21	1	Timp3	1.64E-15
0	Cacna2d1	2.59E-20	1	Fkbp9	1.64E-15
0	Fam198b	3.50E-20	1	Epdr1	2.11E-15
0	Lox	3.63E-20	1	Col5a2	3.79E-15
0	Boc	3.65E-20	1	Tmed3	7.23E-15
0	Cxcl12	1.32E-19	1	Anxa8	7.42E-15
0	Scx	1.30E-18	1	Hist1h2bc	9.00E-15
0	Thbs2	2.71E-18	1	Col14a1	1.01E-14
0	Fn1	4.24E-18	1	Ccnd2	1.46E-14
0	Col6a3	4.42E-18	1	Gpx8	9.48E-14
0	Aspn	5.55E-17	1	Cyb5r3	4.15E-13
0	Ackr3	1.22E-16	1	Mfge8	4.60E-13
0	Mme	8.67E-16	1	Rin2	4.77E-13
0	Anxa8	2.10E-15	1	Ptgis	1.02E-12
0	Dpt	3.62E-15	1	Sdc2	2.31E-12
0	F5	3.80E-15	1	Cdc42ep3	2.67E-12
0	Col15a1	6.98E-15	1	A230065H16Rik	3.75E-12

0	Col5a2	1.37E-14	1	Snhg18	6.45E-12
0	Sfrp2	1.78E-14	1	Srpx2	9.92E-12
0	Postn	6.41E-14	1	Ctsk	2.04E-10
0	Col6a1	1.16E-13	1	Col11a2	2.79E-10
0	Itgbl1	1.92E-13	1	Lmo4	3.54E-10
0	Timp3	4.18E-13	1	Slurp1	4.53E-10
0	Ggct	5.94E-13	1	Clec11a	8.38E-10
0	Tnc	8.43E-13	1	Sod3	2.74E-09
0	Nr4a2	2.59E-12	1	Igfbp6	2.18E-07
0	Igfbp4	4.31E-11	1	Sncg	0.000239962
0	Gsn	1.80E-09	1	Gm42418	0.001284516
0	Cxcl1	7.66E-09	1	Penk	0.286193642
0	Cxcl14	4.55E-08	1	Comp	1
0	Sncg	7.01E-08	1	Serpinf1	1
0	Gm12840	5.73E-07	1	Cytl1	1
2	Lbp	8.29E-46	3	C3ar1	6.38E-148
2	Mmp3	1.76E-43	3	Adgre1	1.02E-137
2	Prg4	2.00E-40	3	Fcgr3	9.28E-133
2	Lcn2	6.59E-40	3	Igf1	6.70E-131
2	Chil1	8.89E-40	3	Fcrls	2.43E-130
2	Bpifb1	3.86E-38	3	Syngr1	1.14E-127
2	Clu	4.50E-37	3	Cd84	2.19E-126
2	Fth1	2.09E-36	3	Bcl2a1b	4.85E-123
2	Tsc22d1	1.17E-35	3	Mpeg1	5.15E-123
2	Saa1	1.42E-35	3	Ms4a7	1.15E-122
2	Serpine2	7.89E-35	3	Ms4a6d	6.19E-122
2	Scara3	4.52E-34	3	Basp1	7.45E-121
2	Gpm6b	6.17E-34	3	Lat2	1.10E-118
2	Spp1	1.30E-33	3	Pla2g7	1.18E-115
2	Mmp13	4.49E-33	3	Lilrb4a	1.18E-110
2	Saa3	1.83E-27	3	Cd72	1.90E-108
2	Gas1	1.12E-22	3	Dpep2	5.07E-106
2	Edil3	6.12E-22	3	Lilr4b	2.71E-105
2	Hp	1.27E-21	3	Slc11a1	2.82E-104
2	Saa2	3.52E-21	3	Itgb2	9.92E-104
2	C3	1.19E-20	3	Cd48	1.62E-103
2	Fap	1.34E-20	3	C1qc	1.08E-102
2	Mt2	1.29E-19	3	C5ar1	2.34E-102
2	Antxr1	1.38E-19	3	AF251705	1.83E-101
2	Nt5dc2	7.76E-19	3	Cd68	1.52E-100
2	Mafb	1.56E-18	3	Gatm	1.69E-99
2	Tspan11	3.85E-18	3	Lcp1	1.88E-98
2	Clmp	2.09E-17	3	Cyth4	9.02E-98
2	Gpx3	2.33E-17	3	Ptpn6	1.29E-96
2	Serpina3n	7.49E-17	3	Ucp2	2.16E-95

2	Abi3bp	1.44E-16	3	Ly86	3.99E-95
2	Mt1	1.84E-16	3	Laptm5	5.92E-94
2	Lrp1	1.12E-15	3	Spi1	8.66E-94
2	Fabp4	2.29E-15	3	C1qa	1.34E-92
2	Sdc4	3.41E-15	3	Ncf4	2.45E-91
2	C1qtnf7	3.63E-15	3	Csf1r	2.77E-90
2	1110008P14Rik	3.90E-15	3	C1qb	2.48E-89
2	Nbl1	4.13E-15	3	Slamf9	5.74E-86
2	Cp	5.31E-15	3	Ctss	4.18E-82
2	Slpi	5.87E-15	3	Apobec1	1.23E-81
2	Cdc42ep3	3.31E-14	3	Aif1	5.39E-81
2	Mxra8	4.87E-14	3	Arrb2	7.82E-79
2	Fxyd1	9.51E-14	3	Tyrobp	7.45E-75
2	Hsd11b1	1.73E-13	3	Cotl1	4.67E-73
2	Dcn	2.40E-13	3	Fcer1g	5.18E-73
2	Gadd45a	2.99E-13	3	Cndp2	3.22E-71
2	Matn4	3.96E-13	3	Coro1a	9.38E-71
2	Gm13889	3.98E-13	3	Rgs1	2.48E-70
2	Gdf10	1.91E-12	3	Zmynd15	2.70E-69
2	Islr	2.11E-12	3	Wfdc17	3.65E-69
2	Pdzrn4	7.35E-12	3	Gpr137b	3.68E-68
2	Wif1	9.16E-12	3	Clec4d	4.18E-68
2	Pdgfra	9.48E-12	3	Cd53	7.53E-68
2	Dbi	1.11E-11	3	Cxcl16	3.66E-67
2	Cdo1	1.74E-11	3	Alox5ap	2.13E-63
2	Ldhb	1.87E-11	3	Hexb	5.85E-63
2	Wfdc21	2.01E-11	3	Trem2	3.71E-62
2	Fam20c	5.91E-11	3	Ctsb	4.61E-62
2	Ldha	1.00E-10	3	Gngt2	8.51E-62
2	Sod2	1.19E-10	3	Unc93b1	7.08E-60
2	Selenbp1	1.31E-10	3	Ccl4	7.98E-60
2	Smoc1	1.48E-10	3	Ftl1	1.22E-59
2	Cxx1b	2.75E-10	3	Ctsz	1.55E-59
2	Enpp2	3.19E-10	3	Lyz2	3.69E-59
2	Igfbp4	6.43E-10	3	Mmp12	1.67E-58
2	Rgcc	7.33E-10	3	Cyba	9.09E-58
2	S100b	7.61E-10	3	Ctsc	2.68E-57
2	Runx1	8.33E-10	3	Grn	7.37E-56
2	Lum	1.03E-09	3	Rgs10	3.64E-54
2	Ier2	1.30E-09	3	Il10rb	5.75E-54
2	Wfdc12	1.36E-09	3	Lgals3	1.30E-53
2	F13a1	2.62E-09	3	Psap	2.52E-53
2	Ptpn2	2.71E-09	3	Ccl3	3.64E-53
2	Cdkn2c	2.90E-09	3	Efhd2	1.85E-52
2	Egr1	3.12E-09	3	Ctsa	5.83E-51

2	Lpl	7.30E-09	3	Lgmn	6.66E-51
2	Cxcl14	1.25E-08	3	Abhd12	7.32E-51
2	Klf4	1.43E-08	3	Plin2	2.23E-50
2	Cxx1a	1.81E-08	3	Sirpa	3.25E-50
2	Rasd1	2.49E-08	3	Ckb	2.59E-49
2	Tob1	4.13E-08	3	Gm10116	2.96E-47
2	Hand2	5.51E-08	3	Tpd52	1.23E-46
2	Cemip	9.61E-08	3	Gpnmb	6.47E-45
2	Pdgfc	3.55E-07	3	Gusb	1.70E-44
2	Plpp3	1.02E-06	3	Ctsd	7.68E-44
2	Phlda1	1.18E-06	3	Tmsb4x	5.76E-43
2	Cd302	1.84E-06	3	Sh3bgrl3	8.67E-43
2	Smoc2	2.08E-06	3	H2-D1	2.63E-42
2	Jun	3.24E-06	3	Capg	3.38E-42
2	Fosb	1.10E-05	3	Cd14	8.06E-42
2	Sox9	1.11E-05	3	Gdf3	1.33E-39
2	Slc7a2	1.20E-05	3	Creg1	2.01E-39
2	Igfbp6	1.57E-05	3	Cstb	4.30E-38
2	Hbegf	0.00010862	3	Man2b1	1.40E-36
2	Rbp4	0.000303771	3	Lsp1	6.50E-31
2	Id1	0.000351868	3	Sepp1	6.45E-30
2	Btg2	0.001012291	3	Pld3	9.36E-30
2	Zfp36l1	0.001244039	3	Pltp	1.34E-19
2	Nr4a1	0.004272478	3	Fabp5	5.39E-16
2	Fos	0.076576412	3	Ctsl	3.19E-08
4	Lect1	9.34E-91	5	Cebpb	0.020145172
4	Scrg1	4.02E-80	5	Ccr2	1.93E-145
4	Ucma	9.03E-71	5	Plbd1	1.98E-136
4	Col11a1	1.31E-69	5	Ms4a6c	1.29E-124
4	Hapln1	6.14E-65	5	Ms4a4c	2.14E-120
4	Mia	9.17E-65	5	Il1b	1.58E-108
4	Bpifb1	1.82E-61	5	Cytip	1.32E-105
4	Atp1a2	5.14E-58	5	Napsa	6.43E-103
4	Mfi2	1.98E-56	5	Spi1	2.51E-101
4	3110079O15Rik	1.06E-53	5	Cd300a	2.45E-98
4	Avpr1a	4.82E-52	5	Sirpb1c	2.51E-97
4	Col9a3	4.82E-48	5	Hck	8.15E-96
4	Ppp1r1b	7.09E-47	5	Lst1	1.79E-93
4	Chil1	7.84E-45	5	Coro1a	7.82E-93
4	Col2a1	5.97E-44	5	Ifitm6	5.70E-92
4	Lcn2	8.44E-41	5	Ptprc	6.15E-92
4	Xylt1	9.81E-41	5	Pld4	1.12E-91
4	Enpp2	9.19E-40	5	Alox5ap	3.05E-88
4	Col11a2	1.21E-39	5	Il1r2	1.13E-86
4	Steap4	1.50E-39	5	H2-DMa	1.80E-85

4	Wif1	1.58E-39
4	Col27a1	6.64E-39
4	Edil3	9.70E-39
4	Lbp	2.57E-38
4	Saa1	3.98E-38
4	Saa2	1.44E-37
4	Chad	2.45E-37
4	Otor	8.91E-36
4	Sdc4	6.75E-34
4	1190002N15Rik	8.64E-34
4	mt-Co1	2.16E-32
4	C3	4.96E-32
4	Fmod	8.80E-32
4	S100b	4.68E-30
4	Gpm6b	1.38E-29
4	Saa3	2.82E-29
4	Serpina3n	2.94E-29
4	Sox9	8.25E-29
4	Acan	1.20E-27
4	Fabp4	3.73E-26
4	Phlda1	3.90E-26
4	Cst3	2.07E-25
4	mt-Cytb	2.12E-25
4	Tsc22d1	9.33E-25
4	Fth1	1.79E-24
4	Trpv4	3.26E-24
4	Mt2	6.80E-24
4	Crispld1	9.49E-24
4	Fzd9	1.64E-23
4	mt-Co2	3.59E-23
4	A230065H16Rik	6.67E-23
4	Ccdc80	1.14E-22
4	Fap	1.19E-22
4	Abi3bp	4.27E-22
4	Slc39a14	6.16E-22
4	Gdf10	6.25E-22
4	Cp	1.72E-21
4	Serpine2	3.36E-21
4	Mdfi	2.19E-20
4	Cox4i2	3.80E-20
4	Omd	6.12E-20
4	Htra3	9.73E-20
4	Hbegf	1.23E-19
4	Nt5e	1.82E-18
4	Mmp3	3.54E-18
5	Ucp2	2.74E-83
5	Selplg	1.09E-82
5	Ms4a6b	5.38E-82
5	Cd52	2.16E-81
5	Clec4a3	2.55E-81
5	Gmfg	7.13E-79
5	Plek	5.97E-75
5	Cd53	1.50E-73
5	Laptm5	1.44E-72
5	Cd83	4.88E-72
5	Cotl1	2.82E-71
5	Psmb8	1.23E-70
5	Chil3	5.74E-70
5	Cfp	7.84E-69
5	Ifi27l2a	8.46E-69
5	Dusp2	1.42E-68
5	Tyrobp	2.42E-68
5	Fcgr2b	6.24E-67
5	Lilrb4a	9.14E-67
5	Lcp1	2.51E-66
5	Ifi30	1.24E-65
5	Csf1r	3.63E-65
5	Fcer1g	3.35E-64
5	Fam49b	1.31E-62
5	Cybb	1.45E-62
5	AF251705	1.93E-62
5	Csf2ra	6.16E-61
5	Cd74	1.36E-59
5	Pim1	3.90E-59
5	Ncf4	8.89E-59
5	Ctss	9.20E-59
5	Rac2	1.07E-58
5	Wfdc17	1.30E-58
5	Clec4e	4.23E-58
5	Clec4n	5.67E-58
5	H2-DMb1	4.09E-57
5	Aif1	1.76E-54
5	Lsp1	9.53E-54
5	Ccrl2	5.44E-52
5	Plac8	6.67E-50
5	Ifitm1	1.05E-49
5	Gngt2	1.21E-49
5	Bcl2a1d	2.93E-47
5	Pfn1	7.79E-47
5	Ctsc	6.79E-46

4	Cdo1	5.65E-18	5	Tmsb4x	1.20E-45
4	Plod2	9.54E-18	5	Klrd1	1.37E-45
4	Wfdc21	6.26E-17	5	Unc93b1	2.72E-44
4	Meg3	7.91E-17	5	H2-Eb1	3.79E-44
4	G0s2	1.87E-16	5	Ccl6	4.78E-44
4	Scara3	2.41E-16	5	Gm2a	3.33E-43
4	Mt1	2.24E-15	5	Ly6c2	5.44E-43
4	Prelp	3.40E-15	5	Tpd52	2.33E-42
4	Dbi	4.77E-15	5	Sub1	8.54E-42
4	Zbtb20	7.63E-15	5	H2-Aa	1.06E-41
4	Smoc2	1.62E-14	5	H2-Ab1	2.53E-41
4	Lrp1	2.41E-14	5	Cyba	5.49E-41
4	Fxyd1	3.50E-14	5	Efhd2	5.97E-41
4	Ctgf	3.93E-14	5	Arhgdib	1.12E-40
4	Rgcc	4.60E-13	5	B2m	1.52E-40
4	Fn1	8.63E-13	5	Cd209a	5.33E-40
4	Btg2	9.97E-13	5	H2afz	1.12E-39
4	C4b	2.70E-12	5	Sh3bgrl3	2.16E-39
4	Hp	2.91E-12	5	Syngr2	2.72E-39
4	Id1	4.51E-12	5	Rgs1	5.71E-39
4	Zfp36l1	5.46E-12	5	Srgn	7.11E-39
4	Dcn	9.09E-11	5	Pglyrp1	3.61E-38
4	Ptgs2	4.09E-10	5	Lyz2	3.47E-36
4	Gpx3	6.95E-10	5	Msrb1	6.73E-35
4	Spp1	7.66E-10	5	Actb	7.61E-35
4	Srgn	8.72E-10	5	Slfn2	1.84E-31
4	Nfkbiz	1.03E-09	5	Cd14	8.81E-31
4	Errfi1	4.71E-09	5	Rgs2	1.87E-30
4	Timp3	4.73E-09	5	Limd2	2.00E-29
4	Frzb	1.09E-08	5	Psap	2.65E-23
4	Mgp	8.81E-07	5	Plaur	2.53E-22
4	Sparc	2.75E-06	5	Nfkbia	1.23E-21
4	Wfdc12	5.30E-06	5	Cdk2ap2	3.05E-16
4	Cytl1	3.82E-05	5	Marcksl1	5.13E-11
4	Trf	0.366904048	5	Cxcl2	1.56E-09
6	Ptprb	1.23E-187	7	Myh11	1.06E-164
6	Tie1	1.53E-186	7	Cnn1	4.38E-117
6	Mmrn2	1.24E-185	7	Aoc3	1.66E-109
6	Cdh5	5.48E-184	7	Itga8	6.16E-106
6	Egfl7	2.87E-174	7	CR974586.5	1.32E-88
6	Rasip1	1.83E-151	7	Tagln	1.87E-78
6	Sox17	6.71E-146	7	Lmod1	1.40E-72
6	Icam2	6.76E-146	7	Igfbp2	4.77E-71
6	Esam	8.69E-142	7	Myl9	1.83E-69
6	Tspan7	3.94E-139	7	Mfap4	2.66E-67

6	Cldn5	1.94E-137	7	Prss23	8.47E-63
6	Tek	5.04E-137	7	Itih4	3.44E-62
6	Edn1	6.43E-131	7	Ccl19	3.10E-50
6	Gja5	1.78E-129	7	Actg2	3.57E-48
6	Myct1	1.11E-120	7	Atp1b1	5.13E-47
6	Vwf	5.84E-120	7	Rgs5	3.15E-46
6	Sdpr	1.22E-117	7	Mylk	6.45E-46
6	Clec14a	7.46E-117	7	Tpm2	1.36E-43
6	Pecam1	4.19E-113	7	Angpt2	1.64E-42
6	Pi16	3.62E-112	7	Nov	2.60E-41
6	Tmem158	3.83E-112	7	Acta2	1.29E-39
6	Ecscr	2.49E-110	7	Fmo2	2.78E-38
6	Emcn	3.34E-110	7	Rarres2	1.02E-37
6	Krt18	4.73E-102	7	Sfrp2	2.26E-37
6	Bmx	1.28E-99	7	Gm12840	3.20E-33
6	Heg1	2.69E-94	7	Ppp1r14a	1.43E-32
6	Spon1	3.79E-94	7	Loxl1	2.01E-32
6	Ctla2a	7.10E-91	7	Postn	2.80E-32
6	Bmp4	8.64E-89	7	Spint2	1.95E-31
6	Lmo2	2.22E-88	7	Fblim1	2.59E-30
6	Ece1	2.41E-86	7	Wisp2	2.99E-30
6	Tinagl1	2.38E-84	7	Eln	2.52E-29
6	Gkn3	7.82E-84	7	Igfbp7	1.46E-28
6	F11r	7.70E-77	7	Cald1	2.45E-28
6	Stmn2	1.77E-75	7	Pde3a	3.84E-28
6	Ramp2	3.69E-73	7	Tpm1	8.53E-28
6	Hs3st1	1.35E-70	7	Fstl1	4.35E-27
6	Mcam	2.24E-70	7	Adamts2	2.39E-26
6	Cd93	3.81E-64	7	Serpinb6b	1.26E-25
6	Sfrp1	4.64E-62	7	Dclk1	4.59E-25
6	Cav1	6.12E-61	7	Lpp	8.72E-25
6	Fblim1	4.43E-58	7	Col4a1	2.08E-24
6	Procr	1.18E-56	7	C1s1	5.53E-24
6	Mall	1.57E-55	7	Map1b	1.45E-23
6	Selp	1.60E-55	7	Lgals1	4.37E-23
6	S1pr1	1.08E-54	7	Myl6	1.58E-22
6	Gja4	1.26E-53	7	Csrp2	1.58E-22
6	Pdlim1	2.82E-53	7	Col18a1	1.80E-22
6	Cd34	4.34E-53	7	F2r	5.27E-22
6	S100a16	1.76E-51	7	Tgfb2	1.02E-21
6	Plvap	6.78E-51	7	Rbpms	1.31E-21
6	Dkk2	9.30E-49	7	Flna	2.90E-21
6	Adam10	1.99E-48	7	Cxcl12	1.01E-20
6	Bpgm	1.89E-46	7	Crispld2	1.27E-20
6	Rab11a	1.15E-44	7	Cyp1b1	2.07E-20

6	Rhob	1.77E-44	7	Col4a2	2.08E-20
6	Slc9a3r2	1.82E-44	7	Mfap5	2.56E-20
6	Slco2a1	5.43E-43	7	Lhfp	8.74E-20
6	Ehd4	4.12E-42	7	Csrp1	1.08E-19
6	Cdh13	1.42E-41	7	Fbn1	1.97E-19
6	Fkbp1a	3.60E-41	7	Sncg	1.29E-18
6	Gng11	5.93E-41	7	Fhl1	1.55E-18
6	Tubb3	2.28E-40	7	Gpc6	3.78E-18
6	Eng	7.98E-40	7	Aebp1	7.73E-18
6	Itgb1	1.21E-39	7	Lox	9.87E-18
6	Tm4sf1	2.81E-39	7	Mmp23	9.32E-17
6	Efna1	1.40E-38	7	Filip1l	1.06E-16
6	Ltbp4	2.99E-38	7	Serping1	1.10E-16
6	Sox4	3.54E-35	7	Col8a1	3.07E-16
6	Cpe	1.42E-33	7	Pcdh7	1.79E-15
6	Actn1	3.24E-33	7	S100a11	2.92E-15
6	Rbp1	6.80E-33	7	Fndc1	3.17E-15
6	Ace	1.65E-32	7	Epas1	4.30E-15
6	Tmsb10	4.48E-32	7	Pls3	4.48E-15
6	Col18a1	4.69E-31	7	C4b	1.84E-14
6	Il6st	2.57E-30	7	Rbp1	4.74E-14
6	F2r	3.51E-30	7	Fbln5	5.60E-14
6	Epas1	3.79E-30	7	Mustn1	6.41E-14
6	Eln	8.50E-30	7	Cx3cl1	8.77E-14
6	Ly6a	1.33E-29	7	Actn1	1.23E-13
6	Hspg2	1.34E-28	7	Tm4sf1	1.59E-13
6	Fbln2	1.74E-28	7	Fgl2	2.73E-13
6	Txndc5	2.56E-28	7	Sod3	4.84E-13
6	Ly6e	3.08E-28	7	Htra1	7.17E-13
6	Tspan6	5.71E-28	7	Smtn	7.91E-13
6	Icam1	3.29E-26	7	Adam9	2.65E-12
6	Tgm2	4.61E-26	7	Cd200	5.43E-12
6	Col4a1	5.08E-26	7	Ltc4s	6.90E-12
6	Cd200	6.56E-26	7	Tns1	8.87E-12
6	Aqp1	7.95E-25	7	Col5a1	9.23E-12
6	Cfh	5.81E-24	7	Ecm1	4.33E-11
6	Gxylt2	3.68E-21	7	Gas6	5.64E-11
6	Lrg1	5.53E-21	7	Col14a1	1.05E-10
6	Cyr61	4.41E-19	7	Tpm4	5.50E-10
6	Pam	1.15E-18	7	Col3a1	9.68E-10
6	Ly6c1	2.92E-14	7	Cnn2	8.95E-09
6	Klf2	4.24E-14	7	Ctgf	3.82E-08
6	Fbln5	1.18E-10	7	Itgbl1	4.66E-08
6	Gadd45g	2.30E-09	7	Pi15	8.13E-07
6	Serpine1	1	7	Crip1	0.000310179

8	Bglap	2.36E-142	9	Ptprcap	1.29E-120
8	Panx3	4.78E-117	9	Cd3e	3.09E-117
8	Alpl	4.67E-105	9	Cd3d	2.74E-106
8	Pln	3.66E-98	9	Cd3g	2.66E-97
8	Bglap3	3.89E-98	9	Cd2	1.23E-91
8	Smpd3	2.10E-82	9	Lat	1.93E-91
8	Bglap2	1.93E-71	9	Cd8a	7.45E-85
8	Slc38a3	3.34E-65	9	Satb1	3.66E-71
8	Omd	2.80E-51	9	Lck	1.87E-67
8	Sp7	5.05E-47	9	Ms4a4b	1.03E-65
8	Col9a3	1.06E-43	9	Skap1	1.58E-65
8	3110079O15Rik	1.23E-41	9	Gm8369	1.62E-64
8	Col10a1	1.64E-40	9	Gimap3	1.62E-64
8	Chad	5.64E-40	9	Cd8b1	4.15E-60
8	Mest	6.92E-37	9	Nkg7	7.73E-55
8	Ibsp	8.87E-36	9	Trbc1	5.41E-50
8	Mia	3.15E-35	9	Trbc2	7.48E-50
8	Pth1r	6.03E-35	9	Cd28	4.96E-49
8	Dhx58os	1.30E-34	9	Ltb	8.84E-46
8	Scin	3.27E-34	9	Ly6d	1.09E-39
8	Hapln1	4.97E-34	9	Gpr18	6.57E-38
8	Haus8	6.62E-32	9	Tcf7	2.61E-36
8	Serinc5	6.75E-31	9	Cd79b	1.62E-33
8	Cst3	7.42E-28	9	Gimap4	2.71E-31
8	Col11a1	9.52E-28	9	Trac	2.78E-29
8	Hpgd	2.96E-26	9	Rac2	1.25E-28
8	Pdzrn4	5.01E-26	9	2810417H13Rik	1.78E-23
8	Col27a1	7.10E-26	9	Top2a	6.80E-23
8	Col2a1	8.89E-26	9	Ptpn18	1.74E-22
8	Pcolce2	1.22E-23	9	1-Sep	1.91E-22
8	Gpx3	2.52E-23	9	Ube2c	4.65E-22
8	Mef2c	4.69E-23	9	Ighm	3.08E-21
8	Ccdc80	4.88E-23	9	Birc5	2.03E-14
8	Fxyd1	1.12E-22	9	Hcst	7.48E-14
8	Tmie	2.42E-22	9	Rrm2	8.78E-14
8	Comp	2.76E-21	9	Thy1	1.92E-13
8	Sgms2	7.25E-21	9	Limd2	1.12E-12
8	Col11a2	1.09E-20	9	Rpl18a	1.35E-12
8	Irx5	1.53E-20	9	Rpl13a	2.02E-12
8	Susd5	5.42E-20	9	Coro1a	2.88E-12
8	C130050O18Rik	1.43E-19	9	Rps24	5.72E-12
8	Cdkn1c	2.09E-19	9	Cd52	5.80E-12
8	Ogfrl1	1.38E-18	9	Hist1h2ap	1.03E-11
8	Fgfr1	3.21E-18	9	Rps5	1.45E-11
8	Fzd9	3.95E-18	9	Rpsa	2.17E-11

8	Rarres1	4.93E-18	9	Rpl32	2.54E-11
8	Sparc	9.27E-18	9	Rps7	4.29E-11
8	Pltp	1.89E-17	9	Rps16	4.56E-11
8	A230065H16Rik	2.63E-16	9	Rps13	5.30E-11
8	Trpv4	3.33E-16	9	Rps6	6.67E-11
8	Srpx	3.28E-15	9	Rps10	2.69E-10
8	Creb3l1	5.35E-15	9	Gmfg	4.18E-10
8	Rbp4	9.11E-15	9	Rplp2	4.95E-10
8	Fap	1.72E-14	9	Vps37b	6.93E-10
8	Acan	3.70E-14	9	Il2rg	8.30E-10
8	Col9a1	5.81E-14	9	Gimap6	8.46E-10
8	Tspan13	5.40E-13	9	Rpl17	9.79E-10
8	Cd200	6.33E-13	9	Gm11808	1.40E-09
8	Ddit4l	1.32E-12	9	Rpl36	1.51E-09
8	Car8	1.50E-12	9	Rps20	1.60E-09
8	Bmp2	3.28E-12	9	Igkc	1.70E-09
8	Wif1	5.13E-12	9	Rps29	1.74E-09
8	Fam104a	7.33E-12	9	Snrpg	3.91E-09
8	Itm2b	1.42E-11	9	Rps15a	4.50E-09
8	Znhit6	4.01E-11	9	Rpl18	6.12E-09
8	Adk	5.28E-11	9	Rps18	6.18E-09
8	Cd24a	6.58E-11	9	Rpl13	7.80E-09
8	Steap4	7.19E-11	9	AW112010	1.60E-08
8	Ucma	8.47E-11	9	Arhgdib	2.74E-08
8	Sox9	8.55E-11	9	Fau	3.26E-08
8	Bambi	1.05E-09	9	Npm1	3.69E-08
8	Chil1	2.17E-09	9	Rpl12	3.86E-08
8	Cpne8	1.77E-08	9	Psmb8	1.16E-07
8	Golph3	2.71E-08	9	Rps27	1.32E-07
8	Serpinh1	4.26E-08	9	H2-DMb2	2.75E-07
8	Cdc42ep3	6.35E-08	9	Rps27rt	6.41E-07
8	Crispld1	2.29E-07	9	Gimap5	6.91E-07
8	Mdfi	2.55E-07	9	Rps19	7.55E-07
8	Serpine2	4.57E-07	9	Ets1	9.29E-07
8	Col1a2	5.21E-07	9	Selplg	6.93E-06
8	Lect1	7.21E-07	9	Tmsb10	1.00E-05
8	Scrg1	2.33E-06	9	Gm9843	1.13E-05
8	Rgcc	2.36E-06	9	H2-T22	1.66E-05
8	Fmod	4.41E-06	9	Hsp90aa1	1.88E-05
8	Btg2	1.91E-05	9	Cd37	0.000147198
8	Hp	3.66E-05	9	H2-Q7	0.000996092
8	Id1	3.74E-05	9	Stk17b	0.001240606
8	Phlda1	6.44E-05	9	Ube2s	0.00275036
8	Neat1	9.41E-05	9	Hmgb2	0.00628967
8	Fosb	0.00023515	9	H2-K1	0.06937247

8	Cdkn1a	0.001396467	9	H2afz	0.134110116
8	Tuba1c	0.00258242	9	Stmn1	0.253354693
8	Col1a1	0.002675769	9	Ccl5	0.386863505
8	Ier2	0.003182112	9	Tmpo	1
8	Pnrc1	0.014936276	9	Hmgb1	1
8	Dnajb1	0.016004089	9	Dut	1
8	Zfp36	0.057364323	9	Tubb5	1
8	Junb	0.066518016	9	Btg1	1
8	Fos	1	9	H2afx	1
8	Jun	1	9	Anp32e	1

III. Methods

Animal Handling and Tissue Processing

Studies were performed on male Myh11-CreER^{T2}, ROSA26 STOP-flox eYFP$^{+/+}$ littermates backcrossed 9 times to C57BL/6. Males were used as the Myh11-CreER^{T2} transgene is located on the Y chromosome. Mice used for atherosclerosis studies were crossed to an Apoe$^{-/-}$ background (SMC-YFP, Apoe$^{-/-}$), whereas carotid ligation studies were performed on both Apoe$^{-/-}$ and Apoe$^{+/+}$ mice (SMC-YFP). Cre-lox mediated recombination of eYFP was induced in 6-8 week old mice after intraperitoneal injections of 1mg of tamoxifen (T-5648, Sigma) per mouse per day for 10 days over two weeks.

PDGFBR studies used male Myh11-CreER^{T2}, ROSA26 STOP-flox eYFP$^{+/+}$, Apoe$^{-/-}$ crossed with PDGFBR-flox mice to generate PDGFBR$^{SMC\ WT/FL}$ lineage tracing mice. PDGFBR$^{SMC\ WT/FL}$ mice were bred to produce littermates with WT and KO pups. Mice were allocated to groups by genotyping and PDGFBR excision was validated by PCR using primers to validate excision of exon 7 of the PDGFBR gene, as well as single cell analysis of SMC by immunofluorescence in the vessel media 18 weeks post tamoxifen. Any animals with less than 95% excision of PDGFBR in SMC in the media were excluded from further analysis.

EC-lineage tracing mice for studies in Chapter 4 were derived by crossing VECadherin-CreER^{T2} mice with the ROSA26 STOP-flox eYFP$^{+/+}$ reporter mouse. Mice were induced with tamoxifen and put on WD for 10 weeks, or underwent lethal irradiation and BMT, outlined below.

On the day of harvest, and 12 hours after fasting (atherosclerosis only), mice were euthanized by CO_2 asphyxiation. Blood was drawn for testing prior to perfusion fixation via the left ventricle with 4% paraformaldehyde (PFA; EMS 15710). To test hyperlipidemia, plasma cholesterol and triglyceride levels were analyzed by the University of Virginia Clinical Pathology Laboratory. Any animal with cholesterol levels beyond 3 standard deviations of the mean.

Bone Marrow Transplant Studies

At 9 weeks of age, mice underwent lethal irradiation, receiving 2 600cGy doses, 3 hours apart, using a cesium-137 irradiator (Mark 1-68a) and reconstituted 30-60 minutes later with >1 x 106 unfractionated bone marrow (BM) cells via tail vein injection as previously described (Iwata et al., 2010). 1200cGy was chosen as the dosage for lethal radiation in mice based on multiple previous reports. BM was harvested from the femur and tibia from donors aged 4-7 weeks.

After BMT, mice were given antibiotics via drinking water (Sulfa water: 80mg/mL sulfamethoxazole, 16mg/mL trimethoprim, Teva Pharmaceuticals) for 6-7 weeks during BM reconstitution before either being placed on Western diet (WD) to induce atherosclerosis development (Harlan Teklad 21% milk fat, 0.15% cholesterol), or undergoing carotid ligation (S. Figure 1B,D). Alternatively, mice were harvested 1, 4, or 7 days post irradiation, BMT, and given a single BrdU pulse at the time of radiation (10 mg/mL; Sigma B5002; Lot#: HMBF4669V), as were their corresponding non-irradiated, non-BMT control littermates.

Bone marrow for atherosclerosis studies and the studies on the acute effects of radiation was as follows: CD45.1 Apoe$^{-/-}$, tdTomato Apoe$^{-/-}$, or dsRed Apoe$^{-/-}$ derived from Tg(CAG-DsRed*MST)1Nagy/J (Jackson Lab #005441). BM for mice in carotid ligation studies used marker tdTomato Apoe$^{+/+}$ derived from B6.129(Cg)-Gt(ROSA)26Sortm4(ACTB-tdTomato,-EGFP)Luo/J (Jackson Lab #007676) or CD45.1 Apoe$^{-/-}$ derived from B6.SJL-Ptprca Pepcb/BoyJ (Jackson Lab #002014), when appropriate. BM was harvested from donors between 4-7 weeks of age from the femur and tibia and >1 x 10^6 unfractionated bone marrow cells were injected via tail vein 30-60 minutes after radiation.

Validating Bone Marrow Reconstitution

Blood samples were acquired by terminal cardiac puncture. Red blood cells and platelets were cleared using 1x RBC lysis buffer (BD PharmLyse) and 1x Hanks Balanced Salt Solution (Gibco). Prior to surface staining, Fc receptors were blocked with TruStain fcX anti-mouse CD16/32 antibody (Biolegend, 10µg/mL). Dead cells were eliminated

from the analysis using Live-Dead Fixable Yellow (ThermoFisher Scientific, 0.55µL/mL). Cells were stained with the following antibodies: CD45.1 (BD Pharminogen, 2.5µg/mL) and CD45.2 (eBiosciences, 2.5µg/mL). OneComp ebeads (eBiosciences, 50µL/sample) were used for single stain controls and all experiments used fluorescent minus one (FMO) controls for each marker. All samples were run on a Beckman Coulter CyAn ADP LX flow cytometer and analyzed using FlowJo v10.

Atherosclerosis Experimental Design

At 8 weeks of age SMC-PDGFBR WT and KO mice were put on Western diet (WD) containing 21% milk fat and 0.15% cholesterol (Harlan Teklad) and remained on WD for 10, 18, or 26 weeks. Mice for BMT atherosclerosis studies were irradiated at 9 weeks of age with Sulfa water and allowed six weeks for BM reconstitution. Experiments were repeated three times, with mice receiving BM from dsRed $Apoe^{-/-}$, tdTomato $Apoe^{-/-}$, or CD45.1 $Apoe^{-/-}$ donors. Mice were then placed on WD for 18 weeks. Littermate controls either received Sulfa water or normal drinking water for the same duration as experimental animals prior to WD feeding. There were no significant differences in control animals who received normal drinking water or Sulfa water. Studies used various BM donors to rule out donor or trace dependent effects on atherosclerosis.

Various locations along the aortic tree that reliably develop lesions including the brachiocephalic artery (BCA), aortic arch, aortic root, abdominal aorta, renal artery, and iliac artery just below the iliac bifurcation were then excised, post-fixed in 4% PFA and embedded in paraffin or put in a sucrose gradient and embedded in OCT. Given the recent finding that the ascending aorta is derived from both neural crest and secondary heart field, the aortic arch sections were taken between the BCA bifurcation and the left subclavian (Sawada et al., 2017). All vessels were sectioned at 10µm. The BCA samples were sectioned as previously described starting past the aortic arch, which allows for lesion analysis at regular intervals. All other samples were sectioned entirely to include areas with lesion deposition.

Carotid Ligation and Femoral Injury Experimental Design

Two groups of SMC-YFP (Apoe$^{+/+}$ or $^{-/-}$) mice underwent carotid ligation or femoral injury surgery, adapted from methods previously described (Herring et al., 2014; Le et al., 2015; Takayama et al., 2015). Briefly, mice that had undergone irradiation and BMT reconstitution or controls were put under anesthesia using the Kent Scientific SomnoSuite Isofluorane delivery system (3% v/wt, 250mL/min). Once mice were anesthetized, 100µL of Bupivacaine HCl (0.25% NDC 55150-167-10) was administered locally. Carotid ligations were performed by making a midline incision and the left (n=5 control, n=5 irradiated) or right (n=5 control, n=5 irradiated) carotid artery was exposed. A 7-0 suture was placed immediately proximal to the internal/external carotid bifurcation. To induce femoral injury, a straight spring wire was inserted into the left femoral artery. The wire was advanced and retracted in a sawing motion ten times to denude the endothelium and produce neointimal hyperplasia. The collateral artery immediately proximal to the deep femoral artery was also ligated to induce neointima formation of lesser severity. The contralateral carotid or femoral artery served as an uninjured control. Mice were euthanized 21 days post ligation. Vessels were sectioned at 10µm from ligation through the first 1.5-2.5mm for analysis.

Delayed Tamoxifen Studies

PDGFBR$^{SMC\ WT/WT}$ and PDGFBR$^{SMC\ FL/FL}$ animals were put on WD starting at 8 weeks of age. Mice were then injected with tamoxifen to induce recombination of eYFP and PDGFBR specifically in MYH11^{+} cells. This method labels approximately 20% of the SMC within the lesion, primarily those located within the fibrous cap. Tamoxifen was injected for 10 days between 16 and 18 weeks of WD and harvested 8 weeks later.

Imatinib Studies

Myh11-CreER^{T2}, ROSA26 STOP-flox eYFP$^{+/+}$, Apoe$^{-/-}$ mice were injected with tamoxifen between 6-8 weeks of age and fed a WD for 18-20 weeks before being randomly allocated to receive either Imatinib or saline as a control treatment via i.p. injection once daily for 7 days. Treatment mice received 100mg/kg/day of Imatinib based on numerous

pre-clinical studies showing its tolerability at this dosage in mice (Pouwer et al., 2018; Reber et al., 2017; Rossi et al., 2010), and its relevance to the human dosing regimen (up to 400mg BID) (Novartis, 2018). Imatinib was purchased as a Mesylate Salt (Selleckchem) and was resuspended in 0.9% medical grade sterile saline prior to each injection. Mice were euthanized if they exhibited symptoms of distress such as hunching or hindlimb paralysis per ACUC guidelines. Saline treated control mice were euthanized after 7 injections, corresponding to the final Imatinib injection.

Immunohistochemistry

Human Tissue

De-identified coronary artery specimens generously donated by collaborators at CVPath Institute, Inc. were paraformaldehyde fixed, paraffin embedded, and sectioned at 5μm thickness. Three separate patients with evidence of erosion, rupture, or stable atherosclerotic lesions were selected. ISH-PLA staining for H3K4me2 at the MYH11 promoter was performed as previously described (Gomez et al., 2013). To assess the percentage of ACTA2+ cells that are derive from SMC, all visible media cells were counted to ACTA2 expression and PLA positivity. Assuming that all ACTA2+ medial cells are derived from SMC (i.e. should be PLA^+), we calculated an efficiency of 28% (top). We used this correction to calculate the PLA^+ $ACTA2^+$ lesion cells (bottom).

$$\frac{media\ PLA+}{media\ ACTA2+}$$

$$\left(\frac{lesion\ PLA+}{correction}\right)/ACTA2$$

Staining Protocol

To assess vessel morphometry and composition, immunohistochemical analyses of murine tissue were performed in paraffin embedded samples at 10μm thickness. Modified Russell-Movat staining was used to assess vessel, lesion, lumen, and media areas at 3 locations, 300μm apart. Necrotic core areas were measured at 2 locations 300μm

apart. Collagen content was visualized by PicroSirius Red staining at 2 locations, 300μm apart. Sample sizes indicated in all graphs as individual dots.

Immunofluorescence staining of BCAs was done to evaluate protein expression in single cells (based on DAPI+ nuclei) with primary antibodies specific for GFP (Abcam ab6673, 1:250), PDGFBR, (Abcam ab32570, 1:250), CD31 (Abcam ab124430, 1:500), LGALS3 (Cedarlane CL8942AP, 1:500), MKi67 (Abcam ab15580, 1:250), cleaved caspase-3 (CASP3; Cell Signaling no. 9661S, 1:75), MYH11 (Kamiya Biomedical Company MC-352, 1:500), or their isotype IgG as negative control. ACTA2 was conjugated to -FITC (Sigma CAT 1:500) or -Cy3 (Sigma clone 1A4, 1:500). TUNEL staining was performed using the CF® 640R TUNEL Assay Apoptosis Detection Kit (Biotium 30074, lot 180417). Cells were counter stained with DAPI (ThermoFisher Scientific D3571). Secondary antibodies for immunofluorescence included the following: donkey anti-goat 488 (Invitrogen A11055, 1:250), donkey anti-goat 647 (Invitrogen A21447, 1:250), donkey anti-rat Dylight 550 (Abcam ab102261, 1:250), and donkey anti-rabbit 555 (Invitrogen A21206, 1:100). Red blood cell analysis was performed using DAB (Acros Organics) using a primary Ter119 antibody (rat anti-mouse Santa-Cruz Biotechnology, Inc; 1:200) and rabbit secondary antibody (Vector Labs BA-4001).

Image Acquisition and Analysis

Immunofluorescence imaging of BCA sections was performed using a Zeiss LSM700 confocal microscope. Figure images were acquired at 2048 x 2048 resolution using a 20x magnification at 0.5 zoom. A series of 1μm Z stack images were acquired for single cell analysis of the entire media, lesion, or fibrous cap areas. Fibrous cap area was determined as the 30μm area under the lumen. Single cell counting, as denoted by DAPI, was performed using Zen 2009 Light Edition Software (Zeiss) to determine cell composition and co-localization of markers within a single DAPI+ nucleus. Linear or brightness adjustments for print were applied equally to all panels within an image. Figure images were pseudo-colored and YFP signal was brightened with gamma expansion for visualization in print, and scale bars were added in Adobe Photoshop

Picrosirius Red was imaged by fiber birefringence under polarized light using an Olympus BX51 camera with a polarized lens. Movat and Ter119 staining was imaged using a Zeiss Axioskope2 fitted with an AxioCamMR3 camera, using AxioVision40 V4.6.3.0 software (Carl Zeiss Imaging Solution). Image Pro Plus software (Media Cybernetics) was used to analyze Ter119, Movat, and Picrosirius Red. Areas of Interest were drawn denoting the external elastic lamina ("EEL"), internal elastic lamina ("IEL"), lesion, and fibrous cap. Lumen area was the difference between IEL and lesion. Pixels were selected for Ter119 and PicroSirius Red analyses to denote positive staining and defined using color-cube based method. Researchers were blinded to mouse genotype.

Metabolic Flux Measurements

Cell Culture

Mouse thoracic aorta SMC were plated on tissue culture plates and grown in DF10 [DMEM-F12 media (Gibco) with 10% FBS (Gibco)] to confluence before being switched to serum free media for 24 hours. Cells were washed with 1x PBS and treated with either PDGFDD (50ng/mL), TGFβ (50ng/mL), or vehicle control (4mM HCl) for 24 hours. For sequential studies, cells were treated with PDGFDD or vehicle for 24 hours and then washed with PBS and subsequently treated with vehicle (4mM HCl + DMSO), TGFβ, or simultaneously with TGFβ + Galloflavin (10μM) or CPI613 (20μM) for 24 hours. RNA was extracted using RNEasy Mini Kit. qRT-PCR was performed using SensiFast SYBR No-ROX and run on a Bio-Rad CFX56 Real-Time System.

Glycolytic and Mitochondrial Stress Test

$4x10^5$ murine smooth muscle cells were seeded onto a Seahorse 24-well tissue culture plate (Agilent Technologies, Santa Clara, CA) with media containing 10% serum. One to three days before the treatment, the culture medium was replaced with serum-free media. Cells were then treated accordingly for 4-48 hours in serum free media prior to metabolic assessment.

To assess respiratory capacity, cells were subjected to a mitochondrial stress test (MST). At the beginning of the assay, the media was changed to DMEM with pyruvate

(Thermo-Fisher, pH=7.35 at 37°C) and cells were allowed to equilibrate for 30 minutes. Oxygen consumption rate (OCR) was measured using a Seahorse XF24 Flux Analyzer (Agilent Technologies, Santa Clara, CA). After three basal OCR measurements, the drugs of interest were injected into the plate and OCR was measured using four-minute measurement periods. Compounds to modulate cellular respiratory function [1μM Oligomycin (Sigma-Aldrich); 2μM BAM15 (Cayman Chemical Company); 1μM Antimycin A & 100nM Rotenone (Sigma-Aldrich)] were injected after every three measurements. Basal respiration was calculated by subtracting the average of the first three measurements by the average of the post-Antimycin A & Rotenone measurements. Maximum respiratory capacity was calculated by subtracting the average of the post-BAM15 measurements by the average of the post-Antimycin A & Rotenone measurements. The reserve capacity was calculated by subtracting the average of the basal measurements from the average of the post-BAM15 measurements.

To assess glycolytic capacity, cells were subjected to a glycolytic stress test (GST). For this test, extracellular acidification rate (ECAR), a measurement of lactate export, was measured using a Seahorse XF24 Flux Analyzer. Cells were seeded onto a Seahorse 24-well tissue culture plate. At the beginning of the assay, the media was changed to unbuffered, glucose-free, DMEM (Sigma-Aldrich Cat#:D5030, pH=7.35 at 37°C), supplemented with 143mM NaCl and 2mM Glutamine. After three basal ECAR measurements, the drugs of interest were injected into the plate and ECAR was measured every three minutes. Compounds to modulate glycolysis [20mM Glucose; 1μM Oligomycin; 80mM 2-Deoxyglucose (Sigma)] were injected after every three measurements. Basal glycolysis was calculated by subtracting the average of the post- 2-Deoxyglucose measurements from the average of the post-Glucose measurements. Maximum glycolytic capacity was calculated by subtracting the average of the post-2-Deoxyglucose from the average of the post-Oligomycin measurements. The glycolytic reserve capacity was calculated by subtracting the average of the post-Oligomycin measurements from the average of the post-Glucose measurements.

RNA-seq Analysis

Bulk RNA-seq

The BCA, aortic arch, and carotid arteries from 18 week Western diet fed SMC-PDGFBR WT (n = 5) KO (n = 5) mice were flash frozen in liquid nitrogen for RNA-seq analysis. Total RNA was extracted from arteries using Trizol (Invitrogen). Directional RNA-sequencing with ribosomal reduction and strand specificity was performed by Hudson-Alpha Institute for Biotechnology (Immunima HiSeq v4, pe, 100bp, 25M reads) and analyzed at the University of Virginia Bioinformatics Core.

Significantly regulated genes were identified using the Benjamini-Hochberg procedure to adjust *P* values (P_{adj}) to less than or equal to 5% false discovery rate. KEGG pathway analysis was performed on all significantly up- or down-regulated genes in the $PDGFBR^{SMC\Delta/\Delta}$ vs. $PDGFBR^{SMCWT/WT}$ samples, as well as the top 50 down-regulated genes based on P_{adj}. This *in vivo* RNA-seq procedure analyzes RNA from all cell types (including endothelial cells and adventitial cells) within the lesions and surrounding vessels and demonstrates the net effect of PDGFBR loss in SMC in advanced atherosclerosis.

Single Cell RNA-seq

Lesions from the BCA, carotids, and aortic arch of SMC-PDGFBR WT (n=3) and KO (n=5) mice were carefully harvested from the underlying media with forceps and put into tubes with FACS buffer (1% BSA in PBS) plus 1µg/mL Actinomycin-D (Gibco). Samples were then minced and digested in LoBind sample tubes (Eppendorf) with 1mL Liberase (Roche) plus 1µg/mL Actinomycin-D for 45 minutes at 37°C. After incubation samples were centrifuged for 10 minutes at 1000xg at 4°C and resuspended in PBS plus 0.04% UltraPure non-Acetylated BSA (ThermoFisher Scientific) and filtered through 30µm filters on ice.

Samples processed as above were stained with Sytox Blue viability dye (1/5,000 dilution) and sorted by the UVA Flow Cytometry Core using the inFlux v7 Sorter based on live cells, singlets, and then allocated into $eYFP^{+}$ or $eYFP^{-}$ tubes containing 100µl 0.04% non-acetylated BSA. Cell viability and count was assessed using a hemocytometer. Cells

were spun down and resuspended to 200 cells/μL for submission to the UVA Genome Analysis Technology Core. 2000 cells were targeted for Chromium 10x Genomics single cell sequencing on the Illumina NextSeq system, 150 cycle high-output. Quality control was conducted by Qubit and Agilent DNA high sensitivity tape station after 10X library prep and NGS library prep. Data was analyzed using Seurat software whereby cells with high mitochondrial or hemoglobin reads were eliminated.

Statistical Analysis

Statistics were performed using GraphPad Prism software. In Chapter 2, SMC investment into lesions and intraplaque hemorrhage were analyzed by two-sided Baptista-Pike Fisher Exact Test with odds ratio and 95% confidence interval. Data in Chapter 3 was assessed for outliers by a ROUT test and excluded if indicated. Data for individual locations between WT and KO animals was assessed by Mann-Whitney U-test. When comparing multiple locations between genotypes, a two-way ANOVA with multiple comparisons and Sidak correction was performed to determine significant differences between genotype and location. Vessel morphometry, necrotic core, and PicroSirius Red images were analyzed using two-way ANOVA with multiple comparisons and Bonferroni correction. Data is presented as mean +/- SEM. All p values reflect significant differences between control and experimental groups and animal numbers are reflected within figures. A p value less than 0.05 was considered significant.

Primers

Genotyping

PDGFBR	Apoe
GCCATCAACATCTCTGTGATCGG	GCCTAGCCGAGGGAGAGCCG
CTCCAGCAGCCGCACGTAGCCAT	TGTGACTTGGGAGCTCTGCAGC
PDGFBR Excision	GCCGCCCCGACTGCATCT
TAGACTTCCCACCGAGCCTAGT	tdTomato
ACGGCCAGTTCCCCTAAACTAC	AAGGGAGCTGCAGTGGAGTA
eYFP	CGGGCCATTTACCGTAAGTTAT
GGAGCGGGAGAAATGGATATG	CCGAAAATCTGTGGGAAGTC
AAGTTCATCTGCACCACCG	CD45.1
TCCTTGAAGAAGATGGTGCG	CTCACAGGCACATGAACGAT
CGTGATCTGCAACTCCAGTC	CGCTTCAAGCATGTCTTCTG
Myh11-Cre	dsRed
TGACCCCATCTCTTCACTCC	CCCATGGTCTTCTTCTGCAT
AACTCCACGACCACCTCATC	AAGGTGTACGTGAAGCACCC
AGTCCCTCACATCCTCAGGTT	CTAGGCCACAGAATTGAAAGATCT
	GTAGGTGGAAATTCTAGCATCATCC

qPCR

ACTA2	FN1
CGCTGTCAGGAACCCTGAGA	TCTGGGAAATGGAAAAGGGGAATGG
CGAAGCCGGCCTTACAGA	CACTGAAGCAGGTTTCCTCGGTTGT
LDHA	SPP1
AACTTGGCGCTCTACTTGCT	CGACTGTAGGGACGATTGGAG
GGACTTTGAATCTTTTGAGACCTTG	CTGCTGCCCGACAACCA
COL15a1	
CTGTCCACTTTCCGAGCCTTT	
AAAGCACTTGGCCCTTGAGA	

References

Acosta, J.C., A. Banito, T. Wuestefeld, A. Georgilis, P. Janich, J.P. Morton, D. Athineos, T.-W. Kang, F. Lasitschka, M. Andrulis, G. Pascual, K.J. Morris, S. Khan, H. Jin, G. Dharmalingam, A.P. Snijders, T. Carroll, D. Capper, C. Pritchard, G.J. Inman, T. Longerich, O.J. Sansom, S.A. Benitah, L. Zender, and J. Gil. 2013. A complex secretory program orchestrated by the inflammasome controls paracrine senescence. Nature cell biology 15:978-990.

Albarran-Juarez, J., H. Kaur, M. Grimm, S. Offermanns, and N. Wettschureck. 2016. Lineage tracing of cells involved in atherosclerosis. Atherosclerosis 251:445-453.

Alexander, M.R., and G.K. Owens. 2012. Epigenetic control of smooth muscle cell differentiation and phenotypic switching in vascular development and disease. Annu Rev Physiol 74:13-40.

Allahverdian, S., A.C. Chehroudi, B.M. McManus, T. Abraham, and G.A. Francis. 2014. Contribution of intimal smooth muscle cells to cholesterol accumulation and macrophage-like cells in human atherosclerosis. Circulation 129:1551-1559.

Allahverdian, S., P.S. Pannu, and G.A. Francis. 2012. Contribution of monocyte-derived macrophages and smooth muscle cells to arterial foam cell formation. Cardiovascular Research

Amento, E.P., N. Ehsani, H. Palmer, and P. Libby. 1991. Cytokines and growth factors positively and negatively regulate interstitial collagen gene expression in human vascular smooth muscle cells. Arterioscler Thromb 11:1223-1230.

Andrae, J., R. Gallini, and C. Betsholtz. 2008. Role of platelet-derived growth factors in physiology and medicine. Genes Dev 22:1276-1312.

Aprile, L., L. Puccetti, S. Galimberti, A. Gozzini, F. Scarpini, M. Defina, F. De Majo, C. Baratè, A. Sicuranza, and V. Candi. 2013. Atherothrombotic Risk and TKIs Treatment In Chronic Myeloid Leukemia Patients: A Role For Genetic Predisposition and Pro-Inflammatory/Pro-Oxidative Status? In Am Soc Hematology.

Baylis, R.A., D. Gomez, Z. Mallat, G. Pasterkamp, and G.K. Owens. 2017a. The CANTOS Trial: One Important Step for Clinical Cardiology but a Giant Leap for Vascular Biology. Arterioscler Thromb Vasc Biol 37:e174-e177.

Baylis, R.A., D. Gomez, and G.K. Owens. 2017b. Shifting the focus of preclinical, murine atherosclerosis studies from prevention to late-stage intervention. Circ Res 120:775-777.

Benditt, E.P., and J.M. Benditt. 1973. Evidence for a monoclonal origin of human atherosclerotic plaques. Proc Natl Acad Sci U S A 70:1753-1756.

Bennett, M.R., S. Sinha, and G.K. Owens. 2016. Vascular Smooth Muscle Cells in Atherosclerosis. Circulation research 118:692-702.

Bentzon, J.F., and E. Falk. 2017. Plaque Erosion: New Insights From the Road Less Travelled. In Am Heart Assoc.

Bentzon, J.F., and M.W. Majesky. 2017. Lineage tracking of origin and fate of smooth muscle cells in atherosclerosis. Cardiovasc Res

Bentzon, J.F., C.S. Sondergaard, M. Kassem, and E. Falk. 2007. Smooth muscle cells healing atherosclerotic plaque disruptions are of local, not blood, origin in apolipoprotein E knockout mice. Circulation 116:2053-2061.

Beranek, J.T., and N.C. Cavarocchi. 1990. Undifferentiated vascular endothelial cells in coronary allograft atherosclerosis. International journal of cardiology 28:127-128.

Bergonie, J., and L. Tribondeau. 1959. Interpretation of some results of radiotherapy and an attempt at determining a logical technique of treatment/De Quelques Résultats de la Radiotherapie et Essai de Fixation d'une Technique Rationnelle. Radiation research 11:587-588.

Bergsten, E., M. Uutela, X. Li, K. Pietras, A. Ostman, C.-H. Heldin, K. Alitalo, and U. Eriksson. 2001. PDGF-D is a specific, protease-activated ligand for the PDGF [beta]-receptor. Nat Cell Biol 3:512-516.

Bernstein, L.R., H. Antoniades, and B.R. Zetter. 1982. Migration of cultured vascular cells in response to plasma and platelet-derived factors. Journal of Cell Science 56:71-82.

Blank, R.S., and G.K. Owens. 1990. Platelet-derived growth factor regulates actin isoform expression and growth state in cultured rat aortic smooth muscle cells. J Cell Physiol 142:635-642.

Bloom, M.W., C.E. Hamo, D. Cardinale, B. Ky, A. Nohria, L. Baer, H. Skopicki, D.J. Lenihan, M. Gheorghiade, A.R. Lyon, and J. Butler. 2016. Cancer Therapy-Related Cardiac Dysfunction and Heart Failure: Part 1: Definitions, Pathophysiology, Risk Factors, and Imaging. Circulation. Heart failure 9:e002661-e002661.

Boucher, P., and M. Gotthardt. 2004. LRP and PDGF signaling: a pathway to atherosclerosis. Trends Cardiovasc Med 14:55-60.

Boucher, P., M. Gotthardt, W.P. Li, R.G. Anderson, and J. Herz. 2003. LRP: role in vascular wall integrity and protection from atherosclerosis. Science 300:329-332.

Boucher, P., W.P. Li, R.L. Matz, Y. Takayama, J. Auwerx, R.G. Anderson, and J. Herz. 2007. LRP1 functions as an atheroprotective integrator of TGFbeta and PDFG signals in the vascular wall: implications for Marfan syndrome. PLoS One 2:e448.

Bowen-Pope, D.F., and E.W. Raines. 2011. History of discovery: platelet-derived growth factor. Arterioscler Thromb Vasc Biol 31:2397-2401.

Braga, T.T., J.S.H. Agudelo, and N.O.S. Camara. 2015. Macrophages During the Fibrotic Process: M2 as Friend and Foe. Frontiers in immunology 6:602-602.

Buetow, B.S., K.A. Tappan, J.R. Crosby, R.A. Seifert, and D.F. Bowen-Pope. 2003. Chimera Analysis Supports a Predominant Role of PDGFRβ in Promoting Smooth-Muscle Cell Chemotaxis after Arterial Injury. The American Journal of Pathology 163:979-984.

Caplice, N.M., T.J. Bunch, P.G. Stalboerger, S. Wang, D. Simper, D.V. Miller, S.J. Russell, M.R. Litzow, and W.D. Edwards. 2003. Smooth muscle cells in human coronary atherosclerosis can originate from cells administered at marrow transplantation. Proc Natl Acad Sci U S A 100:4754-4759.

Chai-Adisaksopha, C., C.M. Hillis, and W. Lam. 2015. Cardiovascular events in patients with chronic myelogenous leukemia treated with tyrosine kinase inhibitors: A systematic review and meta-analysis.

Chappell, J., J.L. Harman, V.M. Narasimhan, H. Yu, K. Foote, B.D. Simons, M.R. Bennett, and H.F. Jorgensen. 2016. Extensive Proliferation of a Subset of Differentiated, yet Plastic, Medial Vascular Smooth Muscle Cells Contributes to Neointimal Formation in Mouse Injury and Atherosclerosis Models. Circ Res 119:1313-1323.

Chaudhary, R., J. Garg, N. Shah, and A. Sumner. 2017. PCSK9 inhibitors: A new era of lipid lowering therapy. World journal of cardiology 9:76.

Chen, C.N., Y.S. Li, Y.T. Yeh, P.L. Lee, S. Usami, S. Chien, and J.J. Chiu. 2006. Synergistic roles of platelet-derived growth factor-BB and interleukin-1beta in phenotypic modulation of human aortic smooth muscle cells. Proc Natl Acad Sci U S A 103:2665-2670.

Chen, P.Y., L. Qin, N. Baeyens, G. Li, T. Afolabi, M. Budatha, G. Tellides, M.A. Schwartz, and M. Simons. 2015. Endothelial-to-mesenchymal transition drives atherosclerosis progression. J Clin Invest 125:4514-4528.

Chen, P.Y., L. Qin, C. Barnes, K. Charisse, T. Yi, X. Zhang, R. Ali, P.P. Medina, J. Yu, F.J. Slack, D.G. Anderson, V. Kotelianski, F. Wang, G. Tellides, and M. Simons. 2012. FGF regulates TGF-beta signaling and endothelial-to-mesenchymal transition via control of let-7 miRNA expression. Cell Rep 2:1684-1696.

Chen, P.Y., L. Qin, G. Li, G. Tellides, and M. Simons. 2016. Smooth muscle FGF/TGFbeta cross talk regulates atherosclerosis progression. EMBO Mol Med 8:712-728.
Cherepanova, O.A., D. Gomez, L.S. Shankman, P. Swiatlowska, J. Williams, O.F. Sarmento, G.F. Alencar, D.L. Hess, M.H. Bevard, E.S. Greene, M. Murgai, S.D. Turner, Y.-J. Geng, S. Bekiranov, J.J. Connelly, A. Tomilin, and G.K. Owens. 2016. Activation of the pluripotency factor OCT4 in smooth muscle cells is atheroprotective. Nat Med advance online publication:
Childs, B.G., D.J. Baker, T. Wijshake, C.A. Conover, J. Campisi, and J.M. van Deursen. 2016. Senescent intimal foam cells are deleterious at all stages of atherosclerosis. Science 354:472-477.
Chung, I.M., S.M. Schwartz, and C.E. Murry. 1998. Clonal architecture of normal and atherosclerotic aorta: implications for atherogenesis and vascular development. Am J Pathol 152:913-923.
Clarke, M., R. Collins, S. Darby, C. Davies, P. Elphinstone, V. Evans, J. Godwin, R. Gray, C. Hicks, S. James, E. MacKinnon, P. McGale, T. McHugh, R. Peto, C. Taylor, and Y. Wang. 2005. Effects of radiotherapy and of differences in the extent of surgery for early breast cancer on local recurrence and 15-year survival: an overview of the randomised trials. Lancet 366:2087-2106.
Clarke, M.C., N. Figg, J.J. Maguire, A.P. Davenport, M. Goddard, T.D. Littlewood, and M.R. Bennett. 2006. Apoptosis of vascular smooth muscle cells induces features of plaque vulnerability in atherosclerosis. Nat Med 12:1075-1080.
Clowes, A.W., M.A. Reidy, and M.M. Clowes. 1983. Kinetics of cellular proliferation after arterial injury. I. Smooth muscle growth in the absence of endothelium. Lab Invest 49:327-333.
Clowes, A.W., and S.M. Schwartz. 1985. Significance of quiescent smooth muscle migration in the injured rat carotid atery. Circ Res
Darby, S., P. McGale, R. Peto, F. Granath, P. Hall, and A. Ekbom. 2003. Mortality from cardiovascular disease more than 10 years after radiotherapy for breast cancer: nationwide cohort study of 90 000 Swedish women. Bmj 326:256-257.
Davies, M.J., P.D. Richardson, N. Woolf, D.R. Katz, and J. Mann. 1993. Risk of thrombosis in human atherosclerotic plaques: role of extracellular lipid, macrophage, and smooth muscle cell content. Heart 69:377-381.
De Donatis, A., G. Comito, F. Buricchi, M.C. Vinci, A. Parenti, A. Caselli, G. Camici, G. Manao, G. Ramponi, and P. Cirri. 2008. Proliferation versus migration in platelet-derived growth factor signaling the key role of endocytosis. Journal of Biological Chemistry 283:19948-19956.
DeBakey, M.E., and D.H. Glaeser. 2000. Patterns of atherosclerosis: effect of risk factors on recurrence and survival-analysis of 11,890 cases with more than 25-year follow-up. Am J Cardiol 85:1045-1053.
DeRuiter, M.C., R.E. Poelmann, J.C. VanMunsteren, V. Mironov, R.R. Markwald, and A.C. GittenbergerdeGroot. 1997. Embryonic endothelial cells transdifferentiate into mesenchymal cells expressing smooth muscle actins in vivo and in vitro. Circulation Research 80:444-451.
Dixon, S.J., D.N. Patel, M. Welsch, R. Skouta, E.D. Lee, M. Hayano, A.G. Thomas, C.E. Gleason, N.P. Tatonetti, and B.S. Slusher. 2014. Pharmacological inhibition of cystine–glutamate exchange induces endoplasmic reticulum stress and ferroptosis. Elife 3:e02523.
Drake, C.J., J.E. Hungerford, and C.D. Little. 1998. Morphogenesis of the first blood vessels. Ann N Y Acad Sci 857:155-179.
Druker, B.J. 2002. STI571 (Gleevec™) as a paradigm for cancer therapy. Trends in Molecular Medicine 8:S14-S18.
Durgin, B.G., O.A. Cherepanova, D. Gomez, T. Karaoli, G.F. Alencar, J.T. Butcher, Y.Q. Zhou, M.P. Bendeck, B.E. Isakson, G.K. Owens, and J.J. Connelly. 2017. Smooth muscle cell-specific deletion of Col15a1 unexpectedly leads to impaired development of advanced atherosclerotic lesions. Am J Physiol Heart Circ Physiol 312:H943-h958.

Endo, A. 2010. A historical perspective on the discovery of statins. Proc Jpn Acad Ser B Phys Biol Sci 86:484-493.
Escaned, J., J. Baptista, C. Di Mario, J.r. Haase, Y. Ozaki, D.T. Linker, P.J. De Feyter, J.R. Roelandt, and P.W. Serruys. 1996. Significance of automated stenosis detection during quantitative angiography: insights gained from intracoronary ultrasound imaging. Circulation 94:966-972.
Evrard, S.M., L. Lecce, K.C. Michelis, A. Nomura-Kitabayashi, G. Pandey, K.-R. Purushothaman, V. d'Escamard, J.R. Li, L. Hadri, and K. Fujitani. 2016. Endothelial to mesenchymal transition is common in atherosclerotic lesions and is associated with plaque instability. Nature communications 7:11853.
Fang, R.C., and R.D. Galiano. 2008. A review of becaplermin gel in the treatment of diabetic neuropathic foot ulcers. Biologics : targets & therapy 2:1-12.
Feil, S., B. Fehrenbacher, R. Lukowski, F. Essmann, K. Schulze-Osthoff, M. Schaller, and R. Feil. 2014. Transdifferentiation of Vascular Smooth Muscle Cells to Macrophage-Like Cells During Atherogenesis. Circ Res
Ferns, G.A., E.W. Raines, K.H. Sprugel, A.S. Motani, M.A. Reidy, and R. Ross. 1991. Inhibition of neointimal smooth muscle accumulation after angioplasty by an antibody to PDGF. Science 253:1129-1132.
Ford, E.S., and S. Capewell. 2011. Proportion of the decline in cardiovascular mortality disease due to prevention versus treatment: public health versus clinical care. Annual review of public health 32:5-22.
Friedman, S.L., D. Sheppard, J.S. Duffield, and S. Violette. 2013. Therapy for fibrotic diseases: nearing the starting line. Sci Transl Med 5:167sr161.
Gabriels, K., S. Hoving, M.J. Gijbels, J.F. Pol, J.A. te Poele, E.A. Biessen, M.J. Daemen, F.A. Stewart, and S. Heeneman. 2014. Irradiation of existing atherosclerotic lesions increased inflammation by favoring pro-inflammatory macrophages. Radiotherapy and Oncology 110:455-460.
Gadson Jr, P.F., M.L. Dalton, E. Patterson, D.D. Svoboda, L. Hutchinson, D. Schram, and T.H. Rosenquist. 1997. Differential response of mesoderm-and neural crest-derived smooth muscle to TGF-β1: regulation of c-myb and α1 (I) procollagen genes. Experimental cell research 230:169-180.
Gan, Q., T. Yoshida, J. Li, and G.K. Owens. 2007. Smooth muscle cells and myofibroblasts use distinct transcriptional mechanisms for smooth muscle alpha-actin expression. Circ Res 101:883-892.
Garcia-Garcia, H.M., N. Gonzalo, E. Regar, and P.W. Serruys. 2009. Virtual histology and optical coherence tomography: from research to a broad clinical application. Heart 95:1362-1374.
Gerthoffer, W.T. 2007. Mechanisms of vascular smooth muscle cell migration. Circ Res 100:607-621.
Giesen, C., H.A. Wang, D. Schapiro, N. Zivanovic, A. Jacobs, B. Hattendorf, P.J. Schuffler, D. Grolimund, J.M. Buhmann, S. Brandt, Z. Varga, P.J. Wild, D. Gunther, and B. Bodenmiller. 2014. Highly multiplexed imaging of tumor tissues with subcellular resolution by mass cytometry. Nat Methods 11:417-422.
Giles, F.J., M.J. Mauro, F. Hong, C.-E. Ortmann, R.C. Woodman, P.D. LeCoutre, and G. Saglio. 2011. Retrospective cohort analysis of peripheral arterial occlusive disease (PAOD) events in patients (pts) with chronic myeloid leukemia in chronic phase (CML-CP). In Am Soc Hematology.
Giles, F.J., M.J. Mauro, F. Hong, C.E. Ortmann, C. McNeill, R.C. Woodman, A. Hochhaus, P.D. le Coutre, and G. Saglio. 2013. Rates of peripheral arterial occlusive disease in patients with chronic myeloid leukemia in the chronic phase treated with imatinib, nilotinib, or non-tyrosine kinase therapy: a retrospective cohort analysis. Leukemia 27:1310-1315.
Gimbrone Jr, M.A., and G. García-Cardeña. 2016. Endothelial cell dysfunction and the pathobiology of atherosclerosis. Circulation research 118:620-636.
Glagov, S., E. Weisenberg, C.K. Zarins, R. Stankunavicius, and G.J. Kolettis. 1987. Compensatory enlargement of human atherosclerotic coronary arteries. New England Journal of Medicine 316:1371-1375.

Goel, S.A., L.W. Guo, X.D. Shi, R. Kundi, G. Sovinski, S. Seedial, B. Liu, and K.C. Kent. 2013. Preferential secretion of collagen type 3 versus type 1 from adventitial fibroblasts stimulated by TGF-beta/Smad3-treated medial smooth muscle cells. Cell Signal 25:955-960.

Gomez, D., R.A. Baylis, B.G. Durgin, A.A.C. Newman, G.F. Alencar, S. Mahan, C. St Hilaire, W. Muller, A. Waisman, S.E. Francis, E. Pinteaux, G.J. Randolph, H. Gram, and G.K. Owens. 2018. Interleukin-1beta has atheroprotective effects in advanced atherosclerotic lesions of mice. Nat Med 24:1418-1429.

Gomez, D., and G.K. Owens. 2012. Smooth muscle cell phenotypic switching in atherosclerosis. Cardiovasc Res 95:156-164.

Gomez, D., and G.K. Owens. 2016. Reconciling smooth muscle cell oligoclonality and proliferative capacity in experimental atherosclerosis. In Am Heart Assoc.

Gomez, D., L.S. Shankman, A.T. Nguyen, and G.K. Owens. 2013. Detection of histone modifications at specific gene loci in single cells in histological sections. Nat Methods 10:171-177.

Gratwohl, A., M.C. Pasquini, M. Aljurf, Y. Atsuta, H. Baldomero, L. Foeken, M. Gratwohl, L.F. Bouzas, D. Confer, and K. Frauendorfer. 2015. One million haemopoietic stem-cell transplants: a retrospective observational study. The Lancet Haematology 2:e91-e100.

Grotendorst, G.R., T. Chang, H.E. Seppa, H.K. Kleinman, and G.R. Martin. 1982. Platelet-derived growth factor is a chemoattractant for vascular smooth muscle cells. J Cell Physiol 113:261-266.

Grotendorst, G.R., H.E. Seppä, H.K. Kleinman, and G.R. Martin. 1981. Attachment of smooth muscle cells to collagen and their migration toward platelet-derived growth factor. Proc Natl Acad Sci U S A 78:3669-3672.

Gröger, C.J., M. Grubinger, T. Waldhör, K. Vierlinger, and W. Mikulits. 2012. Meta-analysis of gene expression signatures defining the epithelial to mesenchymal transition during cancer progression. PloS one 7:e51136.

Haimovici, H., and N. Maier. 1964. FATE OF AORTIC HOMOGRAFTS IN CANINE ATHEROSCLEROSIS. 3. STUDY OF FRESH ABDOMINAL AND THORACIC AORTIC IMPLANTS INTO THORACIC AORTA: ROLE OF TISSUE SUSCEPTIBILITY IN ATHEROGENESIS. Arch Surg 89:961-969.

Hangauer, M.J., V.S. Viswanathan, M.J. Ryan, D. Bole, J.K. Eaton, A. Matov, J. Galeas, H.D. Dhruv, M.E. Berens, S.L. Schreiber, F. McCormick, and M.T. McManus. 2017. Drug-tolerant persister cancer cells are vulnerable to GPX4 inhibition. Nature 551:247-250.

Hautmann, M.B., P.J. Adam, and G.K. Owens. 1999. Similarities and differences in smooth muscle alpha-actin induction by TGF-beta in smooth muscle versus non-smooth muscle cells. Arterioscler Thromb Vasc Biol 19:2049-2058.

Hayflick, L. 1965. The limited in vitro lifetime of human diploid cell strains. Experimental cell research 37:614-636.

He, C., S.C. Medley, T. Hu, M.E. Hinsdale, F. Lupu, R. Virmani, and L.E. Olson. 2015. PDGFRbeta signalling regulates local inflammation and synergizes with hypercholesterolaemia to promote atherosclerosis. Nat Commun 6:7770.

Heldin, C.H. 1992. Structural and functional studies on platelet-derived growth factor. Embo j 11:4251-4259.

Hellstrom, M., H. Gerhardt, M. Kalen, X. Li, U. Eriksson, H. Wolburg, and C. Betsholtz. 2001. Lack of pericytes leads to endothelial hyperplasia and abnormal vascular morphogenesis. J Cell Biol 153:543-553.

Hellstrom, M., M. Kalen, P. Lindahl, A. Abramsson, and C. Betsholtz. 1999. Role of PDGF-B and PDGFR-beta in recruitment of vascular smooth muscle cells and pericytes during embryonic blood vessel formation in the mouse. Development 126:3047-3055.

Herring, B.P., A.M. Hoggatt, C. Burlak, and S. Offermanns. 2014. Previously differentiated medial vascular smooth muscle cells contribute to neointima formation following vascular injury. Vasc Cell 6:21.

Heuchel, R., A. Berg, M. Tallquist, K. Åhlén, R.K. Reed, K. Rubin, L. Claesson-Welsh, C.-H. Heldin, and P. Soriano. 1999. Platelet-derived growth factor β receptor

regulates interstitial fluid homeostasis through phosphatidylinositol-3′ kinase signaling. Proceedings of the National Academy of Sciences 96:11410-11415.
Hoch, R.V., and P. Soriano. 2003. Roles of PDGF in animal development. Development 130:4769-4784.
Hochhaus, A., G. Saglio, T.P. Hughes, R.A. Larson, D.W. Kim, S. Issaragrisil, P.D. le Coutre, G. Etienne, P.E. Dorlhiac-Llacer, R.E. Clark, I.W. Flinn, H. Nakamae, B. Donohue, W. Deng, D. Dalal, H.D. Menssen, and H.M. Kantarjian. 2016. Long-term benefits and risks of frontline nilotinib vs imatinib for chronic myeloid leukemia in chronic phase: 5-year update of the randomized ENESTnd trial. Leukemia 30:1044-1054.
Holtwick, R., M. Gotthardt, B. Skryabin, M. Steinmetz, R. Potthast, B. Zetsche, R.E. Hammer, J. Herz, and M. Kuhn. 2002. Smooth muscle-selective deletion of guanylyl cyclase-A prevents the acute but not chronic effects of ANP on blood pressure. Proceedings of the National Academy of Sciences 99:7142-7147.
Holycross, B.J., R.S. Blank, M.M. Thompson, M.J. Peach, and G.K. Owens. 1992. Platelet-derived growth factor-BB-induced suppression of smooth muscle cell differentiation. Circ Res 71:1525-1532.
Hu, Y., Z. Zhang, E. Torsney, A.R. Afzal, F. Davison, B. Metzler, and Q. Xu. 2004. Abundant progenitor cells in the adventitia contribute to atherosclerosis of vein grafts in ApoE-deficient mice. J Clin Invest 113:1258-1265.
Inomata, K., T. Aoto, N.T. Binh, N. Okamoto, S. Tanimura, T. Wakayama, S. Iseki, E. Hara, T. Masunaga, and H. Shimizu. 2009. Genotoxic stress abrogates renewal of melanocyte stem cells by triggering their differentiation. Cell 137:1088-1099.
Ivar Seldinger, S. 2008. Catheter replacement of the needle in percutaneous arteriography: a new technique. Acta radiologica 49:47-52.
Iwata, H., I. Manabe, K. Fujiu, T. Yamamoto, N. Takeda, K. Eguchi, A. Furuya, M. Kuro-o, M. Sata, and R. Nagai. 2010. Bone marrow-derived cells contribute to vascular inflammation but do not differentiate into smooth muscle cell lineages. Circulation 122:2048-2057.
Iwata, H., I. Manabe, and R. Nagai. 2013. Lineage of bone marrow-derived cells in atherosclerosis. Circ Res 112:1634-1647.
Jacobsen, K., M.B. Lund, J. Shim, S. Gunnersen, E.M. Fuchtbauer, M. Kjolby, L. Carramolino, and J.F. Bentzon. 2017. Diverse cellular architecture of atherosclerotic plaque derives from clonal expansion of a few medial SMCs. JCI Insight 2:
Jaffe, M., C. Sesti, I.M. Washington, L. Du, N. Dronadula, M.T. Chin, D.B. Stolz, E.C. Davis, and D.A. Dichek. 2012. Transforming growth factor-beta signaling in myogenic cells regulates vascular morphogenesis, differentiation, and matrix synthesis. Arterioscler Thromb Vasc Biol 32:e1-11.
Jaussaud, N., S. Chitsaz, A. Meadows, M. Wintermark, N. Cambronero, A.N. Azadani, D.A. Saloner, T.A. Chuter, and E.E. Tseng. 2013. Acute type A aortic dissection intimal tears by 64-slice computed tomography: a role for endovascular stent-grafting? J Cardiovasc Surg (Torino) 54:373-381.
Jawien, A., D.F. Bowen-Pope, V. Lindner, S.M. Schwartz, and A.W. Clowes. 1992. Platelet-derived growth factor promotes smooth muscle migration and intimal thickening in a rat model of balloon angioplasty. J Clin Invest 89:507-511.
Jiang, X., D.H. Rowitch, P. Soriano, A.P. McMahon, and H.M. Sucov. 2000. Fate of the mammalian cardiac neural crest. Development 127:1607.
Kalmanti, L., S. Saußele, M. Lauseker, M. Müller, C. Dietz, L. Heinrich, B. Hanfstein, U. Proetel, A. Fabarius, and S. Krause. 2015. Safety and efficacy of imatinib in CML over a period of 10 years: data from the randomized CML-study IV. Leukemia 29:1123.
Kazi, D.S., J. Penko, P.G. Coxson, A.E. Moran, D.A. Ollendorf, J.A. Tice, and K. Bibbins-Domingo. 2017. Updated Cost-effectiveness Analysis of PCSK9 Inhibitors Based on the Results of the FOURIER Trial. JAMA 318:748-750.
Kazlauskas, A., and J.A. Cooper. 1989. Autophosphorylation of the PDGF receptor in the kinase insert region regulates interactions with cell proteins. Cell 58:1121-1133.

Khavjou, O., D. Phelps, and A. Leib. 2016. Projections of cardiovascular disease prevalence and costs: 2015–2035. Dallas: American Heart Association
Kim, S., H.S. Ip, M.M. Lu, C. Clendenin, and M.S. Parmacek. 1997. A serum response factor-dependent transcriptional regulatory program identifies distinct smooth muscle cell sublineages. Mol Cell Biol 17:2266-2278.
Kim, T.D., D. Rea, M. Schwarz, P. Grille, F.E. Nicolini, G. Rosti, L. Levato, F.J. Giles, H. Dombret, T. Mirault, H. Labussiere, R. Lindhorst, W. Haverkamp, I. Buschmann, B. Dorken, and P.D. le Coutre. 2013. Peripheral artery occlusive disease in chronic phase chronic myeloid leukemia patients treated with nilotinib or imatinib. Leukemia 27:1316-1321.
Kirby, M.L., and K.L. Waldo. 1995. Neural crest and cardiovascular patterning. Circulation research 77:211-215.
Kokkinopoulos, I., M.M. Wong, C.M. Potter, Y. Xie, B. Yu, D.T. Warren, W.N. Nowak, A. Le Bras, Z. Ni, and C. Zhou. 2017. Adventitial SCA-1+ progenitor cell gene sequencing reveals the mechanisms of cell migration in response to hyperlipidemia. Stem cell reports 9:681-696.
Kolodgie, F., R. Virmani, A.a. Burke, A. Farb, D. Weber, R. Kutys, A. Finn, and H. Gold. 2004. Pathologic assessment of the vulnerable human coronary plaque. Heart 90:1385-1391.
Kolodgie, F.D., A.P. Burke, A. Farb, H.K. Gold, J. Yuan, J. Narula, A.V. Finn, and R. Virmani. 2001. The thin-cap fibroatheroma: a type of vulnerable plaque: the major precursor lesion to acute coronary syndromes. Curr Opin Cardiol 16:285-292.
Koyama, N., C.E. Hart, and A.W. Clowes. 1994. Different functions of the platelet-derived growth factor-alpha and -beta receptors for the migration and proliferation of cultured baboon smooth muscle cells. Circulation Research 75:682-691.
Koyama, N., N. Morisaki, Y. Saito, and S. Yoshida. 1992. Regulatory effects of platelet-derived growth factor-AA homodimer on migration of vascular smooth muscle cells. Journal of Biological Chemistry 267:22806-22812.
Kozaki, K., W.E. Kaminski, J. Tang, S. Hollenbach, P. Lindahl, C. Sullivan, J.C. Yu, K. Abe, P.J. Martin, R. Ross, C. Betsholtz, N.A. Giese, and E.W. Raines. 2002. Blockade of platelet-derived growth factor or its receptors transiently delays but does not prevent fibrous cap formation in ApoE null mice. Am J Pathol 161:1395-1407.
Kramann, R., C. Goettsch, J. Wongboonsin, H. Iwata, R.K. Schneider, C. Kuppe, N. Kaesler, M. Chang-Panesso, F.G. Machado, S. Gratwohl, K. Madhurima, J.D. Hutcheson, S. Jain, E. Aikawa, and B.D. Humphreys. 2016. Adventitial MSC-like Cells Are Progenitors of Vascular Smooth Muscle Cells and Drive Vascular Calcification in Chronic Kidney Disease. Cell Stem Cell 19:628-642.
Langley, S.R., K. Willeit, A. Didangelos, L.P. Matic, P. Skroblin, J. Barallobre-Barreiro, M. Lengquist, G. Rungger, A. Kapustin, L. Kedenko, C. Molenaar, R. Lu, T. Barwari, G. Suna, X. Yin, B. Iglseder, B. Paulweber, P. Willeit, J. Shalhoub, G. Pasterkamp, A.H. Davies, C. Monaco, U. Hedin, C.M. Shanahan, J. Willeit, S. Kiechl, and M. Mayr. 2017. Extracellular matrix proteomics identifies molecular signature of symptomatic carotid plaques. J Clin Invest 127:1546-1560.
Larson, R.A., D.-W. Kim, S. Issaragrilsil, P. le Coutre, P.E.D. Llacer, G. Etienne, R.E. Clark, I. Flinn, H. Nakamae, and A. Hochhaus. 2014. Efficacy and safety of nilotinib (NIL) vs imatinib (IM) in patients (pts) with newly diagnosed chronic myeloid leukemia in chronic phase (CML-CP): long-term follow-up (f/u) of ENESTnd. In Am Soc Hematology.
Lassila, M., T.J. Allen, Z. Cao, V. Thallas, K.A. Jandeleit-Dahm, R. Candido, and M.E. Cooper. 2004. Imatinib attenuates diabetes-associated atherosclerosis. Arterioscler Thromb Vasc Biol 24:935-942.
Le, V., C.G. Johnson, J.D. Lee, and A.B. Baker. 2015. Murine model of femoral artery wire injury with implantation of a perivascular drug delivery patch. Journal of visualized experiments: JoVE

Lee, M.-O., S.-H. Song, S. Jung, S. Hur, T. Asahara, H. Kim, S.-M. Kwon, and H.-J. Cha. 2012. Effect of ionizing radiation induced damage of endothelial progenitor cells in vascular regeneration. Arteriosclerosis, thrombosis, and vascular biology 32:343-352.

Leroux-Berger, M., I. Queguiner, T.T. Maciel, A. Ho, F. Relaix, and H. Kempf. 2011. Pathologic calcification of adult vascular smooth muscle cells differs on their crest or mesodermal embryonic origin. Journal of Bone and Mineral Research 26:1543-1553.

Leveen, P., M. Pekny, S. Gebre-Medhin, B. Swolin, E. Larsson, and C. Betsholtz. 1994. Mice deficient for PDGF B show renal, cardiovascular, and hematological abnormalities. Genes & development 8:1875-1887.

Li, J., X. Zhu, M. Chen, L. Cheng, D. Zhou, M.M. Lu, K. Du, J.A. Epstein, and M.S. Parmacek. 2005. Myocardin-related transcription factor B is required in cardiac neural crest for smooth muscle differentiation and cardiovascular development. Proceedings of the National Academy of Sciences 102:8916-8921.

Li, L., J.M. Miano, B. Mercer, and E.N. Olson. 1996. Expression of the SM22alpha promoter in transgenic mice provides evidence for distinct transcriptional regulatory programs in vascular and visceral smooth muscle cells. J Cell Biol 132:849-859.

Li, M., L. You, J. Xue, and Y. Lu. 2018. Ionizing Radiation-Induced Cellular Senescence in Normal, Non-transformed Cells and the Involved DNA Damage Response: A Mini Review. Front Pharmacol 9:522.

Libby, P. 2013. Mechanisms of acute coronary syndromes. The New England journal of medicine 369:883.

Libby, P., P.M. Ridker, and G.K. Hansson. 2011. Progress and challenges in translating the biology of atherosclerosis. Nature 473:317-325.

Lillis, A.P., I. Mikhailenko, and D.K. Strickland. 2005. Beyond endocytosis: LRP function in cell migration, proliferation and vascular permeability. J Thromb Haemost 3:1884-1893.

Lindahl, P., B.R. Johansson, P. Levéen, and C. Betsholtz. 1997. Pericyte Loss and Microaneurysm Formation in PDGF-B-Deficient Mice. Science 277:242-245.

Lindblom, P., H. Gerhardt, S. Liebner, A. Abramsson, M. Enge, M. Hellstrom, G. Backstrom, S. Fredriksson, U. Landegren, H.C. Nystrom, G. Bergstrom, E. Dejana, A. Ostman, P. Lindahl, and C. Betsholtz. 2003. Endothelial PDGF-B retention is required for proper investment of pericytes in the microvessel wall. Genes Dev 17:1835-1840.

Lorenz, E., C. Congdon, and D. Uphoff. 1952. Modification of acute irradiation injury in mice and guinea-pigs by bone marrow injections. Radiology 58:863-877.

Louandre, C., Z. Ezzoukhry, C. Godin, J.C. Barbare, J.C. Mazière, B. Chauffert, and A. Galmiche. 2013. Iron-dependent cell death of hepatocellular carcinoma cells exposed to sorafenib. International journal of cancer 133:1732-1742.

Lutgens, E., M. Gijbels, M. Smook, P. Heeringa, P. Gotwals, V.E. Koteliansky, and M.J. Daemen. 2002. Transforming growth factor-β mediates balance between inflammation and fibrosis during plaque progression. Arteriosclerosis, thrombosis, and vascular biology 22:975-982.

Madsen, C.S., C.P. Regan, and G.K. Owens. 1997. Interaction of CArG elements and a GC-rich repressor element in transcriptional regulation of the smooth muscle myosin heavy chain gene in vascular smooth muscle cells. J Biol Chem 272:29842-29851.

Madura, J.A., 2nd, B.R. Kaufman, D.A. Margolin, D.M. Spencer, P.L. Fox, and L.M. Graham. 1996. Regional differences in platelet-derived growth factor production by the canine aorta. J Vasc Res 33:53-61.

Majesky, M.W. 2007. Developmental basis of vascular smooth muscle diversity. Arterioscler Thromb Vasc Biol 27:1248-1258.

Majesky, M.W., H. Horita, A. Ostriker, S. Lu, J.N. Regan, A. Bagchi, X.R. Dong, J. Poczobutt, R.A. Nemenoff, and M.C. Weiser-Evans. 2017. Differentiated Smooth Muscle Cells Generate a Subpopulation of Resident Vascular Progenitor Cells in the Adventitia Regulated by Klf4. Circ Res 120:296-311.

Mallat, Z., A. Gojova, C. Marchiol-Fournigault, B. Esposito, C. Kamate, R. Merval, D. Fradelizi, and A. Tedgui. 2001. Inhibition of transforming growth factor-beta signaling accelerates atherosclerosis and induces an unstable plaque phenotype in mice. Circ Res 89:930-934.

Manabe, I., and G.K. Owens. 2001. CArG elements control smooth muscle subtype–specific expression of smooth muscle myosin in vivo. The Journal of clinical investigation 107:823-834.

Martin, M., J.-L. Lefaix, and S. Delanian. 2000. TGF-β1 and radiation fibrosis: a master switch and a specific therapeutic target? International Journal of Radiation Oncology* Biology* Physics 47:277-290.

Matoba, T., K. Sato, and K. Egashira. 2013. Mouse models of plaque rupture. Curr Opin Lipidol 24:419-425.

Mautner, S.L., F. Lin, G.C. Mautner, and W.C. Roberts. 1993. Comparison in women versus men of composition of atherosclerotic plaques in native coronary arteries and in saphenous veins used as aortocoronary conduits. Journal of the American College of Cardiology 21:1312-1318.

McArdle, S., G. Chodaczek, N. Ray, and K. Ley. 2015. Intravital live cell triggered imaging system reveals monocyte patrolling and macrophage migration in atherosclerotic arteries. J Biomed Opt 20:26005.

McDonald, O.G., B.R. Wamhoff, M.H. Hoofnagle, and G.K. Owens. 2006. Control of SRF binding to CArG box chromatin regulates smooth muscle gene expression in vivo. J Clin Invest 116:36-48.

McGale, P., S.C. Darby, P. Hall, J. Adolfsson, N.O. Bengtsson, A.M. Bennet, T. Fornander, B. Gigante, M.B. Jensen, R. Peto, K. Rahimi, C.W. Taylor, and M. Ewertz. 2011. Incidence of heart disease in 35,000 women treated with radiotherapy for breast cancer in Denmark and Sweden. Radiother Oncol 100:167-175.

McKenna, A., G.M. Findlay, J.A. Gagnon, M.S. Horwitz, A.F. Schier, and J. Shendure. 2016. Whole organism lineage tracing by combinatorial and cumulative genome editing. Science

Medici, D., S. Potenta, and R. Kalluri. 2011. Transforming growth factor-β2 promotes Snail-mediated endothelial–mesenchymal transition through convergence of Smad-dependent and Smad-independent signalling. Biochemical Journal 437:515-520.

Mertens, A.C., Q. Liu, J.P. Neglia, K. Wasilewski, W. Leisenring, G.T. Armstrong, L.L. Robison, and Y. Yasui. 2008. Cause-specific late mortality among 5-year survivors of childhood cancer: the Childhood Cancer Survivor Study. Journal of the National Cancer Institute 100:1368-1379.

Metharom, P., C. Liu, S. Wang, P. Stalboerger, G. Chen, B. Doyle, Y. Ikeda, and N.M. Caplice. 2008. Myeloid lineage of high proliferative potential human smooth muscle outgrowth cells circulating in blood and vasculogenic smooth muscle-like cells in vivo. Atherosclerosis 198:29-38.

Miano, J.M., P. Cserjesi, K.L. Ligon, M. Periasamy, and E.N. Olson. 1994. Smooth muscle myosin heavy chain exclusively marks the smooth muscle lineage during mouse embryogenesis. Circ Res 75:803-812.

Miller, M.B., and B.L. Bassler. 2001. Quorum sensing in bacteria. Annu Rev Microbiol 55:165-199.

Misra, A., Z. Feng, R.R. Chandran, I. Kabir, N. Rotllan, B. Aryal, A.Q. Sheikh, L. Ding, L. Qin, C. Fernandez-Hernando, G. Tellides, and D.M. Greif. 2018. Integrin beta3 regulates clonality and fate of smooth muscle-derived atherosclerotic plaque cells. Nat Commun 9:2073.

Moreno, P.R., V.c.H. Bernardi, J. Lo´ pez-Cue´ llar, A.M. Murcia, I.F. Palacios, H.K. Gold, R. Mehran, S.K. Sharma, Y. Nemerson, and V.n. Fuster. 1996. Macrophages, smooth muscle cells, and tissue factor in unstable angina: implications for cell-mediated thrombogenicity in acute coronary syndromes. Circulation 94:3090-3097.

Moss, N.S., and E.P. Benditt. 1975. Human atherosclerotic plaque cells and leiomyoma cells. Comparison of in vitro growth characteristics. Am J Pathol 78:175-190.

Motoyama, S., M. Sarai, H. Harigaya, H. Anno, K. Inoue, T. Hara, H. Naruse, J. Ishii, H. Hishida, and N.D. Wong. 2009. Computed tomographic angiography characteristics of atherosclerotic plaques subsequently resulting in acute coronary syndrome. Journal of the American College of Cardiology 54:49-57.
Murry, C.E., C.T. Gipaya, T. Bartosek, E.P. Benditt, and S.M. Schwartz. 1997. Monoclonality of smooth muscle cells in human atherosclerosis. The American journal of pathology 151:697.
Muñoz-Espín, D., M. Cañamero, A. Maraver, G. Gómez-López, J. Contreras, S. Murillo-Cuesta, A. Rodríguez-Baeza, I. Varela-Nieto, J. Ruberte, and M. Collado. 2013. Programmed cell senescence during mammalian embryonic development. Cell 155:1104-1118.
Myllarniemi, M., L. Calderon, K. Lemstrom, E. Buchdunger, and P. Hayry. 1997. Inhibition of platelet-derived growth factor receptor tyrosine kinase inhibits vascular smooth muscle cell migration and proliferation. Faseb j 11:1119-1126.
Nagai, R., D.M. Larson, and M. Periasamy. 1988. Characterization of a mammalian smooth muscle myosin heavy chain cDNA clone and its expression in various smooth muscle types. Proc Natl Acad Sci U S A 85:1047-1051.
Napoli, C., F.P. D'armiento, F.P. Mancini, A. Postiglione, J.L. Witztum, G. Palumbo, and W. Palinski. 1997. Fatty streak formation occurs in human fetal aortas and is greatly enhanced by maternal hypercholesterolemia. Intimal accumulation of low density lipoprotein and its oxidation precede monocyte recruitment into early atherosclerotic lesions. The Journal of clinical investigation 100:2680-2690.
Newby, A.C., and A.B. Zaltsman. 1999. Fibrous cap formation or destruction--the critical importance of vascular smooth muscle cell proliferation, migration and matrix formation. Cardiovasc Res 41:345-360.
Newman, A.A., R.A. Baylis, D.L. Hess, S.D. Griffith, L.S. Shankman, O.A. Cherepanova, and G.K. Owens. 2018. Irradiation abolishes smooth muscle investment into vascular lesions in specific vascular beds. JCI Insight 3:
Nicholls, S.J., K. Wolski, I. Sipahi, P. Schoenhagen, T. Crowe, S.R. Kapadia, S.L. Hazen, E.M. Tuzcu, and S.E. Nissen. 2007. Rate of progression of coronary atherosclerotic plaque in women. J Am Coll Cardiol 49:1546-1551.
Ninomiya, K., A. Takahashi, Y. Fujioka, Y. Ishikawa, and M. Yokoyama. 2006. Transforming growth factor-beta signaling enhances transdifferentiation of macrophages into smooth muscle-like cells. Hypertens Res 29:269-276.
Nissen, S.E., S.J. Nicholls, I. Sipahi, P. Libby, J.S. Raichlen, C.M. Ballantyne, J. Davignon, R. Erbel, J.C. Fruchart, and J.-C. Tardif. 2006. Effect of very high-intensity statin therapy on regression of coronary atherosclerosis: the ASTEROID trial. Jama 295:1556-1565.
Novartis. 2018. Gleevec. In Novartis.
Ohayon, J., G. Finet, A.M. Gharib, D.A. Herzka, P. Tracqui, J. Heroux, G. Rioufol, M.S. Kotys, A. Elagha, and R.I. Pettigrew. 2008. Necrotic core thickness and positive arterial remodeling index: emergent biomechanical factors for evaluating the risk of plaque rupture. American journal of physiology-heart and circulatory physiology 295:H717-H727.
Olson, N., S. Chao, V. Lindner, and M. Reidy. 1992. Intimal smooth muscle cell proliferation after balloon catheter injury. The role of basic fibroblast growth factor. The American journal of pathology 140:1017.
Owens, G.K. 1995. Regulation of differentiation of vascular smooth muscle cells. 487-517 pp.
Owens, G.K., M.S. Kumar, and B.R. Wamhoff. 2004. Molecular regulation of vascular smooth muscle cell differentiation in development and disease. Physiol Rev 84:767-801.
Pasterkamp, G., H.M. Den Ruijter, and P. Libby. 2017a. Temporal shifts in clinical presentation and underlying mechanisms of atherosclerotic disease. Nature Reviews Cardiology 14:21.
Pasterkamp, G., H.M. den Ruijter, and P. Libby. 2017b. Temporal shifts in clinical presentation and underlying mechanisms of atherosclerotic disease. Nat Rev Cardiol 14:21-29.

Pierce, G.F., T.A. Mustoe, B.W. Altrock, T.F. Deuel, and A. Thomason. 1991. Role of platelet-derived growth factor in wound healing. J Cell Biochem 45:319-326.
Pouwer, M.G., E.J. Pieterman, L. Verschuren, M.P.M. Caspers, C. Kluft, R.A. Garcia, J. Aman, J.W. Jukema, and H.M.G. Princen. 2018. The BCR-ABL1 Inhibitors Imatinib and Ponatinib Decrease Plasma Cholesterol and Atherosclerosis, and Nilotinib and Ponatinib Activate Coagulation in a Translational Mouse Model. Front Cardiovasc Med 5:55.
Raines, E.W. 2000. The extracellular matrix can regulate vascular cell migration, proliferation, and survival: relationships to vascular disease. International Journal of Experimental Pathology 81:173-182.
Raines, E.W. 2004. PDGF and cardiovascular disease. Cytokine Growth Factor Rev 15:237-254.
Raines, E.W., and N. Ferri. 2005. Thematic review series: The immune system and atherogenesis. Cytokines affecting endothelial and smooth muscle cells in vascular disease. J Lipid Res 46:1081-1092.
Raines, E.W., H. Koyama, and N.O. Carragher. 2000. The extracellular matrix dynamically regulates smooth muscle cell responsiveness to PDGF. Ann N Y Acad Sci 902:39-51; discussion 51-32.
Reber, L.L., P. Starkl, B. Balbino, R. Sibilano, N. Gaudenzio, S. Rogalla, S. Sensarn, D. Kang, H. Raghu, and J. Sokolove. 2017. The tyrosine kinase inhibitor imatinib mesylate suppresses uric acid crystal-induced acute gouty arthritis in mice. PloS one 12:e0185704.
Red-Horse, K., H. Ueno, I.L. Weissman, and M.A. Krasnow. 2010. Coronary arteries form by developmental reprogramming of venous cells. Nature 464:549.
Reidy, M.A. 1990. Proliferation of Smooth-Muscle Cells at Sites Distant from Vascular Injury. Arteriosclerosis 10:298-305.
Ridker, P.M., E. Danielson, F.A. Fonseca, J. Genest, A.M. Gotto Jr, J.J. Kastelein, W. Koenig, P. Libby, A.J. Lorenzatti, and J.G. MacFadyen. 2008. Rosuvastatin to prevent vascular events in men and women with elevated C-reactive protein. New England Journal of Medicine 359:2195.
Ridker, P.M., B.M. Everett, T. Thuren, J.G. MacFadyen, W.H. Chang, C. Ballantyne, F. Fonseca, J. Nicolau, W. Koenig, and S.D. Anker. 2017a. Antiinflammatory therapy with canakinumab for atherosclerotic disease. New England Journal of Medicine 377:1119-1131.
Ridker, P.M., J.G. MacFadyen, T. Thuren, B.M. Everett, P. Libby, R.J. Glynn, and C.T. Group. 2017b. Effect of interleukin-1beta inhibition with canakinumab on incident lung cancer in patients with atherosclerosis: exploratory results from a randomised, double-blind, placebo-controlled trial. Lancet 390:1833-1842.
Ridker, P.M., T. Thuren, A. Zalewski, and P. Libby. 2011. Interleukin-1beta inhibition and the prevention of recurrent cardiovascular events: rationale and design of the Canakinumab Anti-inflammatory Thrombosis Outcomes Study (CANTOS). Am Heart J 162:597-605.
Rosenbloom, J., E. Macarak, S. Piera-Velazquez, and S.A. Jimenez. 2017. Human Fibrotic Diseases: Current Challenges in Fibrosis Research. Methods Mol Biol 1627:1-23.
Ross, R. 1971. The smooth muscle cell: II. Growth of smooth muscle in culture and formation of elastic fibers. The Journal of cell biology 50:172-186.
Ross, R. 1986. The pathogenesis of atherosclerosis--an update. N Engl J Med 314:488-500.
Ross, R., and S.J. Klebanoff. 1971. The smooth muscle cell: I. In vivo synthesis of connective tissue proteins. The Journal of cell biology 50:159-171.
Rossi, F., Y. Yozgat, E. de Stanchina, D. Veach, B. Clarkson, K. Manova, F. Giancotti, C.R. Antonescu, and P. Besmer. 2010. Imatinib upregulates compensatory integrin signaling in a mouse model of gastrointestinal stromal tumor and is more effective when combined with dasatinib. Molecular cancer research : MCR 8:1271-1283.
Rouget, C. 1874. Note sur le developpement de la tunique contractile des vaisseaux. Compt Rend Acad Sci 59:559-562.

Rovner, A.S., R.A. Murphy, and G.K. Owens. 1986. Expression of smooth muscle and nonmuscle myosin heavy chains in cultured vascular smooth muscle cells. J Biol Chem 261:14740-14745.
Sabatine, M.S., R.P. Giugliano, A.C. Keech, N. Honarpour, S.D. Wiviott, S.A. Murphy, J.F. Kuder, H. Wang, T. Liu, S.M. Wasserman, P.S. Sever, T.R. Pedersen, F.S. Committee, and Investigators. 2017. Evolocumab and Clinical Outcomes in Patients with Cardiovascular Disease. N Engl J Med 376:1713-1722.
Saito, M., T. Iwawaki, C. Taya, H. Yonekawa, M. Noda, Y. Inui, E. Mekada, Y. Kimata, A. Tsuru, and K. Kohno. 2001. Diphtheria toxin receptor-mediated conditional and targeted cell ablation in transgenic mice. Nat Biotechnol 19:746-750.
Sanghavi, M., and M. Gulati. 2015. Sex differences in the pathophysiology, treatment, and outcomes in IHD. Curr Atheroscler Rep 17:511.
Sano, H., T. Sudo, M. Yokode, T. Murayama, H. Kataoka, N. Takakura, S. Nishikawa, S.I. Nishikawa, and T. Kita. 2001. Functional blockade of platelet-derived growth factor receptor-beta but not of receptor-alpha prevents vascular smooth muscle cell accumulation in fibrous cap lesions in apolipoprotein E-deficient mice. Circulation 103:2955-2960.
Sartore, S., A. Chiavegato, E. Faggin, R. Franch, M. Puato, S. Ausoni, and P. Pauletto. 2001. Contribution of adventitial fibroblasts to neointima formation and vascular remodeling: from innocent bystander to active participant. Circ Res 89:1111-1121.
Sata, M., A. Saiura, A. Kunisato, A. Tojo, S. Okada, T. Tokuhisa, H. Hirai, M. Makuuchi, Y. Hirata, and R. Nagai. 2002. Hematopoietic stem cells differentiate into vascular cells that participate in the pathogenesis of atherosclerosis. Nat Med 8:403-409.
Sawada, H., D.L. Rateri, J.J. Moorleghen, M.W. Majesky, and A. Daugherty. 2017. Smooth Muscle Cells Derived From Second Heart Field and Cardiac Neural Crest Reside in Spatially Distinct Domains in the Media of the Ascending Aorta-Brief Report. Arterioscler Thromb Vasc Biol 37:1722-1726.
Schiller, N.K., N. Kubo, W.A. Boisvert, and L.K. Curtiss. 2001. Effect of gamma-irradiation and bone marrow transplantation on atherosclerosis in LDL receptor-deficient mice. Arterioscler Thromb Vasc Biol 21:1674-1680.
Schwartz, S.M., and C.E. Murry. 1998. Proliferation and the monoclonal origins of atherosclerotic lesions. Annu Rev Med 49:437-460.
Schwartz, S.M., R. Virmani, and M.E. Rosenfeld. 2000. The good smooth muscle cells in atherosclerosis. Curr Atheroscler Rep 2:422-429.
Shankman, L.S., D. Gomez, O.A. Cherepanova, M. Salmon, G.F. Alencar, R.M. Haskins, P. Swiatlowska, A.A.C. Newman, E.S. Greene, A.C. Straub, B. Isakson, G.J. Randolph, and G.K. Owens. 2015. KLF4-dependent phenotypic modulation of smooth muscle cells has a key role in atherosclerotic plaque pathogenesis. Nat Med 21:628-637.
Sheikh, A.Q., A. Misra, I.O. Rosas, R.H. Adams, and D.M. Greif. 2015. Smooth muscle cell progenitors are primed to muscularize in pulmonary hypertension. Sci Transl Med 7:308ra159.
Sheikh, A.Q., F.Z. Saddouk, A. Ntokou, R. Mazurek, and D.M. Greif. 2018. Cell Autonomous and Non-cell Autonomous Regulation of SMC Progenitors in Pulmonary Hypertension. Cell Rep 23:1152-1165.
Slepian, M.J., S.P. Massia, B. Dehdashti, A. Fritz, and L. Whitesell. 1998. Beta3-integrins rather than beta1-integrins dominate integrin-matrix interactions involved in postinjury smooth muscle cell migration. Circulation 97:1818-1827.
Soriano, P. 1994. Abnormal kidney development and hematological disorders in PDGF beta-receptor mutant mice. Genes & development 8:1888-1896.
Stary, H.C. 1989. Evolution and progression of atherosclerotic lesions in coronary arteries of children and young adults. Arteriosclerosis (Dallas, Tex.) 9:I19-32.
Steed, D.L. 1995. Clinical evaluation of recombinant human platelet-derived growth factor for the treatment of lower extremity diabetic ulcers. Diabetic Ulcer Study Group. J Vasc Surg 21:71-78; discussion 79-81.

Steegmann, J.L., M. Baccarani, M. Breccia, L.F. Casado, V. García-Gutiérrez, A. Hochhaus, D.W. Kim, T.D. Kim, H.J. Khoury, P. Le Coutre, J. Mayer, D. Milojkovic, K. Porkka, D. Rea, G. Rosti, S. Saussele, R. Hehlmann, and R.E. Clark. 2016. European LeukemiaNet recommendations for the management and avoidance of adverse events of treatment in chronic myeloid leukaemia. Leukemia 30:1648-1671.

Stewart, F.A., S. Heeneman, J. Te Poele, J. Kruse, N.S. Russell, M. Gijbels, and M. Daemen. 2006. Ionizing radiation accelerates the development of atherosclerotic lesions in ApoE-/- mice and predisposes to an inflammatory plaque phenotype prone to hemorrhage. Am J Pathol 168:649-658.

Stewart, H.J., A.L. Guildford, D.J. Lawrence-Watt, and M. Santin. 2009. Substrate-induced phenotypical change of monocytes/macrophages into myofibroblast-like cells: a new insight into the mechanism of in-stent restenosis. J Biomed Mater Res A 90:465-471.

Stone, G.W., A. Maehara, A.J. Lansky, B. de Bruyne, E. Cristea, G.S. Mintz, R. Mehran, J. McPherson, N. Farhat, and S.P. Marso. 2011. A prospective natural-history study of coronary atherosclerosis. New England Journal of Medicine 364:226-235.

Sui, Y., S.-H. Park, J. Xu, S. Monette, R.N. Helsley, S.-S. Han, and C. Zhou. 2014. IKKβ links vascular inflammation to obesity and atherosclerosis. Journal of Experimental Medicine 211:869-886.

Swartz, E.A., A.D. Johnson, and G.K. Owens. 1998. Two MCAT elements of the SM alpha-actin promoter function differentially in SM vs. non-SM cells. Am J Physiol 275:C608-618.

Takayama, T., X. Shi, B. Wang, S. Franco, Y. Zhou, D. DiRenzo, A. Kent, P. Hartig, J. Zent, and L.-W. Guo. 2015. A murine model of arterial restenosis: technical aspects of femoral wire injury. Journal of visualized experiments: JoVE

Thomas, C.M., and E.J. Smart. 2007. Gender as a regulator of atherosclerosis in murine models. Curr Drug Targets 8:1172-1180.

Thomas, J.A., R.A. Deaton, N.E. Hastings, Y. Shang, C.W. Moehle, U. Eriksson, S. Topouzis, B.R. Wamhoff, B.R. Blackman, and G.K. Owens. 2009. PDGF-DD, a novel mediator of smooth muscle cell phenotypic modulation, is upregulated in endothelial cells exposed to atherosclerosis-prone flow patterns. Am J Physiol Heart Circ Physiol 296:H442-452.

Thompson, R.C., A.H. Allam, G.P. Lombardi, L.S. Wann, M.L. Sutherland, J.D. Sutherland, M.A.-T. Soliman, B. Frohlich, D.T. Mininberg, and J.M. Monge. 2013. Atherosclerosis across 4000 years of human history: the Horus study of four ancient populations. The Lancet 381:1211-1222.

Tomas, L., A. Edsfeldt, I.G. Mollet, L. Perisic Matic, C. Prehn, J. Adamski, G. Paulsson-Berne, U. Hedin, J. Nilsson, E. Bengtsson, I. Goncalves, and H. Bjorkbacka. 2018. Altered metabolism distinguishes high-risk from stable carotid atherosclerotic plaques. Eur Heart J 39:2301-2310.

Topouzis, S., and M.W. Majesky. 1996. Smooth muscle lineage diversity in the chick embryo. Two types of aortic smooth muscle cell differ in growth and receptor-mediated transcriptional responses to transforming growth factor-beta. Dev Biol 178:430-445.

Uryga, A.K., and M.R. Bennett. 2016. Ageing induced vascular smooth muscle cell senescence in atherosclerosis. J Physiol 594:2115-2124.

van der Harst, P., and N. Verweij. 2018. Identification of 64 Novel Genetic Loci Provides an Expanded View on the Genetic Architecture of Coronary Artery Disease. Circ Res 122:433-443.

Van Leeuwen, R. 1996. Extracellular proteolysis and the migrating vascular smooth muscle cell. Fibrinolysis 10:59-74.

Vengrenyuk, Y., H. Nishi, X. Long, M. Ouimet, N. Savji, F.O. Martinez, C.P. Cassella, K.J. Moore, S.A. Ramsey, J.M. Miano, and E.A. Fisher. 2015. Cholesterol loading reprograms the microRNA-143/145-myocardin axis to convert aortic smooth muscle cells to a dysfunctional macrophage-like phenotype. Arterioscler Thromb Vasc Biol 35:535-546.

Vernon, M.A., K.J. Mylonas, and J. Hughes. 2010. Macrophages and renal fibrosis. Seminars in nephrology 30:302-317.
Virmani, R., A.P. Burke, and A. Farb. 1999. Plaque rupture and plaque erosion. Thromb Haemost 82 Suppl 1:1-3.
Virmani, R., A.P. Burke, A. Farb, and F.D. Kolodgie. 2006. Pathology of the vulnerable plaque. J Am Coll Cardiol 47:C13-18.
Virmani, R., F.D. Kolodgie, A.P. Burke, A. Farb, and S.M. Schwartz. 2000. Lessons from sudden coronary death: a comprehensive morphological classification scheme for atherosclerotic lesions. Arterioscler Thromb Vasc Biol 20:1262-1275.
Viswanathan, V.S., M.J. Ryan, H.D. Dhruv, S. Gill, O.M. Eichhoff, B. Seashore-Ludlow, S.D. Kaffenberger, J.K. Eaton, K. Shimada, A.J. Aguirre, S.R. Viswanathan, S. Chattopadhyay, P. Tamayo, W.S. Yang, M.G. Rees, S. Chen, Z.V. Boskovic, S. Javaid, C. Huang, X. Wu, Y.Y. Tseng, E.M. Roider, D. Gao, J.M. Cleary, B.M. Wolpin, J.P. Mesirov, D.A. Haber, J.A. Engelman, J.S. Boehm, J.D. Kotz, C.S. Hon, Y. Chen, W.C. Hahn, M.P. Levesque, J.G. Doench, M.E. Berens, A.F. Shamji, P.A. Clemons, B.R. Stockwell, and S.L. Schreiber. 2017. Dependency of a therapy-resistant state of cancer cells on a lipid peroxidase pathway. Nature 547:453-457.
Vitale, C., M. Miceli, and G.M. Rosano. 2007. Gender-specific characteristics of atherosclerosis in menopausal women: risk factors, clinical course and strategies for prevention. Climacteric 10 Suppl 2:16-20.
Wainscoat, J.S., and M.F. Fey. 1990. Assessment of clonality in human tumors: a review. Cancer Res 50:1355-1360.
Wamhoff, B.R., M.H. Hoofnagle, A. Burns, S. Sinha, O.G. McDonald, and G.K. Owens. 2004. A G/C element mediates repression of the SM22alpha promoter within phenotypically modulated smooth muscle cells in experimental atherosclerosis. Circ Res 95:981-988.
Wang, J., A. Uryga, and J. Rienhold. 2016a. Vascular Smooth Muscle Cell Senescence Promotes Atherosclerosis and Features of Plaque Vulnerability. Journal of Vascular Surgery 63:1662.
Wang, S., X.M. Meng, Y.Y. Ng, F.Y. Ma, S. Zhou, Y. Zhang, C. Yang, X.R. Huang, J. Xiao, Y.Y. Wang, S.M. Ka, Y.J. Tang, A.C. Chung, K.F. To, D.J. Nikolic-Paterson, and H.Y. Lan. 2016b. TGF-beta/Smad3 signalling regulates the transition of bone marrow-derived macrophages into myofibroblasts during tissue fibrosis. Oncotarget 7:8809-8822.
Waxman, S., S.R. Dixon, P. L'Allier, J.W. Moses, J.L. Petersen, D. Cutlip, J.-C. Tardif, R.W. Nesto, J.E. Muller, and M.J. Hendricks. 2009. In vivo validation of a catheter-based near-infrared spectroscopy system for detection of lipid core coronary plaques: initial results of the SPECTACL study. JACC: Cardiovascular Imaging 2:858-868.
Weinstein, R., M.B. Stemerman, and T. Maciag. 1981. Hormonal requirements for growth of arterial smooth muscle cells in vitro: An endocrine approach to atherosclerosis. Science 212:818-820.
Weintraub, N.L., W.K. Jones, and D. Manka. 2010. Understanding radiation-induced vascular disease. Journal of the American College of Cardiology 55:1237-1239.
Welch-Reardon, K.M., N. Wu, and C.C.W. Hughes. 2015. A role for partial endothelial-mesenchymal transitions in angiogenesis? Arteriosclerosis, thrombosis, and vascular biology 35:303-308.
Westermark, B., and C.H. Heldin. 1985. Similar action of platelet-derived growth factor and epidermal growth factor in the prereplicative phase of human fibroblasts suggests a common intracellular pathway. Journal of cellular physiology 124:43-48.
Westermark, B., A. Siegbahn, C.H. Heldin, and L. Claesson-Welsh. 1990. B-type receptor for platelet-derived growth factor mediates a chemotactic response by means of ligand-induced activation of the receptor protein-tyrosine kinase. Proceedings of the National Academy of Sciences of the United States of America 87:128-132.
WHO. 2016. The top 10 causes of death.

Widelitz, R., and C.-M. Chuong. 2016. Quorum sensing and other collective regenerative behavior in organ populations. Current opinion in genetics & development 40:138-143.
Wieman, T.J., J.M. Smiell, and Y. Su. 1998. Efficacy and safely of a topical gel formulation of recombinant human platelet-derived growth factor-BB (becaplermin) in patients with chronic neuropathic diabetic ulcers: a phase III randomized placebo-controlled double-blind study. Diabetes care 21:822-827.
Williams, L.T. 1989. Signal transduction by the platelet-derived growth factor receptor. Science 243:1564-1570.
Wilson, C., C.D. Saunter, J.M. Girkin, and J.G. McCarron. 2016. Clusters of specialized detector cells provide sensitive and high fidelity receptor signaling in the intact endothelium. The FASEB Journal 30:2000-2013.
Woodard, A.S., G. Garcia-Cardena, M. Leong, J.A. Madri, W.C. Sessa, and L.R. Languino. 1998. The synergistic activity of alphavbeta3 integrin and PDGF receptor increases cell migration. Journal of Cell Science 111:469-478.
Yang, W., A. Ramachandran, S. You, H. Jeong, S. Morley, M.D. Mulone, T. Logvinenko, J. Kim, D. Hwang, M.R. Freeman, and R.M. Adam. 2014a. Integration of proteomic and transcriptomic profiles identifies a novel PDGF-MYC network in human smooth muscle cells. Cell Commun Signal 12:44.
Yang, W.S., R. SriRamaratnam, M.E. Welsch, K. Shimada, R. Skouta, V.S. Viswanathan, J.H. Cheah, P.A. Clemons, A.F. Shamji, and C.B. Clish. 2014b. Regulation of ferroptotic cancer cell death by GPX4. Cell 156:317-331.
Yoshida, T. 2008. MCAT elements and the TEF-1 family of transcription factors in muscle development and disease. Arterioscler Thromb Vasc Biol 28:8-17.
Yu, H., V. Stoneman, M. Clarke, N. Figg, H.B. Xin, M. Kotlikoff, T. Littlewood, and M. Bennett. 2011. Bone marrow-derived smooth muscle-like cells are infrequent in advanced primary atherosclerotic plaques but promote atherosclerosis. Arterioscler Thromb Vasc Biol 31:1291-1299.
Zhang, X.H., L.Y. Tee, X.G. Wang, Q.S. Huang, and S.H. Yang. 2015. Off-target Effects in CRISPR/Cas9-mediated Genome Engineering. Mol Ther Nucleic Acids 4:e264.